SPIE.

OPTICS
FOR TECHNICIANS

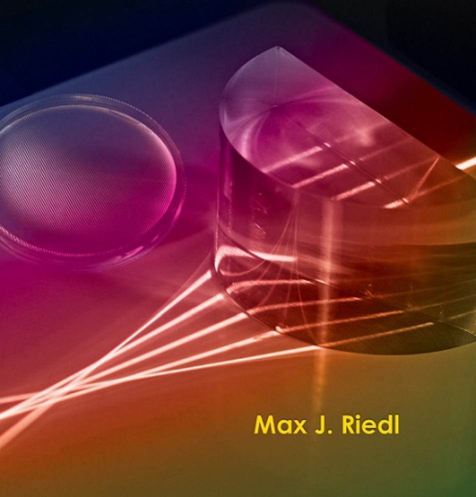

Max J. Riedl

OPTICS

FOR TECHNICIANS

The plano-convex cylinder lens shown on the cover illustrates the increased ray bending toward the edge of the lens. This effect is called *spherical aberration* (see Chapter 4 for more details).

The following computer-generated ray trace confirms the behavior of the pictured lens.

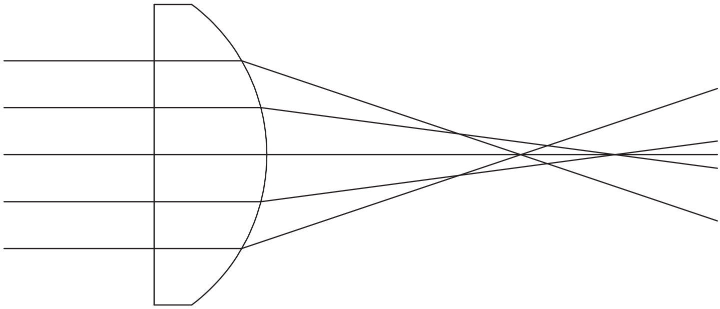

OPTICS

FOR TECHNICIANS

Max J. Riedl

SPIE PRESS
Bellingham, Washington USA

Library of Congress Cataloging-in-Publication Data

Riedl, Max J., author.
Optics for technicians / Max J. Riedl.
pages cm
ISBN 978-1-62841-821-7
1. Optics. I. Title.
QC355.3.R54 2015
621.36–dc23

2015019601

Published by

SPIE
P.O. Box 10
Bellingham, Washington 98227-0010 USA
Phone: +1 360.676.3290
Fax: +1 360.647.1445
Email: books@spie.org
Web: http://www.spie.org

The content of this book reflects the work and thought of the author. Every effort has been made to publish reliable and accurate information herein, but the publisher is not responsible for the validity of the information or for any outcomes resulting from reliance thereon.

Printed in the United States of America.
First printing

Contents

Preface xi

1 Light: What Is It and How Is It Directed? 1

1.1 Introduction 1
1.2 Velocity, Observations 2
1.3 Propagation of Light 3
1.4 Index of Refraction 3
1.5 Fermat's Principle 3
1.6 Snell's Law, Graphically Applied 4
1.7 Creating a Lens 6

2 Optical Elements 9

2.1 Lenses 9
2.2 Positive Lens, Focal Length, and Back Focal Length 10
2.3 Additional Relations 13
2.4 Negative Lens, Focal Length, and Back Focal Length 17
2.5 Imaging with a Negative Lens 19
2.6 Magnifier 21
2.7 Human Eye 22
2.8 Ball Lens 24
2.9 Plane Parallel Plate 25
2.9.1 Plate perpendicular to the optical axis 26

2.9.2 Tilted plate 27
2.9.3 Prisms acting as plane parallel plates 28
2.9.4 Prism and dispersion 29
2.9.5 Abbe number 30
2.9.6 Prism spectrometer 31
2.9.7 Thin prism 32
2.9.8 Lens centering error 32
2.9.9 One-diopter prism 33
2.10 Snell's Law for a Mirror 34
2.11 Spherical Mirrors 34
2.11.1 Imaging with a concave mirror 35
2.11.2 Imaging with a convex mirror 37

3 "Thin Lens" Concept 39

3.1 Postulation 39
3.2 Change and Its Impact 39
3.3 Simplified Image Formation 40
3.4 Quick Reference for Image Location and Orientation 43
3.5 Lens Bending 44

4 Primary Aberrations 47

4.1 Introduction 47
4.2 Thin Lens, Object at Infinity, On-Axis Aberrations 49
4.2.1 Spherical aberration 49
4.2.2 Axial chromatic aberration 53
4.3 Thin Lens Off-Axis Aberrations 56
4.3.1 Coma 56
4.3.2 Astigmatism 56
4.3.3 Field curvature (Petzval curvature) 56
4.3.4 Distortion 57
4.3.5 Lateral color, also termed lateral chromatic aberration 58

4.4 Spherical Convex Mirror, Object at Infinity 58
4.5 Assessment 60

5 Stops, Pupils, and Windows 63

5.1 Aperture Stop 63
5.2 Field Stop 63
5.3 Pupils and Windows 63
5.4 Function of Pupils and Windows 68
5.5 Vignetting 71

6 Two-Element Systems 73

6.1 Introduction 73
6.1.1 Telescopes 73
6.1.2 Microscopes 76
6.1.3 Relay systems 77
6.1.4 Projector systems 78
6.1.5 Telephoto objectives 78
6.1.6 Reverse telephoto objectives 79
6.2 Doublets 80
6.3 Separated Imaging Mirrors 82
6.3.1 Telescope objectives 82
6.3.2 Microscope objectives 84
6.4 Focal Length of Two Separated Elements 86

7 Aspheres, Gradient Index Lenses, and Optical Path Length 91

7.1 Conic Sections 91
7.1.1 Aspheric singlet 93
7.2 Freeform Surfaces 93
7.3 Gradient Index Lenses 94
7.4 Optical Path Length 95

8 Diffraction Limit, Resolution, and Modulation Transfer Function 97

8.1 Diffraction Effect on an Image 97

8.2 Resolution, Image Quality, and Depth of Focus 99
8.3 Modulation Transfer Function 100
8.3.1 What is the modulation transfer function? 101
8.3.2 Equations 102
8.3.3 Additional limit 103
8.4 Real Case Demonstration 105
8.4.1 Aberrations 106
8.4.2 Blur spots 107

9 Optical Coatings 111

9.1 Introduction 111
9.2 Refractive Elements 111
9.3 Antireflective Coatings 114
9.4 Reflective Coatings 116
9.5 Interference Filters 116
9.5.1 Beam splitters 118
9.5.2 Angular sensitivity of filters 119
9.5.3 Effect of placing a filter in a converging or diverging light bundle 119
9.5.4 Thermal sensitivity 121
9.6 Absorption 122
9.7 Interference 123

10 Manufacturing Processes 125

10.1 Introduction with Historical Remarks 125
10.2 Conventional Generation of Spherical Surfaces 125
10.3 Test Plate 129
10.4 Useful Nomogram 132
10.5 Aspheric Surfaces 134
10.6 Surfaces Generated with Single-Point Diamond Turning 135
10.7 Replicated Optical Elements 137
10.7.1 Replication process 137
10.7.2 Lenses 138

10.7.3 Diffraction gratings 139
10.8 Molded Plastic Optical Elements 141

11 Optical Bench 143
11.1 General Remarks 143
11.2 Basic Bench 143
11.3 Evaluating a Concave Mirror 145
11.4 Bessel's Method to Determine the Focal Length 145
11.5 Autoreflecting Microscope and the Autocollimator 148

12 Mounting Optical Components 151
12.1 Declaration 151
12.2 Basic Lens Mounting Methods 151
12.3 Plastic Lenses and Mounts 153
12.4 Mirrors 155
12.5 Prisms 155
12.6 Metal Mirrors 155
12.7 Thermal Effects 158

13 Exercises with Elaborations 161
13.1 Exercise 1.1 161
13.2 Exercise 1.2 163
13.3 Exercise 2.1 166
13.4 Exercise 2.2 167
13.5 Exercise 3.1 168
13.6 Exercise 4.1 170
13.7 Exercise 5.1 171
13.8 Exercise 6.1 172
13.9 Exercise 7.1 173
13.10 Exercise 8.1 175
13.11 Exercise 9.1 176
13.12 Exercise 10.1 177
13.13 Exercise 11.1 179

Index 181

Preface

This book deviates from the usual format of my SPIE Tutorial Texts. It guides the reader in a sometimes conversational style through the pages and provides an elementary understanding of the subjects with the support of more than 100 sketches, diagrams, layouts, and tables. Much effort has been applied in presenting the individual subjects and issues with basic relations, avoiding complicated mathematical expressions.

The numerous examples and exercises will be helpful to gain additional knowledge and understanding of the topics under discussion.

Special emphasis has been placed on the fact that optical elements by themselves are simply components. To serve as an instrument, optical elements must be carefully mounted into mechanical structures.

To pay respect to the great scientists of the past for their discoveries and inventions, some historic remarks have been inserted at proper places for reference.

For those who are eager to dig a bit deeper, derivations and verifications of expressions are included in some instances, which provide further insight into a particular subject.

Whereas this text is intended as a fundamental coverage of the broad field of optics, it may also serve to spark latent imagination for some readers.

I thank Tim Lamkins, Tyler Koshakow, and Scott McNeill of SPIE for their guidance and encouragement, and the reviewers for their helpful recommendations.

Max J. Riedl
July 2015

Chapter 1
Light: What Is It and How Is It Directed?

1.1 Introduction

Light is a very narrow portion of the total electromagnetic radiation range, termed the electromagnetic spectrum, which extends between x-rays (short wavelengths) and radio waves (long wavelengths). The visible spectrum, the so-called "optical" portion, which we perceive with our eyes, covers the wavelength region from 0.4 to 0.76 μm. One $\mu\text{m} = 0.001$ mm, i.e., $0.001/25.4 = 0.00003937 = 3.937 \times 10^{-5}$ in.

When designing optical elements, researchers give special emphasis to the wavelengths 0.5876, 0.4861, and 06563 μm. These wavelengths represent absorption lines in the solar spectrum, named after its discoverer, *Joseph von Fraunhofer*,* in 1814. The three aforementioned lines are, respectively, the d, F, and C lines.

Light exhibits what is known as wave–particle duality: certain properties can be best explained by wave theory and

Joseph von Fraunhofer was a German physicist from Bavaria, born in 1787. He was the 11th child of a glassmaker family and died at the early age of 39 due to lung disease.

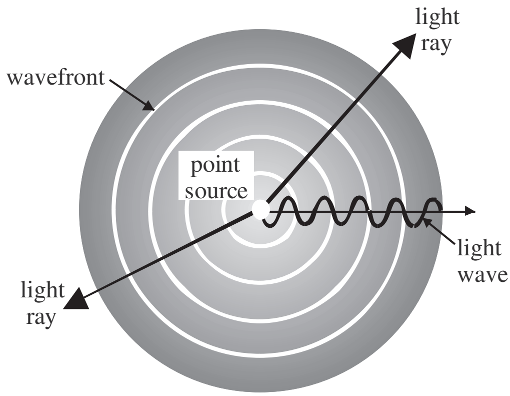

Figure 1.1 Light rays are normal to the wavefront.

others by particle theory. The text in this book primarily considers geometrical optics, whereby the diffraction effect in the image is ignored. In reality, light rays do not exist; they are wavefront-normals, perpendicular lines to the wavefront, as indicated in Fig. 1.1.

1.2 Velocity, Observations

The velocity of light in vacuum is a universal constant and has a value of 2.99792458×10^8 m/s.* This is the maximum speed at which energy can travel.

*The definition of the meter was introduced by the French emperor *Napoleon Bonaparte* in 1791. It was intended to equal one ten-millionth of the length of the meridian from the pole plotted through Paris. To reduce the uncertainty of the length of the artefact known as the platinum–iridium standard, stored in Paris, characterization of the meter was changed from time to time. Today the meter is defined as 1.65076373×10^6 wavelengths of the orange–red radiation of krypton 86.

1.3 Propagation of Light

Light waves uniformly spread in a spherical shape from a point source, as illustrated in Fig. 1.1. Figure 1.1 also illustrates the concept of light rays.

1.4 Index of Refraction

In any other medium, light travels at a slower speed relative to that in vacuum. The ratio of the velocity in vacuum v_{vacuum} to the velocity in the medium v_{medium} is termed the index of refraction n. This is stated as

$$n = \frac{v_{vacuum}}{v_{medium}}. \tag{1.1}$$

The velocity of light in air is somewhat slower than in vacuum, which leads to an index of refraction of 1.000277. Because most optical systems are applied in air, glass indices are termed normal atmospherical conditions with the adjustment of expressing the index for air as 1.

1.5 Fermat's Principle

Pierre de Fermat, a French jurist and mathematician, presented in 1657* his famous theorem in a simple single sentence, which states the following:

"Light takes the path that requires the least time."

Following this statement mathematically leads to the relation

$$n' \sin i' = n \sin i. \tag{1.2}$$

* *Wilibrord Snel van Royen* experimentally determined this relationship 20 years before Fermat, but even van Royen was not the first person to have discovered it. The first discovery was in the year 984 when Ibn Sahl, a Muslim Persian mathematician, stated the law of refraction in the court of Baghdad.

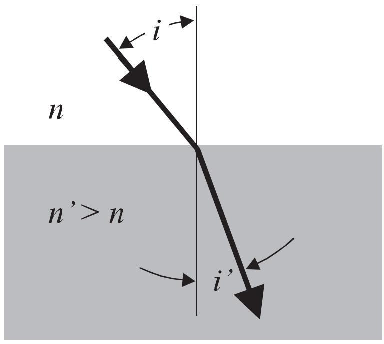

Figure 1.2 Snell's law applied for a ray entering a more-dense medium.

This is known as Snell's law.

In Eq. (1.2), n and n' are the indices of refraction of the media. Terms i and i' are the angles before and after refraction, respectively, indicated in Fig. 1.2.

Exercise 1

A ray enters a glass surface at an angle $i = 30$ deg. The index of refection of the glass is $n' = 1.5$.

Calculate the angle i' at which the ray will travel after refraction.

Solution

Applying Eq. (1.2), we find that $\sin i' = (n/n')(\sin i) = (1/1.5)(\sin 30\ \text{deg}) = 0.666667 \times 0.5 = 0.333333$, which represents an angle $i' = 19.47\ \text{deg}$.

1.6 Snell's Law, Graphically Applied

It is enlightening to apply Snell's law graphically (Fig. 1.3), as in the following exercise.

Procedure

1. Draw a circle with a radius of one unit length, with its center C located at the substrate's top surface. This is the air index circle (for $n = 1$).
2. Draw, around the same center, a circle with radius n'. In our case, the radius is 1.5 times the size of the air index radius because the substrate's index is $n' = 1.5$.
3. Draw the entering ray at the proper angle. For our example, $i = 30$ deg.
4. Draw a line parallel to the substrate surface normal from point 1. The intersection with the index circle is point 2.
5. Draw a line from point 2 through the center C. The extension after point C is the refracted ray, which passes through the substrate at angle i' (measuring with a protractor, you will find that it is 19.5 deg).

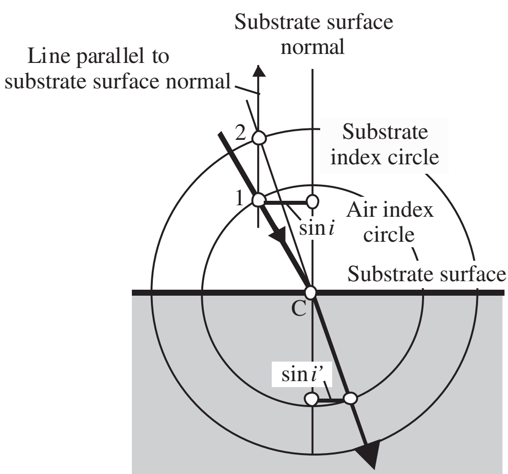

Figure 1.3 Snell's law, graphically applied.

1.7 Creating a Lens

As we will discuss in more detail in Chapter 2, a prism is an optical element; the flat surfaces are tilted with respect to one other. Applying Snell's law to the surfaces of a delta (triangular)-shaped prism shows that rays passing through the prism are always bent towards the thicker end. Placing one

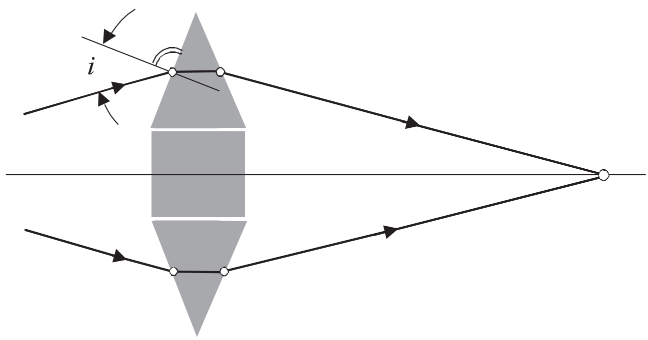

Figure 1.4 Symmetrically arranged prisms.

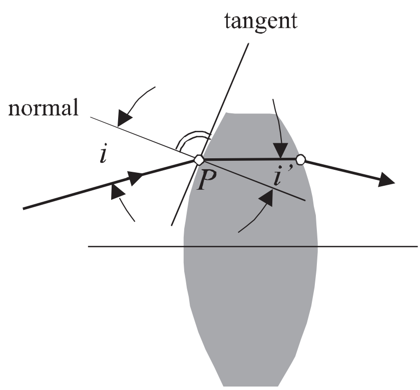

Figure 1.5 Biconvex lens, derived from the fundamental prism arrangement.

prism on top and one prism below a plane parallel block of glass, as depicted in Fig. 1.4, indicates the concept of how a lens functions.

Increasing the number of prisms to an infinite number, and rendering the entire arrangement rotationally symmetrical, forms a lens (see Fig. 1.5).

To apply Snell's law, the tangent at the point where the ray meets the lens surface is termed the "local prism surface."

We have arrived at the foundation of geometrical optics! We have learned the law that describes the direction in which light travels and we have described a device that is suitable for controlling this direction.

Chapter 2
Optical Elements

2.1 Lenses

Optical instruments use a converging lens, most frequently for changing the direction of light. The next type of lens most frequently used is the diverging lens. The first lens type, also known as a positive lens, bends all light rays entering parallel to the optical axis towards the axis, converging to a common point, the focal point F. A diverging lens, also termed a negative lens, directs the rays away from the axis. They appear to be emanating from the focal point F of the lens, except when the ray lies on the optical axis. Both cases are indicated in Fig. 2.1.

Lens surfaces are usually spherical because spherical surfaces are easier to generate than others. However, aspheric surfaces, as the name implies, provide in some cases such great advantages that it has been the dream of lens designers for centuries to be able to generate such surfaces economically. This economical production has been achieved over the past decades. In combination with the expansion of computer programs, the design and manufacturing methods have opened doors to previously unachievable possibilities. In this domain are also "free-form" optical elements. Whereas a free-form is a general asphere, the term asphere is mainly applied

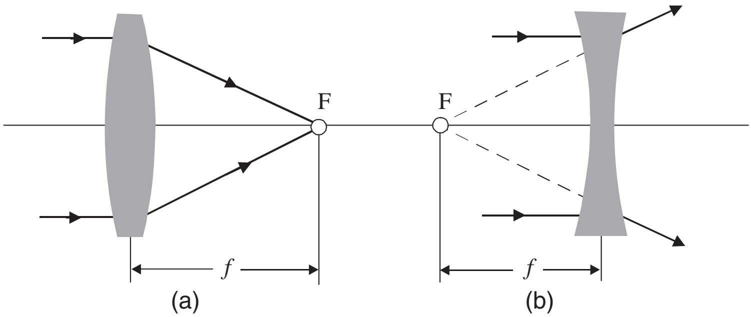

Figure 2.1 (a) Converging (positive focal length) and (b) diverging (negative focal length) lenses, and their behavior.

to rotationally symmetric shapes, such as conic sections, which are parabolas, ellipses, and hyperbolas.

We begin with the positive lens and assume in this examination that the lens is surrounded on both sides by air.

2.2 Positive Lens, Focal Length, and Back Focal Length

As we know, a ray is redirected according to Snell's law on entering and exiting a lens, indicated in Fig. 2.2. The forward-extended entering ray and the backward-extended exiting ray cross at the rear principal plane. The focal length of a lens is the measure from this location to the focal point F_2. The distance from the axial point of the rear surface to the focus is the back focal length (bfl).

The reciprocal of the focal length f is termed the power of the lens and is represented by ϕ.

> The reciprocal of a number is 1 divided by that number. Therefore, the reciprocal of f is $1/f$.

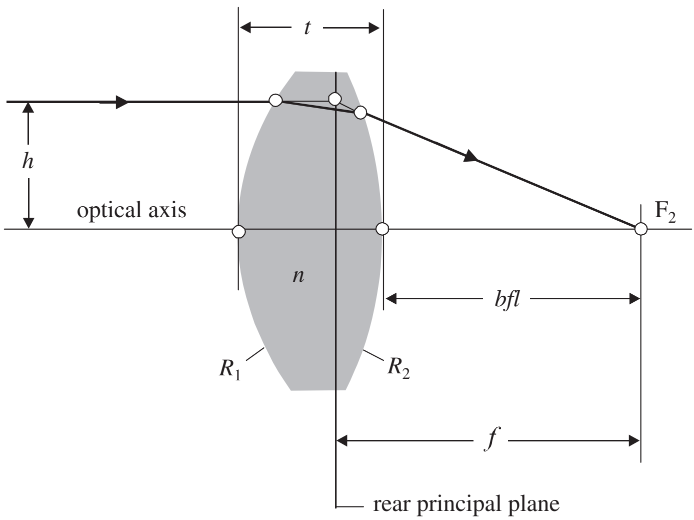

Figure 2.2 Ray entering the lens parallel to the optical axis crosses the axis after exiting at the rear focus F_2.

The reciprocal is not only an expression to indicate the "strength" of a lens to bend light rays; it also simplifies the expression to calculate the focal length of a lens, which is

$$\phi = \frac{1}{f} = (n-1)\left[\frac{1}{R_1} - \frac{1}{R_2} + \frac{(n-1)t}{nR_1R_2}\right], \qquad (2.1)$$

where n is the index of refraction of the lens material, and t is the lens thickness. R_1 and R_2 are the front and rear lens radii, respectively. When the center of a surface radius lies to the right, the radius is positive. If the center of a surface radius is to the left, the radius is negative. Therefore, in Fig. 2.2 R_1 is positive and R_2 is negative. The power of a lens is expressed in diopters. One diopter is the reciprocal of 1 m. Recall that the reciprocal of a number is 1 divided by that number. A lens with a power of 2 diopters therefore has a focal length of $1/2 = 0.5$ m.

Equation (2.1) may look at first a bit cumbersome, but as we will demonstrate with examples it leads quickly to an answer.

The back focal length, also termed the back focal distance, is

$$bfl = f\left[1 - \frac{(n-1)t}{nR_1}\right]. \tag{2.2}$$

Exercise 1

Find the focal length and the back focal distance of a lens with the following prescription.

Front radius $R_1 = 65$ mm, rear radius $R_2 = -200$ mm, thickness $t = 15$ mm, and index of refraction $n = 1.5$.

Approach and Solution

Using Eq. (2.1), we obtain

$$\phi = \frac{1}{f} = (1.5-1)\left[\frac{1}{65} - \frac{1}{-200} + \frac{(1.5-1)\cdot 15}{1.5 \times 65 \times (-200)}\right]$$
$$= 0.01,$$

$$f = \frac{1}{\phi} = \frac{1}{0.01} = 100 \text{ mm}.$$

Equation (2.2) leads to

$$bfl = 100\left[1 - \frac{(1.5-1)\times 15}{1.5 \times 65}\right] = 92.3077 \text{ mm}.$$

This means that the rear principal plane lies 7.6923 mm inside the lens, measured from the vertex of the rear surface.

2.3 Additional Relations

Figure 2.3 identifies additional relations, indicating the locations of the object and image, and the ratio of their heights (magnification) and orientations.

Ray 1 enters the lens parallel to the optical axis. Therefore, the point at which it crosses the axis after exiting the lens is the second focal point F_2. Ray 2 passes through the front focus F_1 and leaves the lens parallel to the optical axis.

The two nodal points are special cardinal points because they lie on the optical axis. A ray aiming at N_1 leaves the lens from N_2 in the same direction as it entered the lens, indicated with ray 3.

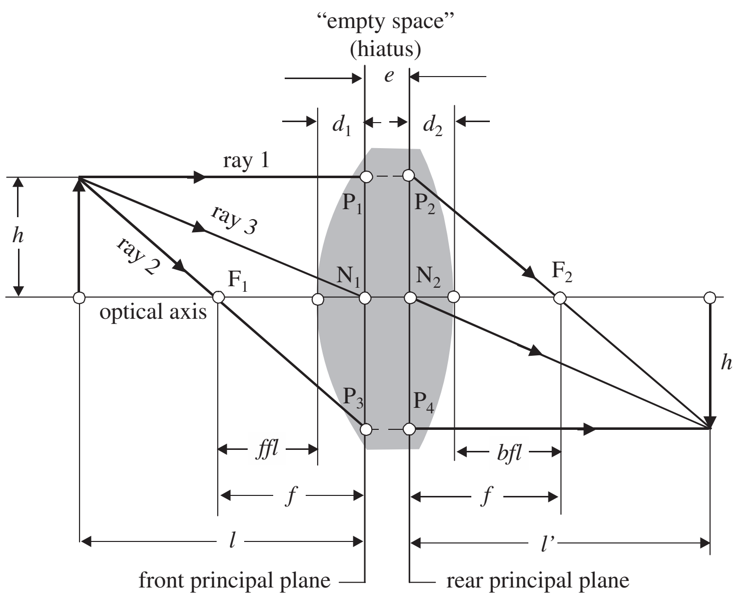

Figure 2.3 Positive lens and its cardinal points. Focal points, F_1 and F_2. Nodal points, N_1 and N_2. Principal points, P_1, P_2, P_3, and P_4.

The principal planes are actually spherical surfaces, but they can be treated as planes in the paraxial region, which is the region close to the optical axis, where the sine and tangent of the ray angles are close to each other, and to the angle expressed in radians.

As a point of reference, $\sin 5\ \text{deg} = 0.08715$, and $\tan 5\ \text{deg} = 0.08748$. Five degrees also equals the 72th part of the 2π full 360-deg circle. Therefore, 5 deg represents $(2\pi/360) \cdot 5 = \pi/36 = 0.08726$ rad. It is a limit of acceptable accuracy in what is termed the paraxial region.

This paraxial treatment is useful even when rays are far from the optical axis because, with the assumption of the trigonometric functions' equality, the equations become linear whereby a simple scaling effect is achieved.

The characteristic feature of the principal planes is that the magnification between them is unity, which means that the rays are transferred at the same height from the front principal plane to the rear principal plane.

In general, a positive lens is used to form an image of an object with a certain magnification.

Sign Convention

- Distances to the left of the front principal plane and heights below the optical axis are negative; distances to the right of the rear principal plane and heights above the optical axis are positive. This indicates that the light is assumed to travel from the left to the right.
- The focal lengths of a positive lens, including the front and back focal lengths, are positive.

It is extremely important to very carefully apply the agreed-upon sign convention.

The following equations refer to the call-outs in Fig. 2.3:

$$\text{Magnification} \qquad m = \frac{l'}{l} = \frac{h'}{h}. \tag{2.3}$$

$$\text{Back focal length} \qquad bfl = f - \frac{(n-1)tf}{nR_1}. \tag{2.4}$$

$$\text{Front focal length} \qquad ffl = f - \frac{(n-1)tf}{nR_2}. \tag{2.5}$$

The distance from the vertex of the front surface to the front principal plane is

$$d_1 = -\frac{(n-1)tf}{nR_2}, \tag{2.6}$$

and the distance from the vertex of the rear surface to the rear principal plane is

$$d_2 = -\frac{(n-1)tf}{nR_1}. \tag{2.7}$$

To demonstrate what is meant by carefully observing the sign convention, we derive the so-called Gaussian expression* for the location of the image. In Fig. 2.3, it can be seen that the following relations exist:

$$\frac{h}{f} = \frac{(h-h')}{-l'}$$

$$\frac{-h'}{f} = \frac{(h-h')}{-l}$$

*_Johann Carl Friedrich Gauss_, a German mathematician, lived from 1777 until 1855 and is well-known for his many contributions in the fields of mathematics and physics.

Rearranging leads to

$$\frac{1}{l'} = \frac{h}{(h - h')} \times \frac{1}{f}, \tag{2.8}$$

$$\frac{1}{l} = \frac{h'}{(h - h')} \times \frac{1}{f}. \tag{2.9}$$

Subtracting Eq. (2.9) from Eq. (2.8) yields

$$\frac{1}{l'} - \frac{1}{l} = \frac{h}{(h - h')} \times \frac{1}{f} - \frac{h'}{(h - h')} \times \frac{1}{f} = \frac{1}{f}\left[\frac{(h - h')}{(h - h')}\right] = \frac{1}{f}.$$

The final Gaussian form is usually presented as

$$\frac{1}{l'} = \frac{1}{l} + \frac{1}{f}. \tag{2.10}$$

To find the image location, one rewrites Eq. (2.10) to read as

$$l' = \frac{lf}{l + f}. \tag{2.11}$$

Exercise 2

Find the image location and height of an object 5 mm high, located 150 mm to the left of the vertex of the lens discussed in exercise 1.

Approach and Solution

Given are $l - d_1 = -150$ mm; $h = 5$ mm. From exercise 1 we know that the focal length $f = 100$ mm, the lens thickness $t = 15$ mm, the index of refraction $n = 1.5$, and the rear radius of the lens $R_2 = -200$ mm.

Using Eq. (2.6), we find the location of the front principal plane

$$d_1 = -\frac{(n-1)tf}{nR_2} = -\frac{(1.5-1)\times 15\times 100}{1.5\times(-200)} = 2.5\text{ mm}.$$

With that, $l = -150 - d_1 = -150 - 2.5 = -152.5$ mm. Equation (2.11) yields

$$l' = \frac{lf}{l+f} = \frac{-152.5\times 100}{-152.5+100} = \frac{-152{,}500}{-52.5} = 2{,}904.76\text{ mm}.$$

The magnification is found with Eq. (2.3), i.e., $m = l'/l = 2{,}904.76/(-152.5) \cong -19$.

The image height, also using Eq. (2.3), is $h' = mh = (-19)\times 5 = -95$ mm.

To find the distance of the image from the vertex of the rear surface of the lens, we must subtract d_2 from l'. Using Eqs. (2.7) and (2.11), we obtain

$$\begin{aligned} l' - d_2 = l' - \frac{(n-1)tf}{nR_1} &= 2{,}904.76 \\ &- \frac{(1.5-1)\times 15\times 100}{1.5\cdot 65} = 2{,}897.07\text{ mm}. \end{aligned}$$

2.4 Negative Lens, Focal Length, and Back Focal Length

A negative lens has a shape as shown in Fig. 2.4. Since its focal length is negative, the locations of the focal points are in reverse order compared to the positive element, as indicated in Fig. 2.4. By choosing the front radius $R_1 = 60$ mm, rear radius $R_2 = 308.35$ mm, thickness $t = 5$ mm, and again

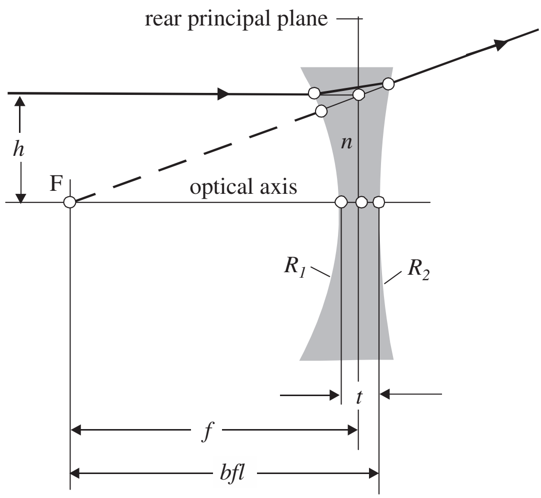

Figure 2.4 Relations for a negative lens.

fabricating the lens with a material for which the index of refraction $n = 1.5$, its power according to Eq. (2.1) is

$$\phi = \frac{1}{f} = (1.5 - 1)\left[\frac{1}{(-60)} - \frac{1}{308.35} + \frac{(1.5 - 1) \times 5}{1.5 \times (-60) \times 308.35}\right]$$
$$= -0.01.$$

The focal length is therefore $f = -100$ mm.
The back focal length according to Eq. (2.2) is

$$bfl = -100\left[1 - \frac{(1.5 - 1) \times 5}{1.5 \times (-60)}\right] = -102.7778 \text{ mm}.$$

The distance from the rear surface vertex to the rear principal plane is therefore $d_2 = -(f - bfl) = -(-100 + 102.78) = -2.78$ mm. This can also be found with Eq. (2.7): $d_2 = -\frac{(n-1)tf}{nR_1} = -\frac{(1.5-1)\times 5\times(-100)}{1.5\times(-60)} = -2.78$ mm. The location

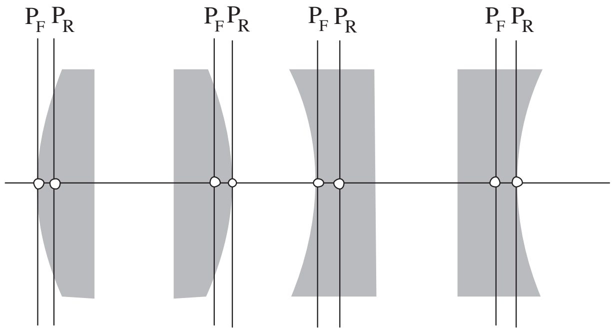

Figure 2.5 Location of the front principal plane for plano-convex and plano-concave lenses.

of the front principal plane, according to Eq. (2.6), is also inside the lens (see Fig. 2.5). The distance from the front surface vertex is

$$d_1 = -\frac{(1.5 - 1) \cdot 5 \cdot (-100)}{1.5 \cdot 308.35} = 0.54 \text{ mm}.$$

Equation (2.6) reveals that the front principal plane is located at the vertex of the first surface if the second surface [having an infinite radius ($R = \infty$)] is flat. If the first surface is flat, the front surface principal plane goes through the vertex of the rear surface. For a meniscus-shaped lens, the principal planes can be located outside the lens.

2.5 Imaging with a Negative Lens

To illustrate the use of the aforementioned equations, we image a 10-mm-high object, again located 150 mm to the left of the front principal plane. The prescription of the lens is given in Sec. 2.3. The setup is shown in Fig. 2.6 (it is not to scale).

Exercise 3

Given: $l = -150$ mm, $h = 10$ mm, and $f = -100$ mm. Find the image location, size, and magnification.

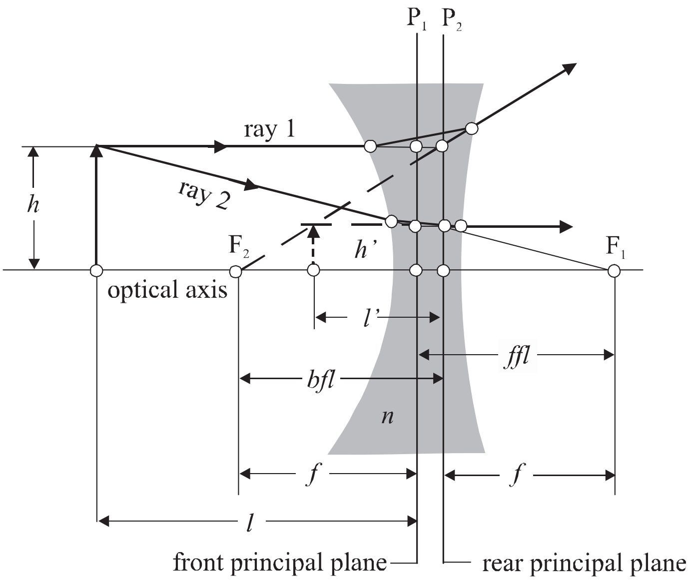

Figure 2.6 More details for the negative lens.

Solution

Using Eq. (2.11) yields

$$l' = \frac{lf}{l+f} = \frac{-150 \times (-100)}{-150 - 100} = -60 \text{ mm}.$$

Equation (2.3) yields

$$m = \frac{l'}{l} = \frac{-60}{-150} = 0.4,$$

and $h' = mh = 0.4 \times 10 = 4$ mm.

Note that the image is upright and virtual, which means that it can be viewed but not projected on a screen. By viewing it, the eye is actually a second system that projects the image onto the retina.

2.6 Magnifier

Figure 2.7 shows the two cases of the use of a magnifying glass. For both cases it is assumed that the eye is close to the lens.

The magnifying power (MP) is expressed by the ratio of the viewing angle of the image with a lens to the angle at which the object extends directly without a lens at the so-called "near point," which is by general agreement 250 mm or 10 in.

With this definition, referring to the near point of 250 mm, the magnification power is

$$MP = \frac{\alpha'}{\alpha} = \frac{\left(\frac{h'}{l'}\right)}{\left(\frac{h}{250}\right)} = \frac{h'}{l'} \times \frac{250}{h}. \tag{2.12}$$

At the limit, when the image location approaches infinity, $h'/l' = 1$, and $h = f$. The magnification is for this case

$$MP_0 = \frac{250}{f}, \tag{2.13}$$

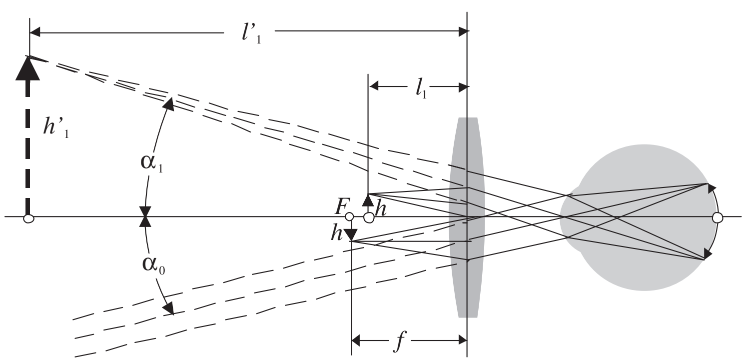

Figure 2.7 In the upper portion, the eye is focused at a distance of 250 mm. In the lower portion, the eye muscles are relaxed; the image is projected at infinity, because the object is placed at the focus of the lens.

where f must be in millimeters. This case is shown in the lower part of Fig. 2.7.

When the image is viewed at the near point distance of $l' = 250$ mm, as indicated in the upper portion of Fig. 2.7, using the subscript 1, we begin to analyze the situation with Eq. (2.10), i.e., $1/l'_1 = (1/l_1) + (1/f)$ and multiply both sides by l'_1. This leads to $l'_1/l'_1 = (l'_1/l_1) + (l'_1/f)$.

Because $(l'_1/l_1)MP_1$, and $l'_1/l'_1 = 1$, we can rewrite $1 = MP_1 + (l'_1/f)$. Finally, having chosen the viewing distance l'_1 to be 250 mm, we obtain for this special case

$$MP_1 = \frac{250}{f} + 1. \tag{2.14}$$

Examples

With a focal length of 50 mm, the magnifying power is $MP_0 = 250/f = 250/50 = 5$ for the relaxed eye. Remember, in that case the object is placed at the focus of the lens. To view the image at 250 mm, the object must be placed accoeding to Eq. (2.10) at

$$l = \frac{fl'}{l' - f} = \frac{50 \times 250}{250 - 50} = 41.667 \text{ mm}.$$

The magnification power is in this case

$$MP_1 = \frac{250}{50} + 1 = 6.$$

2.7 Human Eye

Figure 2.8 shows a very simplified outline of the human eye. The added information defines this fascinating sensing element.

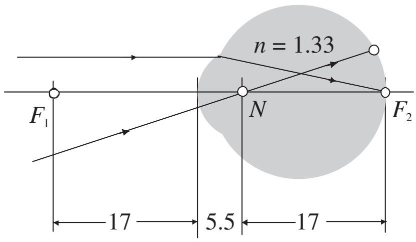

Figure 2.8 Very basic geometrical optics model of the human eye.

The location of the nodal point N is indicated, and the front focal length is 17 mm. In the eye, where the average index of refraction is $n = 1.33$, the focal length is $17 + 5.5 = 22.5$ mm. Much information pertinent to many optical models is available in the literature.

A much more detailed model of the human eye is shown in Fig. 2.9, and its parameters are noted in Table 2.1.

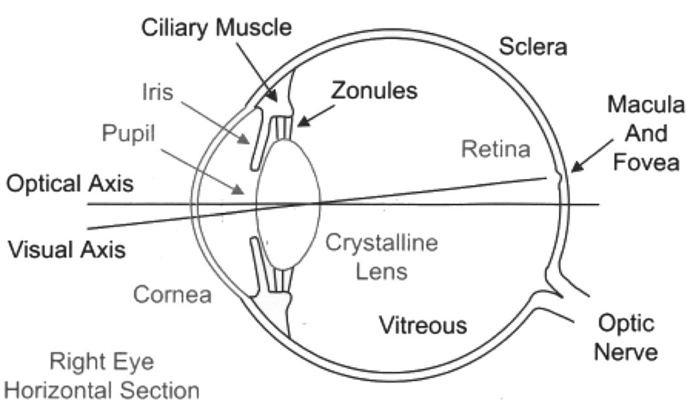

Figure 2.9 Model of the human eye. Image reprinted from *Field Guide to Geometrical Optics* (J. Greivenkamp, SPIE Press 2004).

Table 2.1 Parameters of the eye.

Surface	Radius t (mm)	Thickness t (mm)	Index n
Anterior cornea	7.8	0.55	1.3771
Posterior cornea	6.5	3.05	1.3374
Anterior lens	10.2	4.00	1.4200
Posterior lens	−6.0	16.60	1.3360

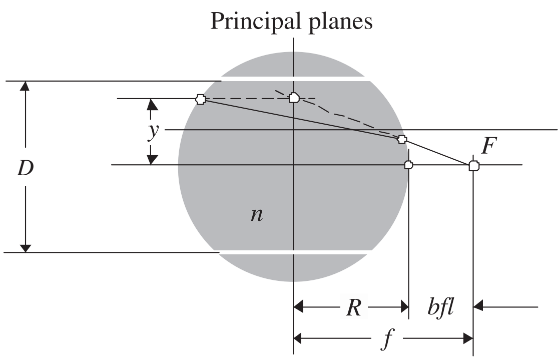

Figure 2.10 Ball lens. White lines suggest that the ball could be formed into a cylinder with a diameter D for easier mounting.

2.8 Ball Lens

A ball lens is an interesting optical element and warrants a closer evaluation. Figure 2.10 indicates its optical behavior and reveals that both principal planes pass through the center of the sphere.

The focal length of the ball lens is

$$f = \frac{nR}{2(n-1)}, \tag{2.15}$$

and the back focal length is

$$bfl = f - R = \frac{(2-n)R}{2(n-1)}. \tag{2.16}$$

Table 2.2 Back focal lengths and locations of ball lenses fabricated from different materials.

Material	Index n	Back focal length
Glass N-BK 10	1.5	$0.5R$
Glass LASF 35	2	0 (focus on rear side)
Zinc selenide	2.4	$-0.143R$ (inside the lens)
Silicon	3.4	$-0.273R$ (inside the lens)
Germanium	4.0	$-0.333R$ (inside the lens)

Caution

Equation (2.16) clearly indicates that there will be no back focus if the index of refraction n equals or is larger than 2. This means that when $n = 2$, the focus falls on the back side of the lens. If n is larger than 2, the focus lies inside the lens, which is the case for materials used in the infrared spectrum. Examples are listed in Table 2.2.

The shifts of the focal points F are indicated with dark spots in Fig. 2.11.

2.9 Plane Parallel Plate

A plane parallel plate can be considered as a special lens with zero power. This does not mean that it has no impact on the light transfer when it is inserted somewhere in the optical system. This is frequently not recognized, especially when optical filters are added or removed from the optical train. First, there is a longitudinal shift, if the rays are not parallel to the optical axis; and second, there is a lateral shift, when the plate is tilted. Furthermore, a plane parallel plate also introduces aberrations, which is often not recognized. Aberrations will be discussed in Chapter 4.

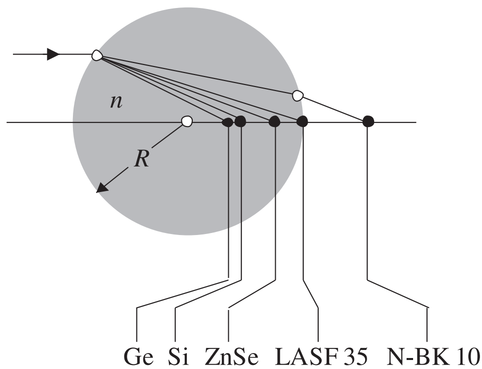

Figure 2.11 Focal point falls inside the ball when the index of refraction is larger than 2.

2.9.1 Plate perpendicular to the optical axis

The amount of the longitudinal shift (Fig. 2.12) is stated as

$$\Delta L = \left(1 - \sqrt{\frac{1 - \sin^2 u}{n^2 - \sin^2 u}}\right) t, \tag{2.17}$$

where u = the angle of the descending ray.

Exercise

If $n = 1.5$, $t = 20$ mm, and u is 15 deg, the image shift from P to P' amounts to

$$\begin{aligned}\Delta L &= \left(1 - \sqrt{\frac{1 - \sin^2 u}{n^2 - \sin^2 u}}\right) t \\ &= \left(1 - \sqrt{\frac{1 - \sin^2 15\ \text{deg}}{1.5^2 - \sin^2 15\ \text{deg}}}\right) \times 20 = 6.925\ \text{mm}.\end{aligned}$$

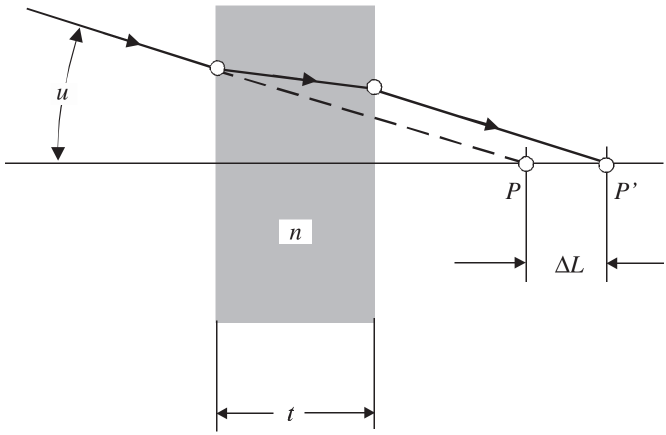

Figure 2.12 Longitudinal shift ΔL cause by inserting a plane parallel plate.

2.9.2 Tilted plate

Tilting the plate introduces an additional shift. It displaces the image laterally. The lateral displacement (Fig. 2.13) is

$$\Delta T = \left(1 - \sqrt{\frac{1 - \sin^2 u_{tilt}}{n^2 - \sin^2 u_{\mathrm{tilt}}}}\right) t \sin u_{tilt}. \qquad (2.18)$$

Tilting the plate from the aforementioned example by 20 deg results in a lateral displacement of point P of

$$\begin{aligned}\Delta T &= \left(1 - \sqrt{\frac{1 - \sin^2 u_{tilt}}{n^2 - \sin^2 u_{tilt}}}\right) t \sin u_{tilt} \\ &= \left[1 - \sqrt{\frac{1 - \sin^2(20\ \mathrm{deg})}{1.5^2 - \sin^2(20\ \mathrm{deg})}}\right] \times 20 \times [\sin(20\ \mathrm{deg})] \\ &= 2.439\ \mathrm{mm}.\end{aligned}$$

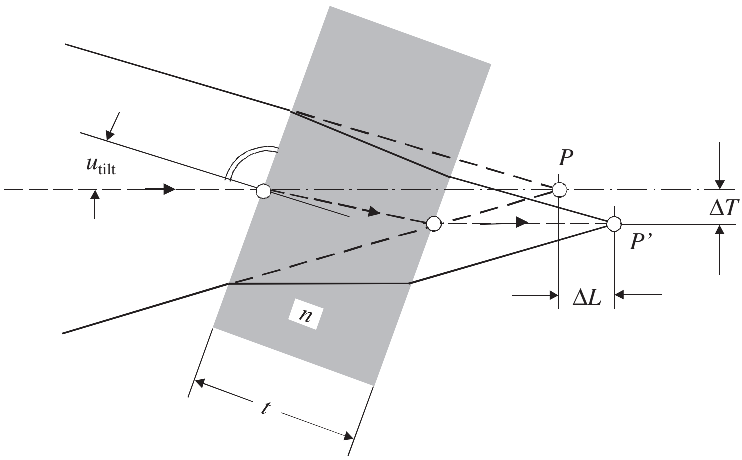

Figure 2.13 Added displacement ΔT.

2.9.3 Prisms acting as plane parallel plates

In many familiar cases, prisms act as plane parallel plates in an optical train. This is indicated in Figs. 2.14 and 2.15.

It is therefore important to remember that prisms displace the image according to Eqs. (2.17) and (2.18).

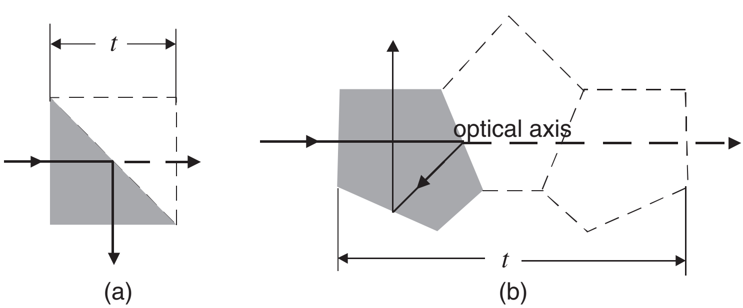

Figure 2.14 (a) Right-angle prism and (b) penta-prism act as plane parallel plates, perpendicular to the optical axis.

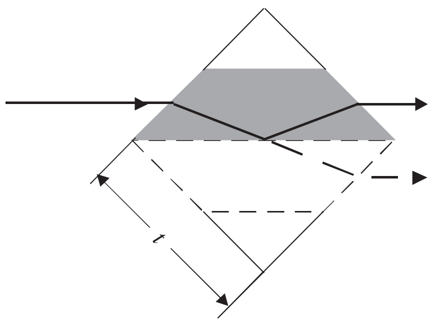

Figure 2.15 Dove prism compared to a tilted plane parallel plate.

2.9.4 Prism and dispersion

Dispersion is the separation of white light into a color spectrum. It is the process that is responsible for chromatic aberrations, which will be discussed in Chapter 4. Dispersion is caused by the variation of the index of refraction with the wavelength of light. The index for blue light is higher than that for red light. Therefore, according to Snell's law, the blue light is bent more than the red light as it travels through a prism. This is indicated schematically in Fig. 2.16.

The fact that white light is a combination of different colors was discovered by the great British scientist Isaac

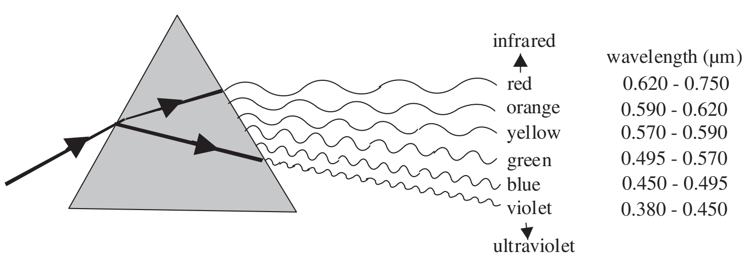

Figure 2.16 Separation of white light into color bands.

Newton (1642 to 1726). He was the one who applied a prism to prove this fact. He went even farther and applied a second prism to demonstrate that the colors could not be further split.

The principal dispersion for the visible spectrum is defined by the difference of the indices for the F and C Fraunhofer lines of a particular glass, $n_F - n_C$.

2.9.5 Abbe number

Ernest Abbe, a German scientist and social reformer, found it helpful in his optical calculations to state dispersion as

$$\nu = \frac{n_d - 1}{n_F - n_C}. \tag{2.19}$$

This expression is termed the *reciprocal relative dispersion*, better known as the *Abbe number*.

Figure 2.17 shows that relation for a typical glass used in the visible spectrum.

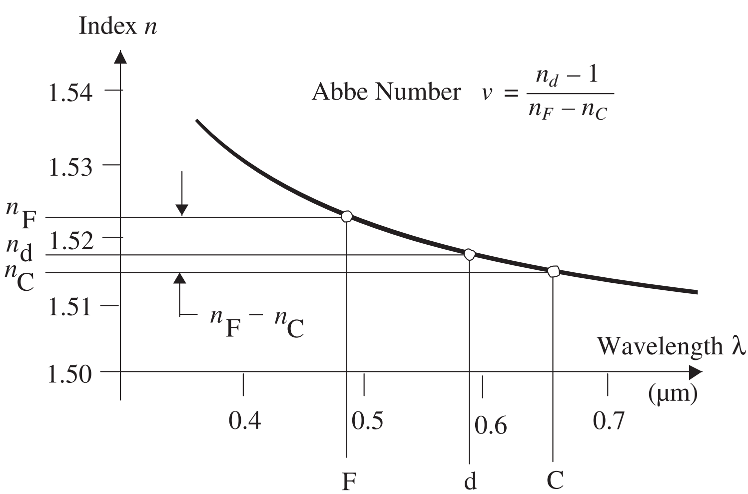

Figure 2.17 Principal dispersion and Abbe number for BK7. Image adapted from *Optical Glass* (P. Hartman, SPIE Press 2014).

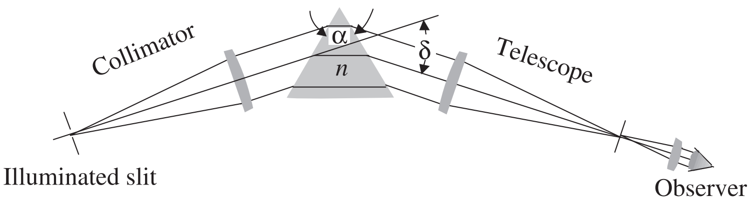

Figure 2.18 Schematic arrangement of prism spectrometer with the special case of a symmetric pass through a prism with a 60-deg apex angle.

The subject will be revisited in Chapter 4, when the chromatic aberration of lenses will be covered.

2.9.6 Prism spectrometer

The symmetric arrangement shown in Fig. 2.18, where the rays inside the prism pass parallel to the prism's base, is the setup where the minimum deviation occurs. The minimum deviation is applied to determine the index of refraction of an optically transmitting substrate. The relation between the index of refraction n, the deviation angle δ, and the apex mirror α of the prism is

$$n = \frac{\sin\left[\frac{\alpha+\delta}{2}\right]}{\sin\left[\frac{\alpha}{2}\right]}. \tag{2.20}$$

If the apex angel α of the prism is chosen to be 60 deg, then Eq. (2.20) converts to $n = \{\sin[0.5(60+\delta)]\}/(\sin 30)$. This reduces to

$$n = 2\sin(30 + 0.5\delta). \tag{2.21}$$

Example

The deviation angle δ was measured to be exactly 37 deg for a chosen wavelength when analyzing a prism with the aforementioned setup. Find the index of refraction of the prism material.

Solution

Applying Eq. (2.21) yields

$$n_\lambda = 2\sin(30 + 0.5 \times 37) = 2\sin 48.5 = 2 \times 0.748956$$
$$= 1.497911.$$

2.9.7 Thin prism

When two flat surfaces of a substrate are not quite parallel, they form a wedge, which is called a thin prism. If the wedge angle is small, the deviation angle of a perpendicularly entering ray after passing through the element is

$$\delta = \alpha(n - 1). \tag{2.22}$$

Figure 2.22 shows the relations.

At a deviation angle $\delta = 17.5$ deg, the result obtained with Eq. (2.22) is within 1% of the accurate value found using Eq. (2.20) for a prism with an index of refraction $n = 1.5$.

2.9.8 Lens centering error

The lens diameter is usually ground to size after the surfaces have been polished. Depending on the mounting technique used for this process, in general there remains an offset

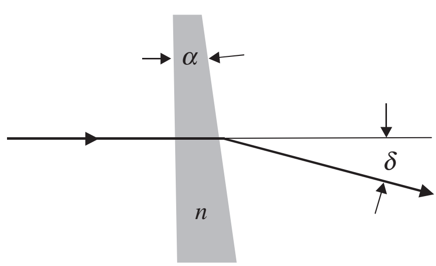

Figure 2.19 Ray deviation after passing through a thin prism (wedge).

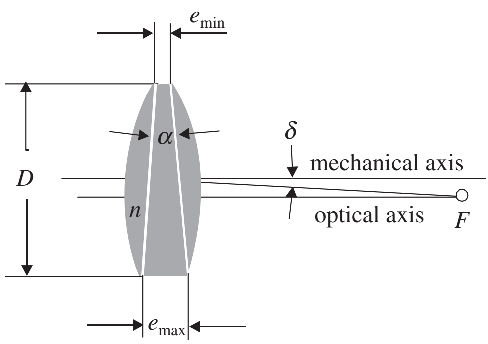

Figure 2.20 Decentered lens.

between the mechanical and optical axis. This undesired result can be interpreted as having a thin prism inserted in an otherwise perfect lens, as indicated in Fig. 2.20.

The wedge angle $\alpha = (e_{max} - e_{min})/D = (\Delta e)/D$, and the deviation angle $\delta = (n-1)\alpha = [(n-1)\Delta e]/D$. One can easily see that such a situation creates a problem in aiming at a target. This error is therefore termed the *Bore-sight error*.

2.9.9 One-diopter prism

By definition, a "one-diopter" prism is one that produces a deviation angle of 0.01 rad. This means that a ray is displaced by 1 cm at a 1-m distance (see Fig. 2.21).

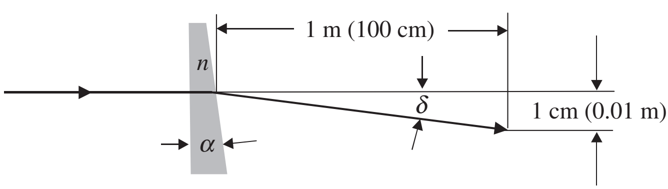

Figure 2.21 Power of a prism measured in diopters.

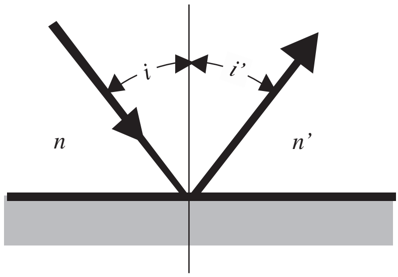

Figure 2.22 Snell's law applied to a flat mirror.

2.10 Snell's Law for a Mirror

Figure 2.22 shows how an impinging ray is reflected by a flat mirror.

With reference to the surface normal, the entrance and exit angles are equal, but of course in opposite directions. Assuming that the mirror is surrounded by air, for which the index of refraction n is 1, Snell's law can be applied if the index after reflection n' is set to -1. With that, the general form $n' \sin i' = n \sin i$ changes for the mirror to $\sin i' = -\sin i$. This means, of course, that $i' = -i$, as stated previously.

2.11 Spherical Mirrors

Spherical mirrors are also image-forming optical elements, just like lenses. The advantage of a mirror is that it responds equally to all wavelengths in the optical spectrum. This is of great importance in several ways.

A reflective optical system, such as a telescope, for example, used in the infrared spectrum can be aligned in the visible spectral band because there is no focus shift. Mirrors can also be made much larger than lenses. The primary mirror of the famous Hubble telescope, for example, measures 2.4 m in diameter.

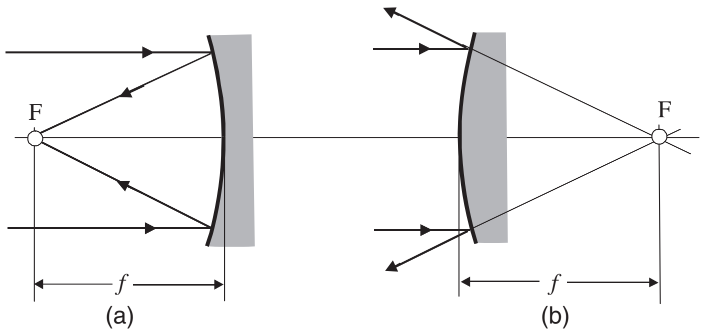

Figure 2.23 (a) Converging (positive focal length) and (b) diverging (negative focal length) spherical mirrors.

Because there is only one surface, the expression for the focal length is very simple. It is half of the surface radius. To take the reversal of an incoming ray into consideration, reflective surfaces are treated in the ray-tracing equations as elements having an index of refraction of -1, as stated previously. This changes the sign for the distances in the longitudinal direction. The focal length is

$$f = -\frac{R}{2}. \tag{2.23}$$

2.11.1 Imaging with a concave mirror

Figure 2.24 shows how an image is formed with a concave mirror.

Exercise

A 20-mm-high object is located 100 mm to the left of the mirror. The concave mirror has a surface radius of -60 mm. Determine the focal length, the image size, and its location.

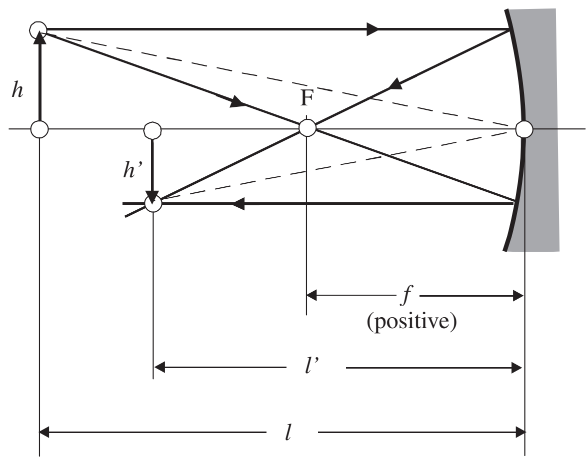

Figure 2.24 Object–image relations for a concave mirror. Dotted ray can also be used to determine the image height.

Approach and Solution

The focal length is, according to Eq. (2.23), $f = -R/2 = -(-60/2) = 30$ mm. The Gauss equation [Eq. (2.11)] can also be used for imaging with a mirror if the change in direction of the reflected ray is recognized. Therefore,

$$l' = -\frac{lf}{l+f} = -\frac{-100 \times 30}{-100 + 30} = -\frac{-3{,}000}{-70} = -42.857 \text{ mm}.$$

With the same stipulation, according to Eq. (2.3), the magnification is $m = -\frac{l'}{l} = -\frac{-42.857}{-100} = -0.42857$.

The image height is then $h' = mh = -0.42857 \times 20 = -8.571$ mm.

2.11.2 Imaging with a convex mirror

Figure 2.25 shows the arrangement for a convex mirror. Because in this case the surface radius is positive, the focal length becomes negative [see Eq. (2.23)].

To extend the aforementioned exercise, we replace the concave mirror with a convex mirror with the same nominal radius, just opposite in sign. This results in the focal length $f = -R/2 = -60/2 = -30$ mm. The image distance $l' = (lf)/(l+f) = [-100 \cdot (-30)]/(-100 - 30) = 3{,}000/(-130) = -23.077$ mm, and the magnification $m = l'/l = (-23.077)/(-100) \cong 0.231$.

Finally, the image height $h' = mh = 0.231 \times 20 = 4.62$ mm.

Such convex mirrors also find use in automobiles as outside rear-view mirrors, sometimes with the warning, “Objects in the mirror are closer than they appear.” This refers to the magnification, which is reduced to increase the field of view.

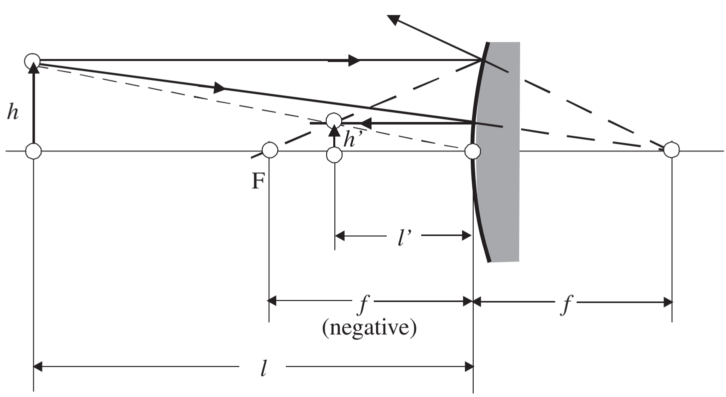

Figure 2.25 Object–image relations for a convex mirror. Fine dotted ray can also be used to determine the image height.

Chapter 3
"Thin Lens" Concept

3.1 Postulation

Proposing the idea of a lens with zero thickness appears at first glance to be somewhat unrealistic. However, as will be seen, this idea simplifies a great deal with respect to addressing the behavior of lenses.

3.2 Change and Its Impact

The equation for the reciprocal focal length, the power of a thick lens, was given in Chapter 2 as [Eq. (2.1)]

$$\phi = \frac{1}{f} = (n-1)\left[\frac{1}{R_1} - \frac{1}{R_2} + \frac{(n-1)t}{nR_1R_2}\right].$$

By eliminating the thickness t, this equation changes to

$$\phi = \frac{1}{f} = (n-1)\left[\frac{1}{R_1} - \frac{1}{R_2}\right] \tag{3.1}$$

Defining the reciprocal of a lens radius R as the surface curvature c leads to the expression

$$\phi = \frac{1}{f} = (n-1)(c_1 - c_2). \tag{3.2}$$

Let us investigate the impact on the focal length by neglecting the lens thickness. With Eq. (2.1), we find the power of a lens produced from BK7, and with an index of refraction of 1.5185, a front radius of 80 mm, a rear radius of −144.2264 mm, and a thickness of 5 mm, to be

$$\phi = \frac{1}{f} = (1.5185 - 1)\left[\frac{1}{80} - \frac{1}{-144.2264} + \frac{(1.5185 - 1) \times 5}{1.5185 \times 80 \times (-144.2264)}\right] = 0.01\ \mathrm{mm}^{-1}$$

The focal length is therefore $f = 1/\phi = 1/0.01 = 100$ mm.

The thin lens power determined according to Eq. (3.1) is

$$\phi = \frac{1}{f} = (n - 1)\left[\frac{1}{R_1} - \frac{1}{R_2}\right]$$
$$= (1.5185 - 1)\left[\frac{1}{80} - \frac{1}{(-144.2264)}\right] = 0.0100763\ \mathrm{mm}^{-1}$$

The focal length $f = 1/\phi = 1/0.0100763 = 99.243$ mm. This is a deviation of less than 1%.

This deviation is due to the fact that the thickness (5 mm in this case) is usually much smaller than the product of the two radii in the denominator.

3.3 Simplified Image Formation

Using the concept of thin lenses in the paraxial domain, further simplifications are provided for the image-forming relations (as indicated in Fig. 3.1).

The sign of the angle for a ray aiming up, away from the optical axis, is positive. The sign of the angle for a ray aiming down is negative. Therefore, u is positive. Terms u', u_p, and u_p' are negative. It is customary to use plain letters for

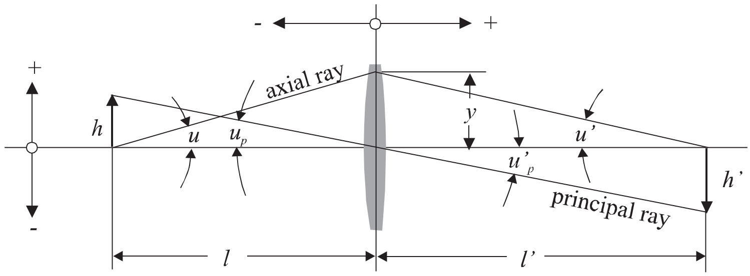

Figure 3.1 Basic relations and sign convention for a thin lens in the paraxial region.

identification in the object space and primed letters in the image space. Remember the traditional agreement that light approaches an optical system from the left, if not otherwise specified.

From Fig. 3.1, one can derive an additional relation for the magnification. Using $u = y/l$ and $u' = y/l'$, we form the fraction

$$\frac{u}{u'} = \frac{y}{l} \cdot \frac{l'}{y} = \frac{l'}{l} = m = \frac{h'}{h}. \tag{3.3}$$

The *principal ray* is the ray that travels from the edge of the object through the center of the lens, and is also called the *chief ray* if the free lens diameter limits the entering light bundle. In that case, the free lens diameter $D = 2y$ is the aperture stop diameter of the system, because there is no separate stop present. A ray aiming for the edge of the aperture stop is termed a *marginal ray*. Therefore, the *axial ray* shown in Fig. 3.1 is termed the *axial marginal ray*, because it enters the lens at the free lens diameter, which is the aperture stop.

Figure 3.2 shows the situation in which the light source is located at infinity ($u = 0$). This special case is used to identify particular relations.

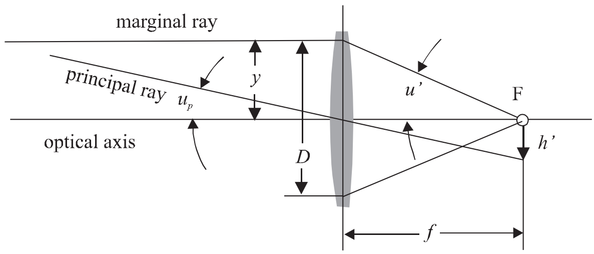

Figure 3.2 Relations for the case when the object is located at infinity.

In this situation, the image is formed in the focal plane.

The expression $n' \sin u'$ is termed the *numerical aperture* (NA). This term is primarily used for microscope objectives when the object to be viewed is immersed in a liquid, with an index n', to increase the magnification. For other applications, when the object is located at infinity, the ratio between the focal length aperture diameter f/D is termed the *relative aperture* or *F-number*, written $f/\#$. The relation between the relative aperture and numerical aperture is

$$(f/\#) = \frac{1}{2NA}. \tag{3.4}$$

For the case where the image is not formed in the focal plane, the ratio between the image distance and the aperture diameter is termed the *working relative aperture*, or *working F-number*. For a thin lens

$$(f/\#)_{working} = \frac{l'}{D}. \tag{3.5}$$

The general expression is

$$(f/\#)_{working} = \frac{1}{2u'} \tag{3.6}$$

where u' is the slope of the exiting marginal ray.

3.4 Quick Reference for Image Location and Orientation

As indicated in Fig. 3.1, an upside-down image is formed by a positive lens of an object located at a distance l to the left of the lens. This image can be projected onto a screen located a distance l' to the right of the lens. When l is shorter than the focal length f, the situation changes dramatically. The image becomes virtual, which means that it cannot be projected onto a screen. Its location is at the same side as the object, to the left of the lens. It is right-side up and can be visualized. This is the application of a positive lens as a magnifier, also termed a loupe.

An object located at the front focal point is imaged at infinity. This is the principle of a collimator, the purpose of which is to bring an object located at infinity into the laboratory. For testing infrared systems, the object is frequently simply a tiny pinhole aperture irradiated by a blackbody radiation source.

Figure 3.3 presents an overview of these relations, and can be used to quickly assess specific situations.

Examples

1. If an object is located -60 units, such as millimeters, centimeters, or inches, in front of the lens, which has a focal length of 20 units, we find that a real image is formed at 30 units to the right of the element. We simply draw a line through the respective values at the l and f scales and extend it until it crosses the l' axis.
2. By moving the object inside the front focal point to $l = -10$, the image is formed also to the left of the lens, at $l' = -20$, in the virtual image domain.

According to Eq. (3.3), the magnification for the first example is $m = l'/l = 30/-60 = -0.5$, and for the second example, it is $m = -20/-10 = +2$.

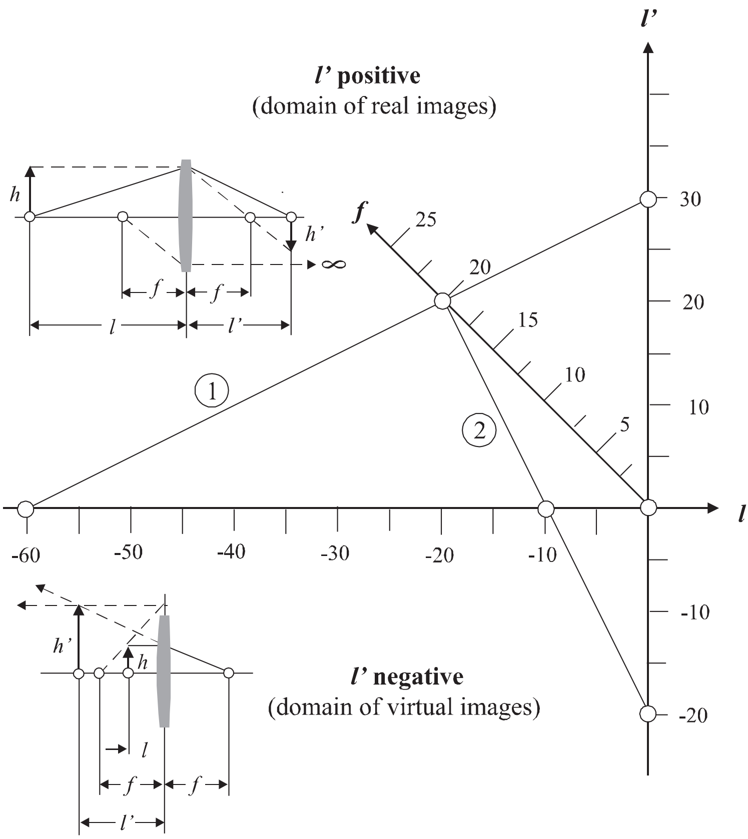

Figure 3.3 Quick reference for image location and orientation.

3.5 Lens Bending

Closely evaluating Eq. (3.2) discloses a very interesting fact. It is the *difference* in the curvatures that matters for determining the focal length of a lens. Table 3.1 contains a number of selected curvature differences, which have been chosen for a lens in which the index of refraction is 1.5

Table 3.1 Bending of a glass lens ($n = 1.5$), maintaining a focal length of 100 mm.

Radius R_1	Radius R_2	Curvature c_1	Curvature c_2	Lens shape
−50	−25	−0.02	−0.04	
plano	−50	0	−0.02	
100	−100	0.01	−0.01	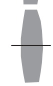
50	plano	0.02	0	
25	50	0.04	0.02	

(glass). The focal length is 100 mm. The power is therefore $1/100 = 0.01\ \text{mm}^{-1}$.

Using the chosen parameters, Eq. (3.2) leads to $c_1 - c_2 = \phi/(n-1) = 0.01/(1.5-1) = 0.02$ to $c_2 = c_1 - 0.02$.

Table 3.1 contains a selection of constant curvature differences for this 100-mm lens with an indication of how the shape of the lens changes. This by itself may not sound to be of much importance, except in terms of choosing different curvatures, but maintaining the difference between the two curvatures changes the shape of the lens, which in turn impacts the spherical aberration, which is one of the most severe primary aberrations.

This will be discussed in Chapter 4.

Chapter 4
Primary Aberrations

4.1 Introduction

In previous Chapters, comments were made about imaging aberrations. This means that a lens has shortcomings with respect to imaging a point as one without degradation. This degradation is due to aberrations defined as

1. Spherical aberration.
2. Axial chromatic aberration.
3. Coma.
4. Astigmatism.
5. Field curvature (Petzval curvature).
6. Distortion.
7. Lateral color.

When determining aberration size, we will refer only to expressions which relate to the so-called *thin lens third-order aberration theory*.

This theory is based on truncation of a sine series to the third order to simplify the calculations.

The full series is expressed by

$$\sin x = x - \frac{x^3}{1 \times 2 \times 3} + \frac{x^5}{1 \times 2 \times 3 \times 4 \times 5} - \frac{x^7}{1 \times 2 \times 3 \times 4 \times 5 \times 6 \times 7} + \cdots\cdots .$$

As the name implies, only the first two terms of this series are considered in this aberration theory.

Let us demonstrate this theory with an angle of 30 deg; recall that $\sin(30 \text{ deg}) = 0.5$.

Thirty degrees expressed in radians is $\pi/6$. Taking the sine,

$$\sin\left(\frac{\pi}{6}\right) = \frac{\pi}{6} - \frac{1}{6}\left(\frac{\pi}{6}\right)^3 = 0.523599 - \frac{0.143548}{6} = 0.523599 - 0.023925 = 0.499674.$$

The error in this value is within 0.065%.

This scheme was first applied by the German scientist *Philipp Ludwig von Seidel* (1821 to 1896). This is why the third-order aberration theory is also termed the Seidel aberration theory.

Details of this theory will not be discussed here, but the results of the on-axis image degradations, the *spherical* and *axial chromatic aberrations*, will be treated with examples for a single thin lens and a spherical concave mirror for the case when the object is located at infinity.

Readers who are inclined to learn more about the *thin lens third-order aberration theory* may consult the book by Smith, W. J., *Modern Optical Engineering*, 4th Ed, McGraw–Hill, New York, 2008, or Wellford, W. T., *Aberrations of Optical Systems*, J. W. Arrowsmith Ltd., Bristol, 1986.

As a general remark, aberrations are measured as deviations from the ideal, the paraxial image location. The

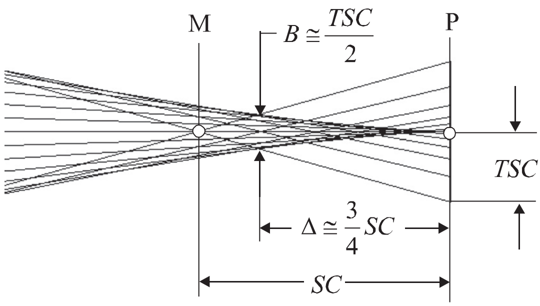

Figure 4.1 Spherical aberration is the variation in focus in accordance with the size of the aperture.

other deviations, the so-called *off-axis aberrations*, including the *field curvature*, named after the Hungarian mathematician *Josef Max Petzval*, will be presented only graphically for identification and recognition.

4.2 Thin Lens, Object at Infinity, On-Axis Aberrations

4.2.1 Spherical aberration

Because rays closer to the edge of a positive lens with spherical surfaces are bent more than rays closer to the optical axis, the result is that an object point is imaged as a circular blur (illustrated in Fig. 4.1).

Figure 4.1 shows ray traces for an $f/2$ glass lens with a 100-mm focal length. The object is located at infinity. Figure 4.1 indicates the location of the marginal image point M and paraxial image plane P, which in this case is also the paraxial focal plane. Figure 4.1 shows that the minimum blur spot size B is approximately half the size of the transverse spherical aberration TSC. This minimum blur spot is also termed the *circle of least confusion* and lies approximately

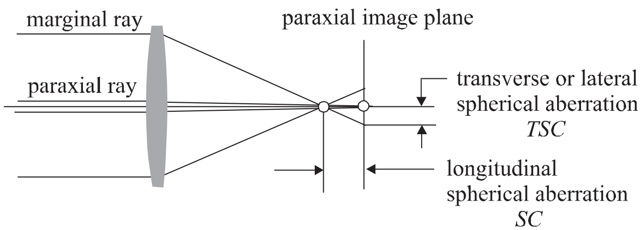

Figure 4.2 Identifications and relations.

three-quarters of the measure of the *longitudinal spherical aberration SC* to the left of the paraxial image plane. The minimum blur spot is the amount of refocusing required to obtain the best possible image of an object point. These definitions refer to the thin lens third-order theory. The traces are of a thick lens, created with a computer program, applying the unabridged geometric sine function for the calculation. This is done to offer some confidence in the use of the thin-lens third-order approximation. Frequently, especially in the field of infrared optics, the blur spot size is reported as an angular measure, commonly in milliradians. This means that the linear size is divided by the image distance from the lens, which is the focal length if the object is located at infinity.

When the marginal ray crosses the optical axis ahead of the paraxial image plane, as shown in Fig. 4.2, the lens is considered to be undercorrected. Spherical aberration is negative.

At the end of Chapter 3 it was noted that spherical aberration varies with the shape of the lens. In 1772, the Swiss mathematician Leonhard Euler* developed an expression for

*Leonhard Euler was born 1707 in Basel, Switzerland, and he was the most prolific writer of all time. His complete works contains 886 books and papers. Amazingly, after 1765, when Euler was 58, he produced almost half of his works, despite being completely blind.

the optimal shape of a thin lens resulting in the minimum remaining spherical aberration.

The two radii are

$$\text{front radius } R_1 = \frac{2(n+2)(n-1)}{n(2n+1)} f, \tag{4.1}$$

$$\text{rear radius } R_2 = \frac{2(n+2)(n-1)}{n(2n-1)-4} f. \tag{4.2}$$

These are the radii for a lens, when the object is located at infinity, which means that the rays entering the lens are parallel to the optical axis, as shown in Fig. 4.2. The best shape for the 100-mm focal length glass lens with an index of 1.5 is therefore

$$\begin{aligned} R_1 &= \frac{2(n+2)(n-1)}{n(2n+1)} f = \frac{2(1.5+2)(1.5-1)}{1.5(2\times 1.5+1)} \cdot 100 \\ &= 58.333 \text{ mm}, \\ R_2 &= \frac{2(n+2)(n-1)}{n(2n-1)-4} f = \frac{2(1.5+2)(1.5-1)}{1.5(2\times 1.5-1)-4} \cdot 100 \\ &= -350 \text{ mm}. \end{aligned}$$

The expression for the minimum blur spot diameter, caused by spherical aberration for such an optimally shaped lens, is

$$B_{sphere} = \frac{n(4n-1)f}{128(n-1)^2(n+2)(f/\#)^3}. \tag{4.3}$$

For our 100-mm lens with a relative aperture $f/\# = 2$, the minimum blur spot diameter is therefore

$$B_{sphere} = \frac{1.5(4\times 1.5-1)\cdot 100}{128(1.5-1)^2(1.5+2)(2)^3} = 0.84 \text{ mm}.$$

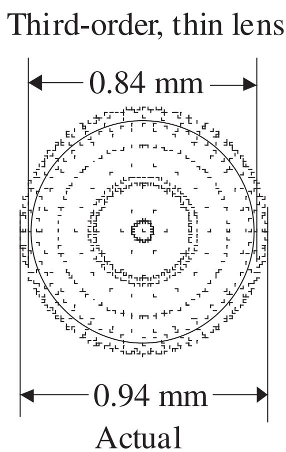

Figure 4.3 Comparison between actual blur spot size and the result based on third-order, thin lens calculations.

The angular dimension of β_{sphere} is $B_{sphere}/f = 0.84/100 = 8.4$ mrad.

Figure 4.3 compares the two blur spot sizes, obtained with real ray traces and the thin lens third-order aberration equation. The fit is even closer with "slower" systems, which are systems with a larger F-number.

There are two interesting facts underpinned by Eqs. (4.1) and (4.2). The index of refraction n of germanium, a lens material, which is mainly used in the longwave infrared spectrum region, is 4. Inserting this value into Eqs. (4.1) and (4.2) shows that for the best shape, $R_1 = f$, and $R_2 = 1.5f$, a relation that is easy to remember. The other fact can be deduced from the denominator of Eq. (4.2). For the second surface to be flat, $n(2n - 1) - 4$ must be zero. This is the case for $n = 1.686$. The index of refraction for sapphire, a material used in the mid-infrared region, is close to this value; the glasses SF5 and LAKN13 fit this criterion in the visible spectral range.

4.2.2 Axial chromatic aberration

If an optical system is used over a spectral range, which is usually the case with the exception of laser applications, chromatic aberrations are present. Figure 4.4 demonstrates the fact that the foci for different wavelengths have different positions along the optical axis. Figure 4.5 illustrates the result from a different angle.

This is due to the fact that the index of refraction varies with wavelength. Therefore, according to Snell's law [Eq. (1.2)], rays representing different wavelengths exit a lens at different angles.

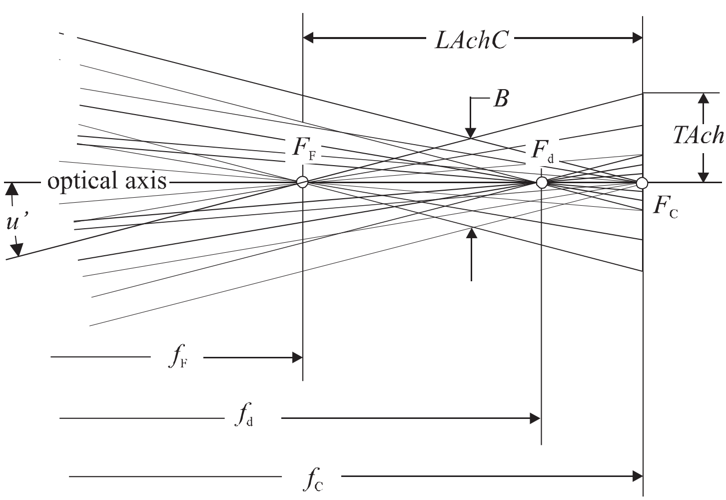

Figure 4.4 Focus shift for different wavelengths. The circle of least confusion, the smallest blur spot, is located approximately halfway between the foci F_F and F_C.

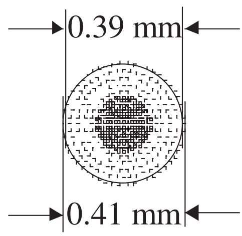

Figure 4.5 Comparison between the actual chromatic blur spot size and the result obtained with the first-order, thin lens equation. Q7

Table 4.1 Index of refraction for BK7 at different wavelengths.

Fraunhofer line	d	F	C
Wavelength λ (μm)	0.5876	0.4861	0.6563
Index of refraction n	1.51680	1.52238	1.51432

As stated in Chapter 1, in the visible spectrum, it is common to select a wavelength spread from 0.48613 through 0.65628 μm. These wavelengths identify, respectively, the Fraunhofer lines F and C. The center of the band serves the d-line; the wavelength is 0.55756 μm. One of the glasses most commonly used in the visible spectrum is BK7, which has the characteristics shown in Table 4.1; see also Fig. 2.18 in Chapter 2.

As previously mentioned in Chapter 2, an additional value given for a glass is the Abbe number*

$$\nu = \frac{n_d - 1}{n_F - n_C}. \tag{4.4}$$

**Ernst Abbe* was born in northern Germany in 1840 and lived there until 1905. He is known for his lifelong association with *Zeiss*, the world-renowned optical company. Zeiss became famous through Abbe's contributions.

For BK7 glass,

$$\nu = \frac{n_d - 1}{n_F - n_C} = \frac{1.51680 - 1}{1.52238 - 1.51432} = 64.12.$$

This repetition was necessary for the manner in which chromatic aberration is expressed. The *longitudinal chromatic aberration contribution* is

$$LAchC = \frac{f_d}{\nu}. \tag{4.5}$$

The *transverse axial contribution* is

$$TAchC = LAchCu' = \frac{f_d}{2\nu(f/\#)}. \tag{4.6}$$

Both quantities are identified in Fig. 4.4. Figure 4.4 shows that the transverse axial contribution is also the approximate blur spot size. Therefore, for an object at infinity,

$$B_{chrom} = \frac{f_d}{2\nu(f/\#)}. \tag{4.7}$$

Expressed as an angular measure,

$$\beta_{chrom} = \frac{B_{chrom}}{f_d} = \frac{1}{2\nu(f/\#)}. \tag{4.8}$$

For the 100-mm focal length $f/2$ lens, produced from BK7, the chromatic blur spot is therefore

$$B_{chrom} = \frac{f_d}{2\nu(f/\#)} = \frac{100}{2 \cdot 64.12 \cdot 2} \cong 0.39 \text{ mm}.$$

We compare again the results obtained with this simple equation via real computer ray traces and observe the excellent match.

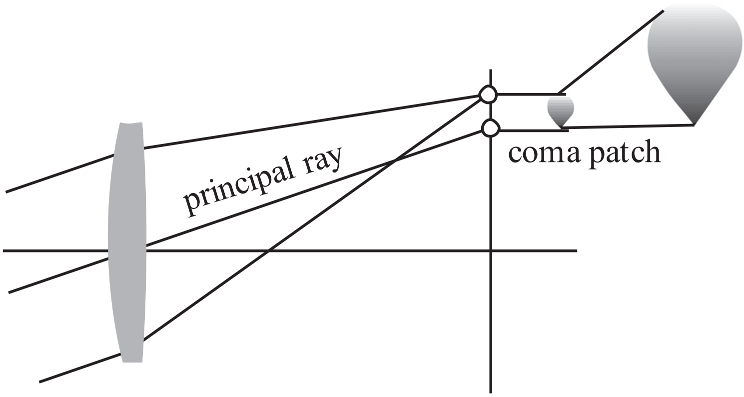

Figure 4.6 Coma is caused by the rays through the edge of the lens focusing at a different height than the principal ray.

4.3 Thin Lens Off-Axis Aberrations

4.3.1 Coma

The blur spot shape resembles the form of a comet, as can be seen in the enlargement (see Fig. 4.6), which lead to this aberration's name.

4.3.2 Astigmatism

Stigmatic means coming together to a point. Therefore, when light rays do not come together to a point, there is astigmatism. This is the name given to the situation that exists when a lens forms separated image lines, as shown in Fig. 4.7.

4.3.3 Field curvature (Petzval curvature)

It is not surprising that for a positive lens the field is inwardly curved, because the distance to an image plane is shorter on the optical axis than away from the optical axis (see Fig. 4.8).

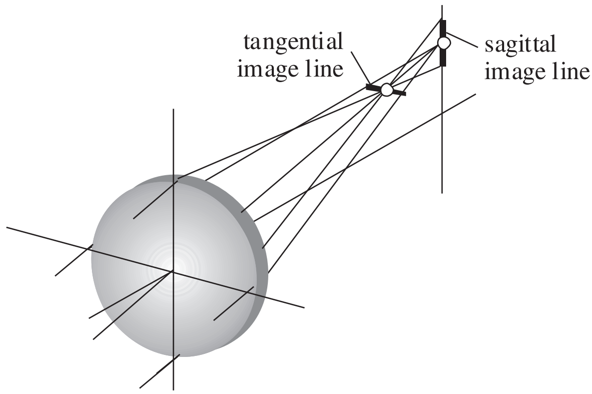

Figure 4.7 Astigmatism.

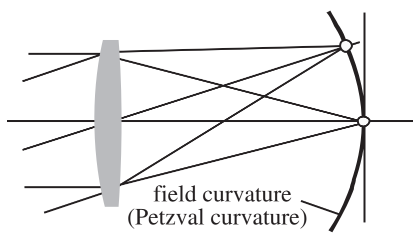

Figure 4.8 Field curvature, i.e., Petzval curvature, when no astigmatism is present.

4.3.4 Distortion

Whereas distortion does not feature image degradation, there is a change of magnification across the field. Depending on the lens design, it can be pincushion-shaped, as shown in Fig. 4.9. In this case, the distortion is considered to be positive. The negative type, i.e., the barrel-shaped distortion, has been added in Fig. 4.9 as a white outline.

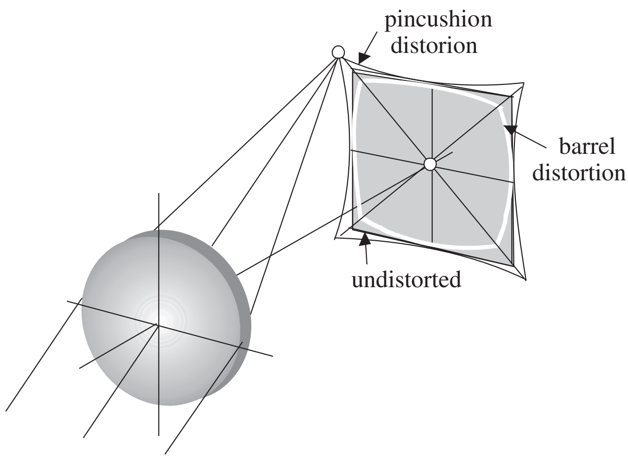

Figure 4.9 Distortion, a change in magnification across the field.

4.3.5 Lateral color, also termed lateral chromatic aberration

Lateral color is attributable to the fact that the index of refraction for long wavelengths is higher than for short wavelengths (Table 4.1). This causes different bending angles according to Snell's law, producing a lateral spread in the image plane (indicated in Fig. 4.10).

4.4 Spherical Convex Mirror, Object at Infinity

As mentioned previously, mirrors reflect equally at all wavelengths, which means that mirrors do not introduce chromatic aberrations. Therefore, there is only one axial aberration, the spherical aberration (illustrated in Fig. 4.11).

The linear third-order blur spot size is

$$B_{sphere} = \frac{f}{128(f/\#)^3}. \tag{4.9}$$

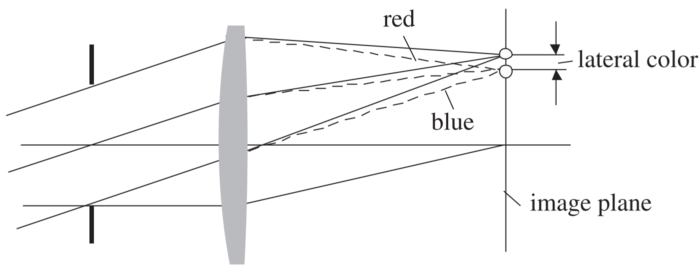

Figure 4.10 Lateral color, the magnification difference according to color.

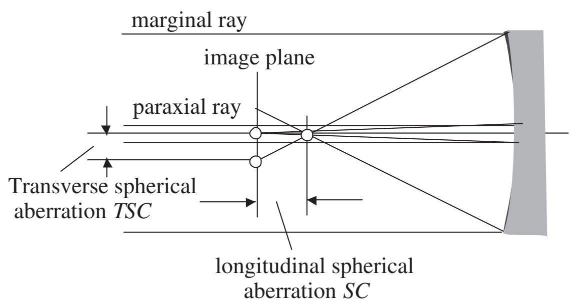

Figure 4.11 Spherical aberration at a concave spherical mirror.

The angular third-order blur spot size is

$$\beta_{sphere} = \frac{1}{128(f/\#)^3}. \tag{4.10}$$

We examine a spherical mirror with the same focal length $f = 100$ mm, as for the lens previously discussed. The diameter $D = 50$ mm; therefore, the relative aperture $f/\# = f/D = 100/50 = 2$. Using Eq. (4.9), we find the blur spot sizes of $B_{sphere} = 0.098 \cong 0.1$ mm.

Equation (4.10) states that

$$\beta_{sphere} = \frac{1}{128(f/\#)^3} = \frac{1}{128 \times 2^3} = \frac{1}{128 \times 8} \cong 1 \text{ mrad}.$$

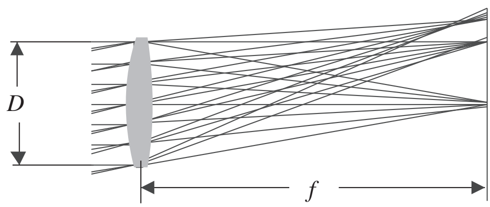

Figure 4.12 On- and off-axis ray bundle patterns through a single element.

Comment

Recognize that the blur spot size due to spherical aberration is approximately 8× smaller for a spherical mirror than for an optimally shaped lens fabricated from BK7 with the same focal length and relative aperture. Furthermore, as mentioned previously, the mirror is free from chromatic aberration.

Of course, a mirror has off-axis aberrations, which deviate somewhat from those of a lens.

4.5 Assessment

Whereas aberrations were identified and presented individually, they are always present simultaneously and overlap. It is the task of the lens designer to apply methods to minimize these image-impairing effects. Of course, one must keep the application in mind. A camera objective requires much more attention than, for example, a light source system. The performance of a 100-mm focal length system with an $f/3$ relative aperture and a total angular field coverage of 28 deg is illustrated in Figs. 4.12 and 4.13. Figure 4.12 gives an indication of how much the individual rays deviate from the desired point image.

The position of the image plane has been optimized in both cases to balance the blur spot sizes across the field.

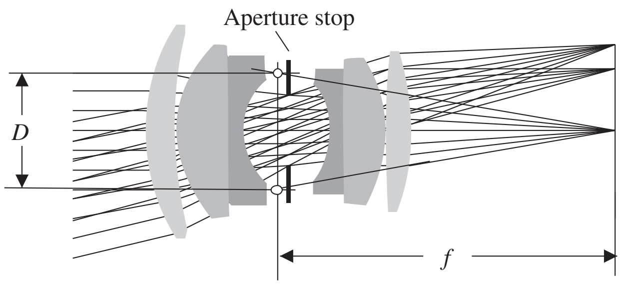

Figure 4.13 Double-Gauss camera objective.

To improve the performance such that the lens is suitable as a camera objective, elements of different shapes and diverse materials must be added. An example of a suitable configuration is shown in Fig. 4.13. It is known as the *double-Gauss* objective.

The ray pattern in this cross section is indicative of focusing improvements. Figure 4.13 also shows an aperture stop, the purpose of which is to control the size of the light beam passing through the system and reduce the aberrations by its location. Chapter 5 discusses the aperture spot's function in more detail.

A comparison of the generated blur spots reveals that the double-Gauss design reduces blur spots by a factor of approximately 40.

Chapter 8 discusses how the performance of a lens is judged in addition to its generated blur spot sizes.

Chapter 5
Stops, Pupils, and Windows

5.1 Aperture Stop

The limiting opening that controls the size of a light bundle passing through an optical system is called the *aperture stop*. The aperture stop is usually round. So far we have assumed that the aperture stop is located at the lens, such that the free lens diameter is the stop. Off-axis aberrations are influenced if a separate stop is inserted at a specific place along the optical axis. This fact is applied to minimize such aberrations.

5.2 Field Stop

As the name implies, the field stop controls the size of the field. In the case of a camera, the field stop can be the film mask itself or the sensor array. In microscopes and other viewing devices, the field stop is a separate element.

5.3 Pupils and Windows

There are *entrance and exit pupils* and *entrance and exit windows*. The pupils are images of the aperture stop. The image of the aperture stop in the object space is the entrance pupil. The image of the aperture stop in the image space is the exit pupil. The entrance window and the exit window are, respectively, the images of the field stop in the object space and image spaces (the object space is to the left of the first lens; the image space is to the right of the last lens).

All of these components are shown and identified in Fig. 5.1. The symbols have the following meanings:

- AS, aperture stop
- EP, entrance pupil, the image of the aperture stop in the object space formed by the front lens
- EP', exit pupil, the image of the of the aperture stop in the image space formed by the rear lens
- FS, field stop
- EW, image of field stop in the object space
- EW', image of field stop in the image space (in the example, there is no separate field stop, as is the case with a camera, where the film frame or the detector array acts as the field stop; the entrance window is in this case located in the object plane).

It can be seen that rays emanating at the object, aiming at the edge of the entrance pupil, are redirected by the front lens to pass through the edge of the aperture stop. Likewise, these rays arriving at the image plane appear to be coming from the edge of the exit pupil. The actual rays have been redirected by the rear lens. The same effect is shown for the axial point.

The layout indicates that the image size is determined by the sensor (film) dimensions. Therefore, the sensor is the field stop and also the exit window. Its image in the object plane is the entrance window.

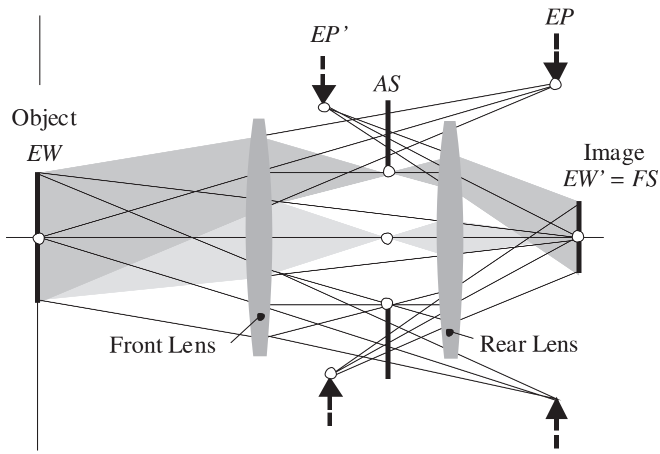

Figure 5.1 Interaction among stops, pupils, and windows.

In the layout shown in Fig. 5.1, the front lens has been placed by its focal lengths to the right of the object. This causes the ray to leave the lens parallel to the optical axis; the result is that the ray crosses the optical axis again at the focal point of the rear lens, which is the image plane.

Exercise

Find the sizes and locations of the entrance and exit pupils and the size of the entrance window of a system with the following attributes:

- focal length of front lens $f_F = 35$ mm
- distance from the front lens to the aperture stop $l_F = 20$ mm
- distance from the aperture stop to the rear lens $l_R = -10$ mm
- focal length of rear lens $f_R = 20$ mm
- aperture stop diameter 20 mm $y_A = 10$ mm
- full field stop size 12 mm $h' = -6$ mm.

Approach and Solution

We determine the locations of the pupils with Eqs. (2.11) and (2.3).

Entrance pupil

Since the aperture stop is located to the right of the front lens to which it must be imaged, the direction of the rays is from the right to the left. Therefore, the easiest approach is to turn the system around for the calculation.

$$l'_{EP} = \frac{l_{EP} f_F}{l_{EP} + f_F} = \frac{-20 \times 35}{-20 + 35} = -46.666667 \text{ mm}$$

Now, we again reverse the direction and note that $l_{EP}{}' = 46.666667$ mm.

The magnification is

$$m_{EP} = \frac{l'_{EP}}{l_{EP}} = \frac{46.666667}{20} = 2.333333 = \frac{EP}{2y_A} = \frac{EP}{2 \times 10} = \frac{EP}{20}.$$

The diameter of the entrance pupil $EP =$ 46.666667 mm (Fig. 5.2).

Exit pupil

We calculate the location of the exit pupil (Fig. 5.3) as $l'_{EP'} = \frac{l_{EP'} f_R}{l_{EP'} + f_R} = \frac{-10 \times 20}{-10 + 20} = 20$ mm.

Its size is $m_{EP'} = \frac{l'_{EP'}}{l_{EP'}} = \frac{20}{20} = 1 = \frac{EP'}{2y_A} = \frac{EP'}{2 \times 10} = \frac{EP'}{20}$.

The diameter of the exit pupil $EP' = 20$ mm.

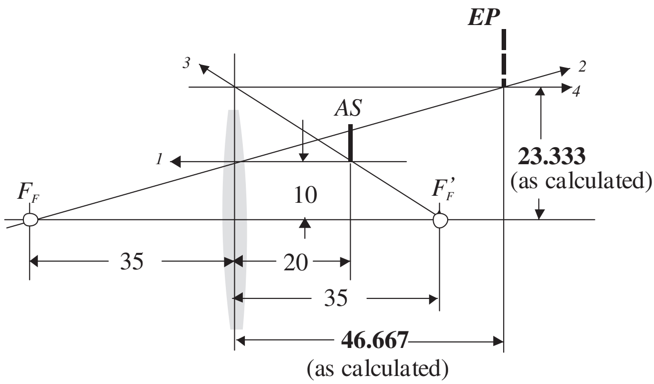

Figure 5.2 Determining graphically the size and location of ***EP***.

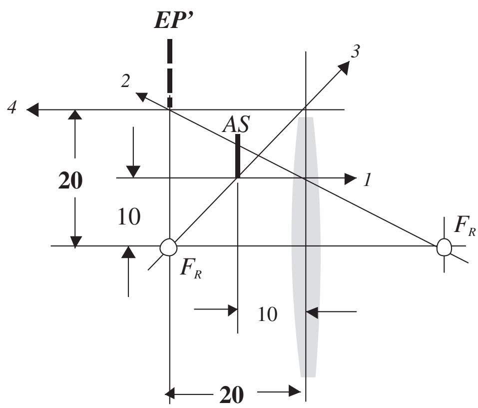

Figure 5.3 Determining graphically the size and location of ***EP***′.

Entrance window

Figure 5.4 identifies h and h' as the half sizes of the entrance and exit windows, respectively.

Figure 5.4 also identifies the slope angles u and u'. Equation (3.3) states that $u/u' = l'/l = m$. In our

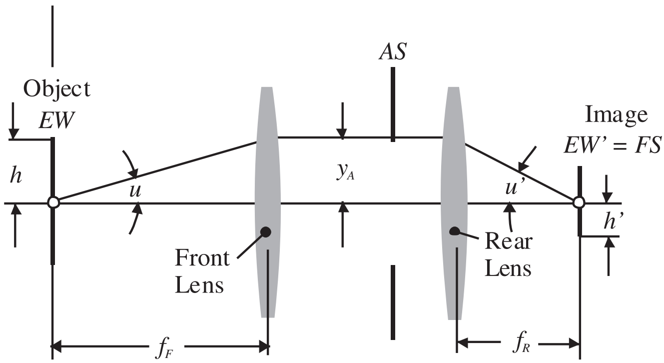

Figure 5.4 Determining the size of *EW*.

example, the object is located at the focal plane of the front lens and the image appears at the focal plane of the rear lens. Therefore, $m = -f_R/f_F = -20/35 = -1/1.75$. Since the magnification is also $m = -h'/h$, $h = h'/m = -1.75 \times 6 = 10.5$ mm. The entrance window EW is therefore 21 mm.

5.4 Function of Pupils and Windows

What is the function of pupils and windows? They control the amount of radiation (light) that passes through the system. Specific sizes and separations are needed to calculate the radiation transfer from the object (target) to the sensor, which can be a detector, a film, or the eye.

The expression

$$\Gamma = \frac{EP \times EW}{s^2} = \frac{EP' \times EW'}{s'^2}, \tag{5.1}$$

is called the *throughput* or *étendue* of the system. It is the product of the pupil area and the solid angle of the field of view.

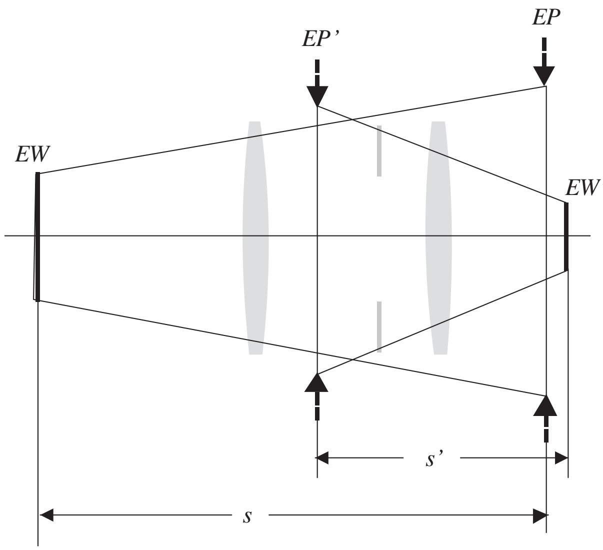

Figure 5.5 Layout for throughput calculations.

We will verify both of the equalities in Eq. 5.1 in our example. We assume that the aperture stop is round and the field stop is square-shaped (shown in Fig. 5.5).

The separations of the pupils and windows are

$$s = f_F + l_{EP} = 35 + 46.666667 = 81.666667 \text{ mm},$$

$$s' = -l'_{EP'} + f_R = 20 + 20 = 40 \text{ mm}.$$

Throughput determined for the entrance pupil

$$\Gamma = \frac{EP \times EW}{s^2} = \frac{D_{EP}^2 \pi 4h^2}{4s^2} = \frac{46.666667^2 \pi \times 4 \times (10.5)^2}{4 \times 81.666667^2}$$
$$= 113.097336.$$

2. Throughput determined for the exit pupil

$$\Gamma = \frac{EP' \times EW'}{s'^2} = \frac{D^2_{EP'}\pi 4h'^2}{4s'^2} = \frac{40^2\pi \times 4 \times 6^2}{4 \times 40^2}$$
$$= 113.097336.$$

The results are in agreement.

Special Case

The fact that either the object or the image side of the system can be used for the calculation is very beneficial when the object is located at infinity. In that case, $s = -\infty$ and the first part of the equation has no solution. The interesting aspect of this special case is $s' = f$, the system's focal length. This fact changes Eq. (5.1) to a simple expression when the aperture stop is round and the field stop is square

$$\Gamma = \frac{EP' \times EW'}{s'^2} = \frac{\pi d^2}{4(f/\#)^2} \tag{5.2}$$

Remark

It is common in photography to control the throughput in discrete steps by a factor of 2. This is achieved by reducing or increasing the relative aperture $f/\#$ by the factor of $\sqrt{2}$. The well-known sequence, derived from Eq. (5.2), is

$$(f/1), (f/1.4), (f/2), (f/2.8), (f/4), (f/5.6), (f/8)\ldots\ldots$$

These F-numbers are controlled with the iris, an adjustable diaphragm that is the aperture stop of the camera.

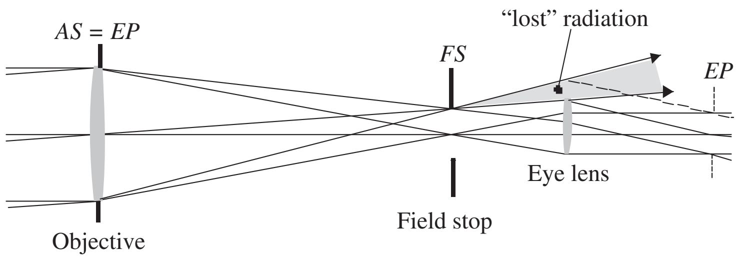

Figure 5.6 Vignetting. Part of the radiation misses the eye lens and causes an energy fall-off at the edge of the field.

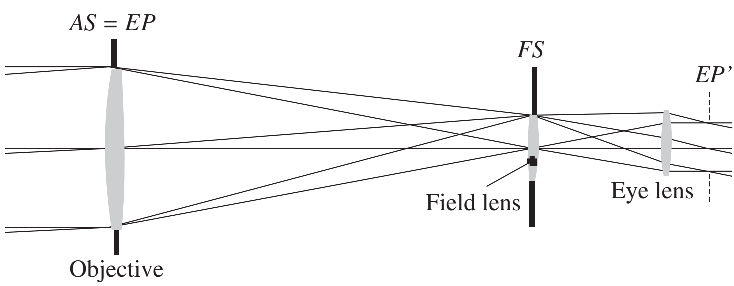

Figure 5.7 Inserting a suitable field lens, at the field stop, eliminates vignetting.

5.5 Vignetting

When oblique light beams are unable to pass through the entire optical system because of obstruction or an insufficient element size, as shown in Fig. 5.6, part of the entering energy is lost by blockage or "clipping." This effect is termed vignetting.

In this case, inserting a proper lens at the field stop redirects the rays such that all of the energy is received by the exit pupil (shown in Fig. 5.7).

It is advisable to position the field lens in a somewhat displaced position along the optical axis. By placing the field lens exactly at the field stop, where the image is formed and observed, any surface defects, such as scratches of the field lens, are clearly visible, because they are "in focus."

Even though vignetting causes loss of light throughput, it is nevertheless a powerful technique, applied in complex optical systems to reduce off-axis aberrations, balancing the acceptable illumination reduction.

Chapter 6
Two-Element Systems

6.1 Introduction

Two-element systems have a wide variety of arrangements and applications. The following selected examples show basic systems with two lens elements without addressing design details (necessary to correct aberrations) of the components.

6.1.1 Telescopes

Telescopes served in Chapter 5 to demonstrate and explain the vignetting effect. Here we want to identify them as instruments used to observe the image of a distant object, formed by a lens (the telescope objective), and viewed with a second element (the eyelens, also called the ocular). Figure 6.1 shows the basic arrangement of the so-called *Kepler* telescope, also known as the *astronomical* type. The image to be viewed is upside down, which is of no concern for astronomical observations. If the device is used for terrestrial applications, a relay lens is inserted between the objective and the eyepiece to render the image orientation upright, which indicates, of course, that it is a three-element system.

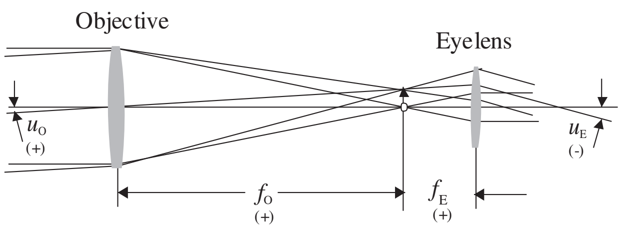

Figure 6.1 Refractive telescope according to Kepler.

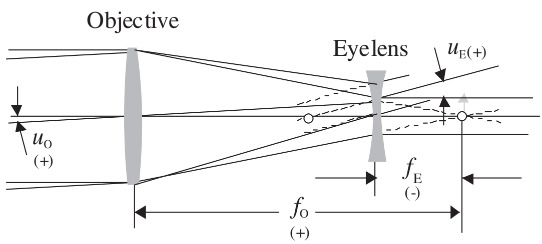

Figure 6.2 Galilean telescope (operetta glass).

The second telescope type, the refractive design, has been credited to Kepler's contemporary, *Galileo Galilei*, even though he was not the inventor. His basic design is shown in Fig. 6.2.

The field of view for this device is very limited, and the fact that the exit pupil is located to the left of the eyepiece leads to a viewing constraint. This will be discussed and demonstrated with an example in Chapter 13 with reference to stops, pupils, and windows. As previously indicated, its use is primarily intended for observing stage performances.

The magnification of either telescope is expressed as

$$MP = \frac{u_E}{u_O} = \frac{-f_O}{f_E}. \tag{6.1}$$

Example 1

The focal length of a Kepler telescope* has an objective lens $f_0 = 200$ mm. The eye lens focal length $f_E = 20$ mm. The half field angle $u_0 = 2\ \text{deg}$.

What is the magnification and what is the exit angle u_E?

Answer

Applying Eq. (6.1), $MP = -f_O/f_E = -200/20 = -10$.

Consequently, $u_E = MP \times u_O = -10 \times 2 = -20\ \text{deg}$.

Example 2

Analyze a Galilean telescope# with the same objective focal length and the same eye lens focal length (the same size, yet negative).

Answer

Using Eq. (6.1), we get $MP = -f_O/f_E = -200/-20 = +10$. The exit angle $u_E = MP \times u_O = +10 \times 2 = +20\ \text{deg}$.

This indicates that the magnification is the same size for both cases. The signs indicate that that for the Kepler telescope there is an image reversal, whereas with the Galilean type there is none.

**Johannes Kepler* lived from 1571 until 1630. The discovery of the laws of planetary motion is probably the foremost of his many achievements in the fields of mathematics and physics.

#*Galileo Galilei*, a great Italian philosopher and physicist, was a contemporary of Kepler who lived from 1564 until 1642. He improved the telescope design named after him. It was invented one year prior (1608) to his improvement by the Dutch eyeglass maker *Hans Lippershey*.

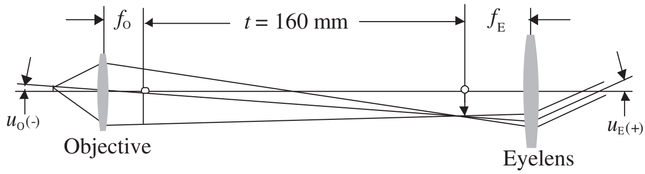

Figure 6.3 Principal layout of a compound microscope.

6.1.2 Microscopes

Contrary to the telescope, which is used to observe distant objects, a microscope focuses on very small objects, as the name implies. Its basic design is shown in Fig. 6.3.

Regarding the compound microscope, the magnification can be expressed as the product of the objective magnification and the magnification of the eyelens.

Therefore,

$$MP = M_O \times M_E. \tag{6.2}$$

The indicated distance t between the rear focal point of the objective and the front focus point of the eye lens is termed the microscope's *tube length*, which is most frequently 160 mm. Consequently, Eq. (6.2) becomes

$$MP = \frac{-160}{f_O} \times M_E. \tag{6.3}$$

The eyelens is a magnifier with a magnification of $MP_0 = 250/f$, as was noted in Eq. (2.13). Therefore, the final expression for the magnification of the compound microscope is expressed as

$$MP = \frac{-160}{f_O} \times \frac{250}{f_E}. \tag{6.4}$$

Remark

In these equations, the focal lengths must be in units of millimeters.

Example

The objective of a compound microscope has a focal length $f_O = 16$ mm. The eyelens focal length $f_E = 20$ mm. What is the total magnification?

Answer

Using Eq. (6.4), the magnification is the following:

$$MP = \frac{-160}{f_O} \times \frac{250}{f_E} = \frac{-160}{16} \times \frac{250}{20} = -10 \times 12.5 = -125.$$

Again, the minus sign indicates a reversal of the image direction.

6.1.3 Relay systems

In cases for which an image must be repositioned in an optical train, a relay system is inserted. Two possible layouts are presented here. In the first arrangement, shown in Fig. 6.4, the

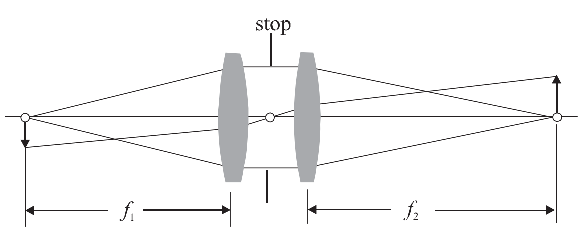

Figure 6.4 Relay system with the image to be relayed located in the focal plane of the first lens, and the projected image located in the focal plane of the second lens.

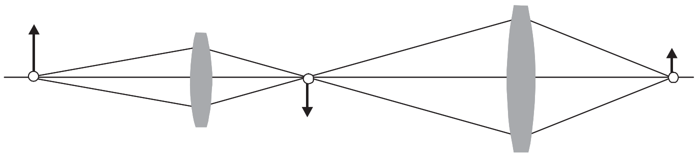

Figure 6.5 System with the elements' focal lengths chosen to maintain the image orientation at the desired magnification.

image to be relayed is located in the focal plane of the first lens, projecting its image at infinity. The rays between the two lenses are parallel; the relay system forms an image at its focal plane. This arrangement has an advantage in that each element can be individually moved along the optical axis for optimal focus conditions, whereby the magnification is maintained, which is simply the focal length ratio of the two elements. Notice that the image orientation is reversed in this setup.

In the second arrangement, shown in Fig. 6.5, an intermediate image is formed to achieve a double image orientation reversal. As in the first setup, the magnification is controlled by the choice of the element's focal lengths as well as the object and image distances.

6.1.4 Projector systems

In this example for two lenses, the first lens is the illumination lens, termed the *condenser*. The second lens is the *projection lens* (shown in Fig. 6.6). One can see the interaction between the two lenses to achieve uniform illumination of the object to be projected onto the screen.

6.1.5 Telephoto objectives

In this arrangement of a two-element system, a negative element is placed at a proper distance behind a positive element, as shown in Fig. 6.7. Such a layout results in a compact, long focal length device.

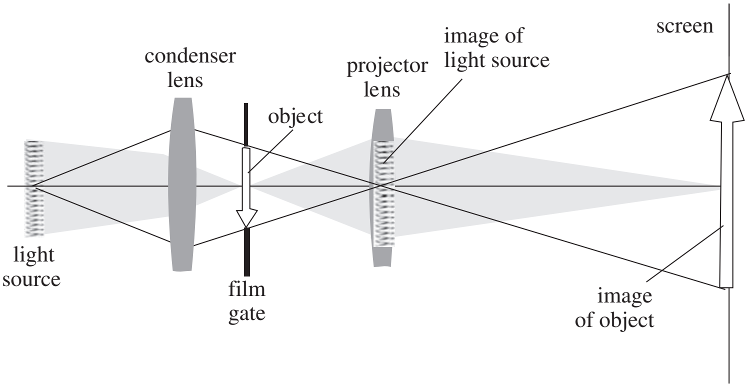

Figure 6.6 Projector system.

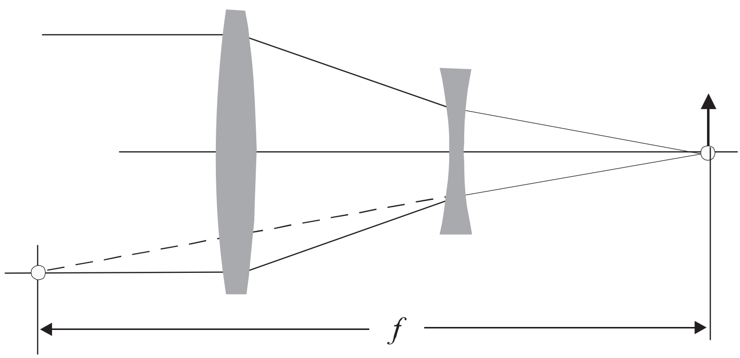

Telephoto objective, a compact assembly.

Figure 6.7 Telephoto objective, a compact assembly.

6.1.6 Reverse telephoto objectives

As the name implies, this arrangement is the reversal of the telephoto objective shown in Fig. 6.7. The negative lens is now in front, as can be seen in Fig. 6.8.

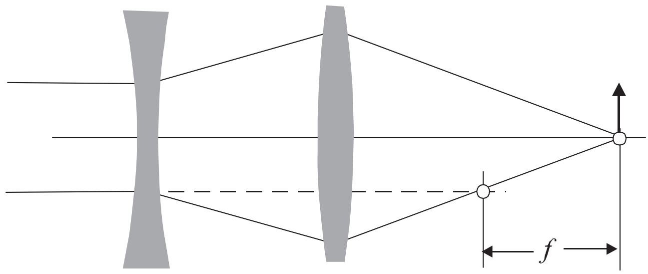

Figure 6.8 Reversed telephoto objective, also known as a retrofocus objective, which has a short focal length and a long free working distance, the space behind the last element. It is the basis for the wide-angle objective.

6.2 Doublets

Doublets are defined as two elements in close proximity. For the visible spectrum, doublets are commonly cemented together. Of course, the elements are constructed from different glasses. Elements for doublets used in the mid-wave infrared (MWIR) and longwave infrared (LWIR) spectral bands must be separated, because optical cement does not transmit beyond a wavelength of approximately 2.7 μm. The MWIR section extends from 3 to 5 μm, and the LWIR region covers the range from 8 to 12 μm. Although this necessary separation renders mounting of the elements somewhat more costly, there is the advantage of being able to bend each element independently.

We limit our observations to the cemented doublet, the *achromat* used in the visible spectrum. As the name implies, this lens is designed to correct *chromatic aberration*. This is achieved for two colors on-axis. The remaining uncorrected aberration is termed the *secondary spectrum*.

With properly chosen radii of the elements, spherical aberration and also coma can be eliminated. The front element is usually a positive element, constructed from crown glass. The second is a negative flint glass component. Figure 6.9 shows the arrangement of a cemented achromat. The joining of the long and short wavelength in the focal point is indicated.

> There is an interesting story behind the achromat. This is the way it is told in the second edition of *Introduction to Classical and Modern Optics* (J. R. Meyer-Arendt, Prentice-Hall 1972).
>
> "This method of correcting for chromatic aberration goes back to 1729, when Chester Moor-Hall (1704–1771), British judge of peace and amateur astronomer, designed the first achromatic contact doublet. Apparently, Moor-Hall had discovered that glass containing lead oxide, of the type used to make fine table ware, had higher dispersion than window glass. To keep his discovery secret, he ordered one element for his doublet from a certain lens maker in London, the other from another. As it happened, both men subcontracted the work to a third optician, who, on finding that both lenses were for the same customer and had one radius in common, placed them in contact and saw that the image was free of color. News of this discovery slowly spread to other opticians, among them John Dolland (1706–1761), whose son Peter (1739–1820) urged him to apply for a patent so that he could collect royalties. Naturally, the other London opticians objected and took the case to court, producing Moor-Hall as a witness. The court agreed that indeed Moor-Hall was the inventor, but in a much-quoted decision, the judge, Lord Camden, ruled in favor of Dolland, saying 'It is not the person who locked up his invention in his scritoire that ought to profit by a patent for such an invention, but he who brought it forth for the benefit of the public.'"
>
> This is just one of so many interesting stories that tell about people who contributed much in the field of optics. It is not only fascinating to learn more about these people; these stories are instructive and sometimes sad, as is the case with Josef Max Petzval, a Hungarian mathematician (1807 to 1891). In 1859 burglars broke into his home and destroyed many of the notes he had made over the years, including his derivations of higher-order aberrations calculations.

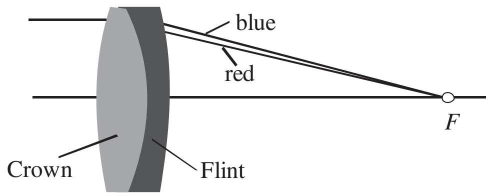

Figure 6.9 Achromat, bringing two wavelengths to a common image point.

Table 6.1 Refractive indices and Abbe numbers for typical achromat glasses.

Crown glass (BK7)	$n_d = 1.5168$	$\nu = 64.167$
Flint glass (F2)	$n_d = 1.620$	$\nu = 36.367$

Crown glass has a relatively low index of refraction and a high Abbe number. The index of refraction for *flint glass* is relatively high and its Abbe number is low. Typical values for such glasses used for an achromat are shown in Table 6.1.

To correct for a third color, one must add another element. Such an arrangement is termed an *apochromat*.

6.3 Separated Imaging Mirrors

6.3.1 Telescope objectives

The most well-known arrangement of two separated imaging mirrors is probably the *Cassegrain* telescope configuration, shown in Fig. 6.10.

Laurent Cassegrain was a French priest, born in 1629. Not much is known about his education. His two-mirror arrangement has taken a special place in telescope design, and is termed the "classic two-mirror configuration."

In the original *Cassegrain* layout, the shape of the primary mirror is parabolic, and that of the secondary mirror is

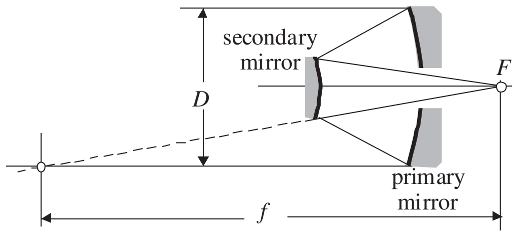

Figure 6.10 Cassegrain telescope configuration.

hyperbolic. These shapes are so-called conic sections. They will be discussed in Chapter 7.

Astronomical telescopes are of this type. They have usually large relative apertures. The famous *Hubble* telescope, for example, has a focal length of 57.6 m and a free-aperture of 2.4 m, rendering it a very "slow" $f/24$ system. The advantage, of course, is to limit the angular field, reducing the off-axis aberrations. In the case of the *Hubble* telescope, it is for one application only 25 arc s (linear dimension = 7 mm). A second arrangement provides 52 arc s (14.5 mm).

To correct for coma, both mirrors are hyperbolas. This configuration was invented in 1910 by two astronomers, American *George Willis Ritchey* and Frenchman *Henri Chrétien*. Making both mirrors hyperbolas corrects coma over a narrow field. Today, the majority of two-mirror telescope systems is of this category and is termed the *RC* type.

Two astronomers from Holland, *Alan Dall* and *Horace Kirkham*, wanted to eliminate the difficulty in manufacturing and measuring the hyperbolic shape of the secondary mirror. In 1928, they replaced the secondary mirror with a spherical mirror, which rendered the primary mirror a prolate ellipse. This manufacturing advantage, however, has a bit of a

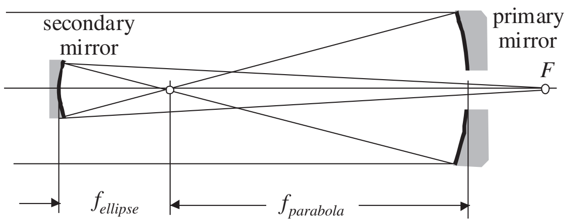

Figure 6.11 Gregorian telescope.

performance drawback over the already very narrow field coverage.

Before Cassegrain, there was a Scottish astronomer named *James Gregory* (1638 to 1679), who invented in 1663 the first two-mirror telescope. Its configuration consists of a parabolic primary mirror, and an elliptical secondary mirror, as shown in Fig. 6.11. Its disadvantage is its overall length, which is determined by the sum of the two mirrors' focal lengths. The fact that the final image is right-side up, however, is advantageous.

A few years later, in 1668, the great British scientist Sir *Isaac Newton* (1642 to 1726) introduced his design, which consists of only one active element, a parabolic mirror. The second mirror has a flat surface and is tilted 45 deg to bring the focus of the imaging mirror outside of the incoming beam (indicated in Fig. 6.12).

To avoid the diffraction effects caused by the holding structure of the folding mirror, termed the spider, an arrangement of the type shown in Figure 6.13 is employed.

6.3.2 Microscope objectives

The most well-known reflective microscope objective was invented by the German physicist *Karl Schwarzschild* (1873 to

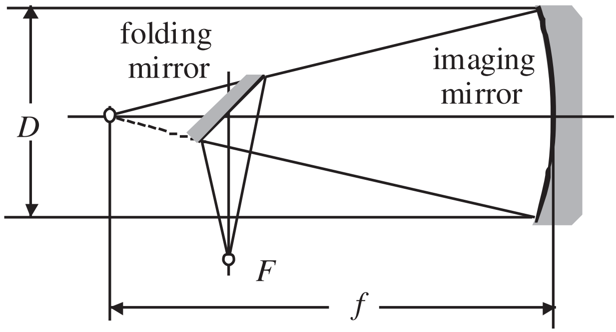

Figure 6.12 Classic Newtonian telescope.

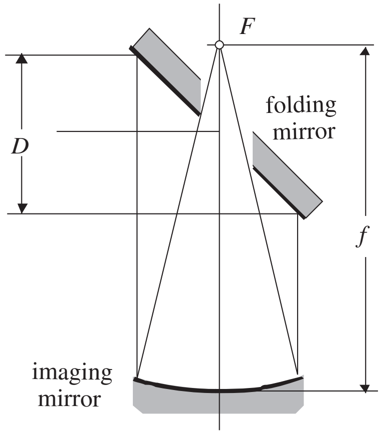

Figure 6.13 "Inverted" Newtonian telescope.

1916). It is a very clever design, because by arranging two concentric spherical concave mirrors, spaced by twice the objective's focal length, it is free of third-order spherical aberration, coma, astigmatism, and distortion, if the aperture stop is placed at the common center C of the mirrors. The objective is shown in Fig. 6.14.

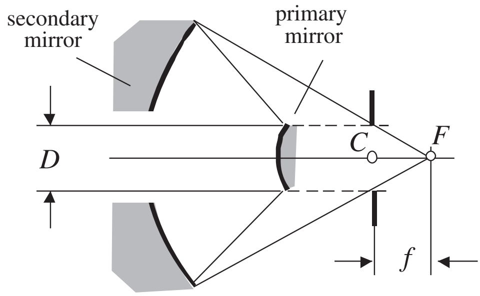

Figure 6.14 Classic Schwarzschild microscope objective.

In most cases, the aperture stop is not installed, especially when the field to be covered is narrow. In that case, coma and astigmatism are negligible and spherical aberration is not affected. Furthermore, the *free working distance* (the distance between the last component of the objective and the object to be viewed) is increased. Such objectives are sold as shelf items available from a number of suppliers.

There are variations of this basic design that uses aspheric surfaces and have shorter free-working distances.

Such objectives find applications beyond the visible spectrum because, as previously mentioned several times, mirror surfaces are not wavelength-selective.

Remark

Relay configurations are an additional two-mirror arrangement. For laser applications, two-mirror beam expanders are employed. These consist preferably of two parabolic reflectors, one positive and one negative.

6.4 Focal Length of Two Separated Elements

There is a very simple expression, based on the thin lens theory, which states that the focal length of a two-element

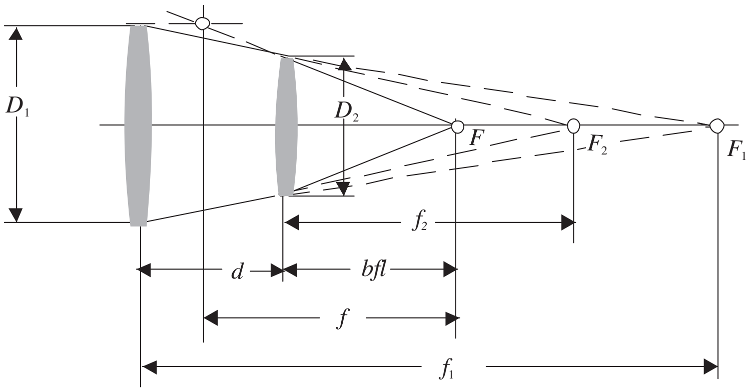

Figure 6.15 Two separated elements.

system in air, in which the elements are separated by a distance d, is as follows:

$$\frac{1}{f} = \frac{1}{f_1} + \frac{1}{f_2} - \frac{d}{f_1 f_2}. \tag{6.5}$$

Figure 6.15 defines the variables.

Solving for the system's focal length f yields

$$f = \frac{f_1 f_2}{f_1 + f_2 - d}. \tag{6.6}$$

The distance from the second lens to the focus is the back focal length, sometimes also termed the back focal distance. It is expressed as

$$bfl = \frac{f(f_1 - d)}{f_1}. \tag{6.7}$$

Exercise 1

A system consists of two positive lens elements. The first element has a focal length $f_1 = 100$ mm. The focal length of the second element is $f_2 = 50$ mm. The elements are spaced by $d = 25$ mm. What is the system's focal length f and what is the back focal length? Make a sketch of the lens. The relative aperture is $f/2$.

Solution

We apply Eq. (6.6) and find the system's focal length to be

$$f = \frac{f_1 f_2}{f_1 + f_2 - d} = \frac{100 \times 50}{100 + 50 - 25} = \frac{5000}{125} = 40 \text{ mm}.$$

The back focal length is

$$bfl = \frac{f(f_1 - d)}{f_1} = \frac{40(100 - 25)}{100} = \frac{3000}{100} = 30 \text{ mm}.$$

The requirement of the system having a relative aperture renders the front element diameter $D_1 = f/(f/\#) = 40/2 = 20$ mm. The diameter of the second lens is derived from the ratio $D_1/f_1 = D_2/(f_1 - d)$ (see Fig. 6.15). Solving for D_2, we find

$$D_2 = \frac{(f_1 - d)}{f_1} D_1 = \frac{(100 - 25)}{100} \times 20 = \frac{75}{5} = 15 \text{ mm}.$$

Now we are ready to sketch the system (Fig. 6.15).

Exercise 2

To demonstrate that Eqs. (6.6) and (6.7) may be also applied to mirror systems, we investigate an $f/4$ Cassegrain telescope (see Fig. 6.10).

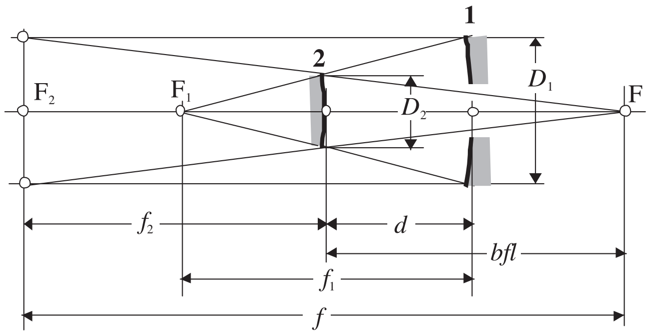

Figure 6.16 Sketch for exercise 2.

Problem

The primary mirror's focal length $f_1 = 100$ mm and the secondary mirror's focal length $f_2 = -100$ mm. The mirrors are separated by $d = 50$ mm.

Find the system's focal length and back focal distance. How large are the mirror diameters?

Solution

The system's focal length, according to Eq. (6.6), is

$$f = \frac{f_1 f_2}{f_1 + f_2 - d} = \frac{100 \times (-100)}{100 - 100 - 50} = 200 \text{ mm}.$$

The back focal distance [Eq. (6.7)] is

$$bfl = \frac{f(f_1 - d)}{f_1} = \frac{200 \times (100 - 50)}{100} = 100 \text{ mm}.$$

With a relative aperture of $f/4$, the diameter of the primary mirror is

$$D_1 = \frac{f}{4} = \frac{200}{4} = 50 \text{ mm} \quad D_2 = \frac{100}{4} = 25 \text{ mm}.$$

Figure 6.16 shows the arrangement.

Chapter 7
Aspheres, Gradient Index Lenses, and Optical Path Length

Aspheres have a special place in optics and a long history as imaging mirrors, as was noted in Chapter 6. As the name implies, any surface that is not a sphere is an asphere.

Of particular interest are conic sections for imaging mirrors because they form stigmatic images, which means that all rays from an axial object point pass through the same image point. Therefore, they do not create spherical aberration. It all started with the use of parabolic reflectors for astronomical telescopes. The ellipsoid and hyperboloid found their place as suitable shapes for the secondary mirror of the Gregorian and Cassegrain telescopes, respectively, as noted in Chapter 6.

7.1 Conic Sections

Figure 7.1 illustrates how different slices through the double cone generate optically useful curves.

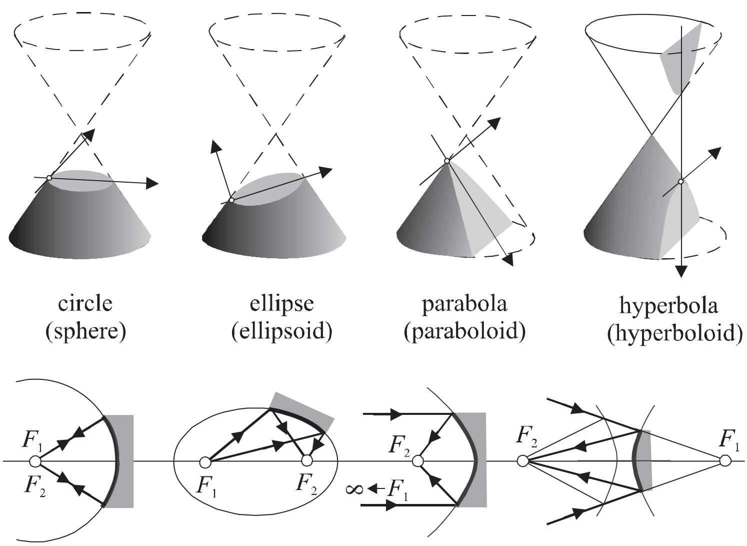

Figure 7.1 Lower sketches indicate the location of the focal points of mirrors with different conic cross sections.

A circle is obtained with a cut perpendicular to the vertical axis of rotation of the double cone. If the cut occurs at an angle smaller than the cone angle, the contour is an ellipse. If the cutting angle is parallel to the cone angle, a parabola is generated. Finally, by slicing the cone parallel to its axis of rotation, a symmetrical hyperbola results.

In the lower part of Fig. 7.1, applications of these shapes as optical mirror imaging surfaces are depicted.

To improve the aberration correction, additional so-called higher-order deformation coefficients are added to the basic conic sections equation.

With the development of computer-controlled manufacturing equipment, optical components with asymmetric surface contours, so-called freeform surfaces, are increasingly utilized.

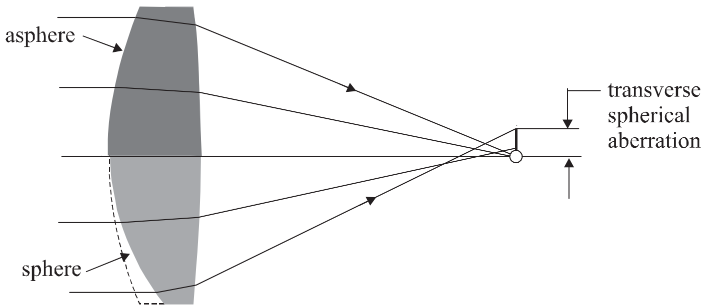

Figure 7.2 Performance comparison between an aspherized and an all-spherical surface singlet.

7.1.1 Aspheric singlet

The upper part of the lens shown in Fig. 7.2 has an aspheric front surface, adjusted to direct all the exiting rays to one point on the optical axis. The lower section of the lens is spherically shaped. It can be seen that a sphere bends rays too much towards the edge of the lens, resulting in spherical aberration.

7.2 Freeform Surfaces

As the name indicates, freeform surfaces can exhibit any shape. A good general reference is the profile of a saddle-shaped potato chip (Fig. 7.3). Whereas the shape in the sketch may be a bit over-magnified, it indicates the surface contour freedom that is now available to the lens designer. Such surfaces find applications as reflectors as well as for refractive elements. Typical examples are progressive eyeglass lenses, which provide continuous focus changes over the field of view, and automobile headlight optics, which optimize the desired light distribution. Such freeform optical surfaces are difficult to describe mathematically, and of course are also problematic

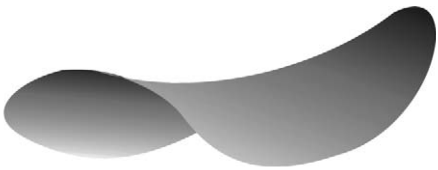

Figure 7.3 Example of a freeform surface.

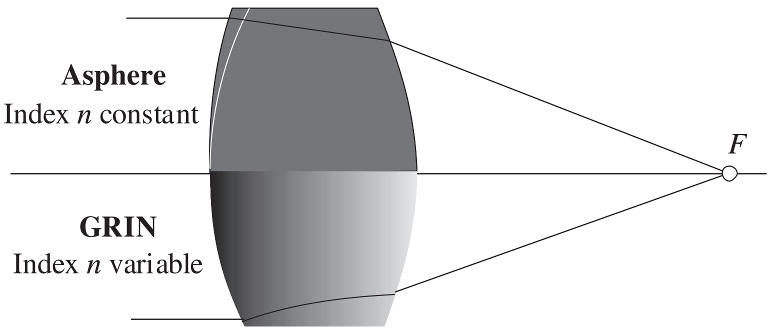

Figure 7.4 Comparison of controlling the ray direction.

to produce. However, with the aid of modern computers, both challenges have been met and further progress can be expected in an increasing number of applications.

7.3 Gradient Index Lenses

Gradient index (GRIN) lenses consist of a material in which the index of refraction varies either radially as a function of the distance from the optical axis or axially in the direction of the optical axis. This second type is especially useful for correcting spherical aberration. Figure 7.4 demonstrates this principle.

The darker-shaded section towards the front of the lens indicates a higher index, which decreases towards the back of

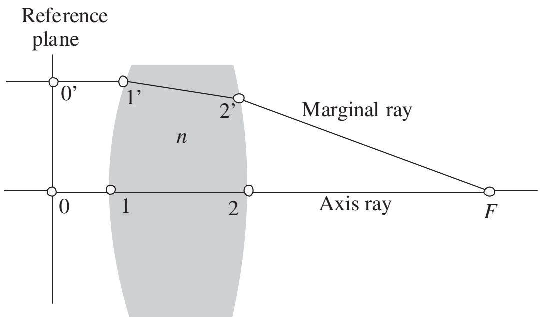

Figure 7.5 Two different optical paths.

the lens, resulting in less bending of the ray, as predicted by Snell's law. The upper portion of Fig. 7.4 shows how the direction of the ray is controlled by an aspheric surface shape. The white line indicates the extension of the spherical surface from below. This comparison between the two types of ray direction control leads us to the next subject.

7.4 Optical Path Length

The optical path length (OPL) is the product of the index of refraction and the distance traveled by the light, stated as

$$OPL = nd. \tag{7.1}$$

For an aberration-free lens, the OPL must be the same for any ray traveling from an object point to the corresponding image point. Figure 7.5 indicates two paths from a reference plane for a lens, imagining an object located at infinity.

The requirement for zero spherical aberration is as follows:

$$\begin{aligned} OPL_{marginal} &= \overline{0'1'} + n\overline{1'2'} + \overline{2'F} = OPL_{axis} \\ &= \overline{01} + n\overline{12} + \overline{2F}. \end{aligned}$$

We know that this can be achieved with an aspheric surface, as shown in Fig. 7.2.

Now we have a second method to vary the index of refraction through the GRIN lens, which actually means we are taking a bit of a detour (i.e., the bow shown in Fig. 7.4), and adjusting the speed to arrive at F at the same spot as the ray traveling on the optical axis. The optical path difference (OPD) is 0.

Chapter 8
Diffraction Limit, Resolution, and Modulation Transfer Function

8.1 Diffraction Effect on an Image

Based on the wave hypothesis of light, there is an effect termed diffraction. Simply stated, when a plane wave-front passes an edge, there is a lateral spreading effect, termed diffraction, schematically depicted in Fig. 8.1.

This diffraction effect is the reason that an object point cannot be imaged as a point, even if it can be predicted as such by geometric ray tracing.

Lord *George Biddell Airy*, a brilliant British mathematician and astronomer, who lived from 1801 to 1892, developed in 1835 the expression for the intensity distribution of a point source imaged by a perfect lens. As indicated in Fig. 8.2, the energy contained in the "Airy disc," that is, the central circle of the diffraction pattern, contains 83.9% of

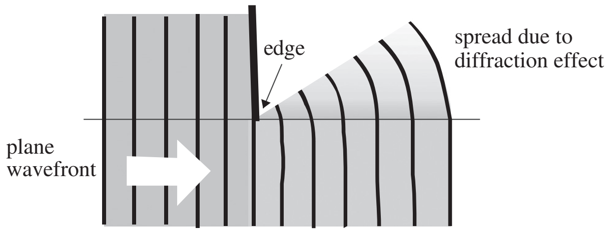

Figure 8.1 Wave-front spread due to diffraction at an edge.

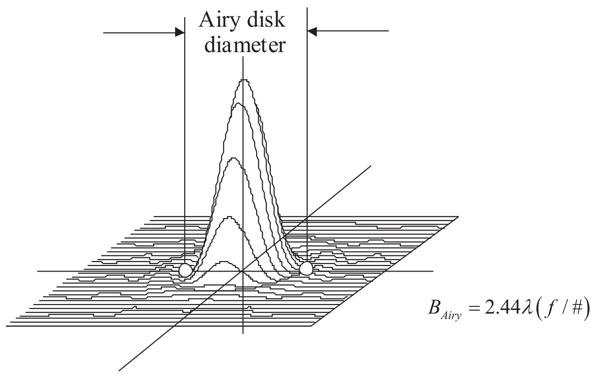

Figure 8.2 Pattern caused by diffraction; 83.9% of the energy is contained in the Airy disk.

the transmitted energy. Its diameter for an object point at infinity is

$$B_{Airy} = 2.44\lambda(f/\#). \tag{8.1}$$

As previously stated in Chapter 1, the visible (VIS) spectral region extends from 0.4 to 0.76 μm. The main spectral regions utilized in the infrared are the mid-wave infrared (MWIR) and the longwave infrared (LWIR) regions. The MWIR region ranges from 3 to 5 μm. The LWIR extends from 8 to 12 μm.

Table 8.1 Airy disk size in different spectral regions.

Spectral region	Center wavelength (μm)	Airy disc diameter (μm)
VIS	0.5	$1.22(f/\#)$
MWIR	4	$3.74(f/\#)$
LWIR	10	$24.4(f/\#)$

Table 8.1 indicates how the diameter of the Airy disk increases as a function of wavelength.

An example will demonstrate this fact. An $f/2$ lens designed for the visible spectrum has a blur spot size of only 2.44 μm, if it is "diffraction-limited." This is the term used to refer to a lens that is free of aberrations. The Airy disk for this case is magnified 1000× in Fig. 8.2.

8.2 Resolution, Image Quality, and Depth of Focus

A measure for the resolution of an optical system was introduced by Lord *Rayleigh* (John William Strutt), a British physicist (1842 to 1919). This *Rayleigh criterion* states that two points are *resolved* if their images, formed by a diffraction-limited optical system, are separated by a distance equal to the radius of the Airy disk, which is $1.22\lambda(f/\#)$, depicted in Fig. 8.3.

Lord Rayleigh also reasoned that an image is considered to be acceptably perfect if the wavefront, forming the image, is within one-quarter of a wavelength. This so-called *quarter wave criterion* is expressed by the allowable longitudinal out of focus tolerance of

$$\Delta f = \pm 2\lambda(f/\#)^2. \tag{8.2}$$

Examples

Table 8.2 lists the out-of-focus allowance for an $f/2$ system in different spectral regions.

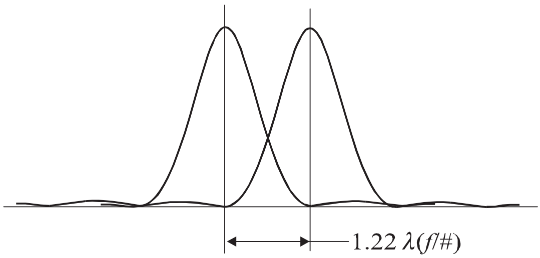

Figure 8.3 Lord Rayleigh's resolution criterion.

8.3 Modulation Transfer Function

Another measure of resolution is the modulation transfer function (MTF), where the contrast of the image is stated at a selected spatial frequency, which is simply another term for *line pairs per millimeter*.

The modulation transfer function is a testimony of quality and predicts the performance a lens. It does not, however, reveal any details about aberrations.

Before MTF measurement equipment became a standard quality control device, lenses were tested by visually observing the *sharpness* of a projected resolution pattern on a screen.*

*As is the case with many inventions and discoveries, this concept of testing the performance of optical systems is not the achievement of one individual. In 1936, *Helmut Frieser*, a staff member of Zeiss–Ikon in Berlin, had noticed that periodic sinusoidal patterns maintain their shape when projected but their amplitude and position deteriorate. He recognized that imaging coarse and fine structures would be sufficient to evaluate the quality of a lens. In a broader context the French physicist *Pierre-Michelle Duffieux* introduced in 1946 the exact relationship of the subject by employing the mathematical tools invented by his compatriot *Jean-Batista Fourier*, who lived from 1768 to 1830. There was also an American physicist *Harry Nyquist* who had published his sampling theorem in 1928, which is very much related to the subject of the modulation transfer function.

Table 8.2 Defocusing tolerances for $\lambda/4$ systems.

Spectral region	Center wavelength (μm)	Out-of-focus tolerance (μm)
VIS	0.5	4
MWIR	4	32
LWIR	10	80

This subjective judgment varied not only from person to person, but also from morning to evening and Monday to Friday.

To provide a simple overview of the subject, we present a few steps.

8.3.1 What is the modulation transfer function?

As previously stated, the modulation transfer function is the ratio of the image contrast to that of the object, as a function of a line bar pattern with varying line width. This is illustrated in Fig. 8.4. Whereas the true modulation function is based on a sine wave response, for practical reasons, square wave patterns are used in the process and the relation to the sinusoidal pattern is achieved mathematically with a process invented by Frenchman Jean-Baptiste Joseph Fourier (1768 to 1830).

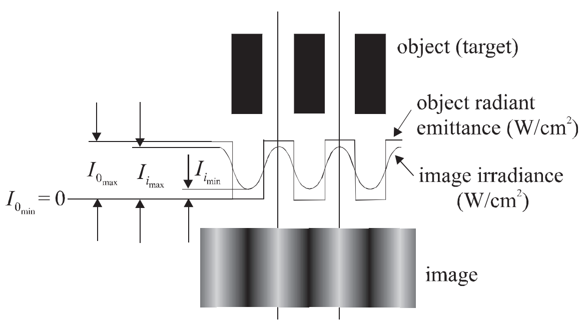

Figure 8.4 Perfect black/white object lines are imaged with blurring effects.

This is caused not only by existing aberrations, but also by the diffraction effect. Figure 8.4 explains the relationship between the object brightness (radiant emittance) and the image illumination (irradiance) distributions. From that, the modulation for the object is defined as

$$M_{object} = \frac{I_{0_{max}} - I_{0_{min}}}{I_{0_{max}} + I_{0_{min}}}. \tag{8.3}$$

For the image, the modulation is

$$M_{image} = \frac{I_{i_{max}} - I_{i_{min}}}{I_{i_{max}} + I_{i_{min}}}. \tag{8.4}$$

Term I represents the brightness of the object and the illumination of the image.

The modulation transfer function is

$$MTF = \frac{M_{image}}{M_{object}}. \tag{8.5}$$

When $I_{0_{\max}} = 1$ and $I_{0_{\min}} = 0$, $M_{object} = (I_{0_{max}} - I_{0_{min}})/(I_{0_{max}} + I_{0_{min}}) = 1$. As the target bars become progressively narrower (increase in frequency), the contrast in the image becomes increasingly low. The MTF is a plot of this relationship, as shown in Fig. 8.5.

8.3.2 Equations

For a diffraction-limited optical system, which is a system with negligible aberration effects, the MTF is stated as an approximation through the equation

$$MTF_{diffr} \cong 1 - 1.218\left(\frac{\nu}{\nu_0}\right), \tag{8.6}$$

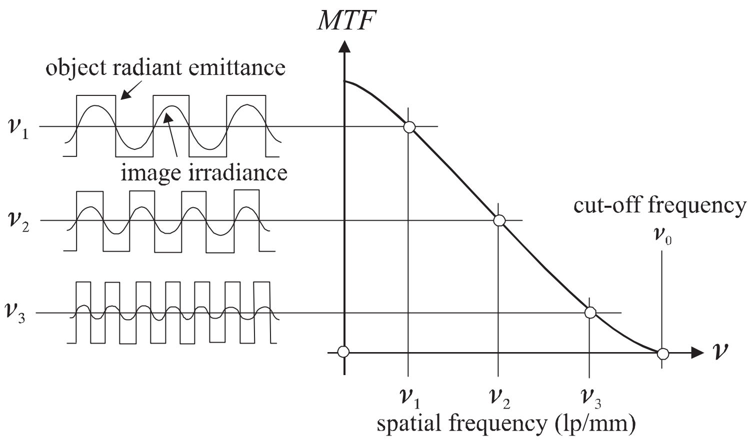

Figure 8.5 Construction of the modulation transfer function.

within the boundaries of $0 < (\nu/\nu_0) < 0.6$. Term ν_0 is the cut-off frequency where modulation stops, as indicated in Fig. 8.5. It is expressed as

$$\nu_0 = \frac{1}{\lambda(f/\#)} \tag{8.7}$$

The precise relationship for a diffraction-limited system and for an aberrated system can be found in *Optical Design Fundamentals for Infrared Systems, Second Edition* (M. J. Riedl, SPIE Press 2001)

Figure 8.6 compares the actual MTF curves with the straight line approximations for three spectral regions.

8.3.3 Additional limit

There is another limit that must be considered when a detector array is part of the optical system. In that case, the limiting resolution is defined by the pixel size of the array. One

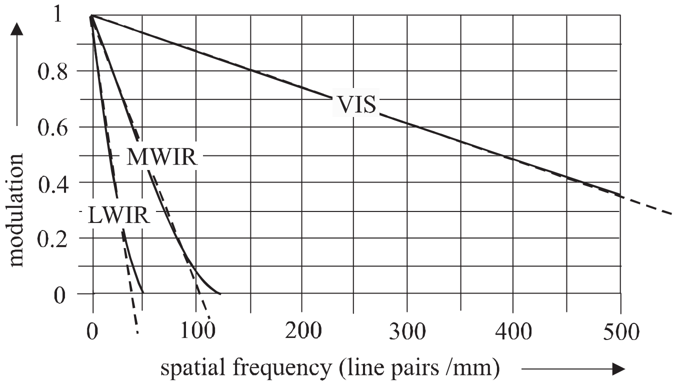

Figure 8.6 Transfer functions for diffraction-limited $f/2$ lenses for three spectral regions. Dotted lines are the linear approximations, indicating the good fit over a wide modulation range.

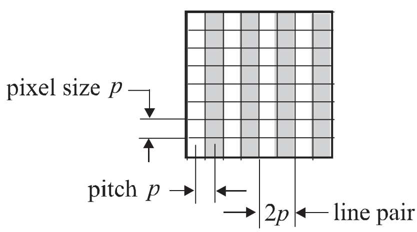

Figure 8.7 Focal plane array (FPA); pixel size and Nyquist frequency.

line pair has the width of two pixels. This boundary is referred to as the Nyquist frequency ν_N, stated as

$$\nu_N = \frac{1}{2p}. \tag{8.8}$$

The relation is shown in Fig. 8.7.

Figure 8.8 demonstrates the relationship between contrast and resolution. To answer which lens is better can only be answered with, "it depends on the application." One simply must think about intentionally smoothening a person's

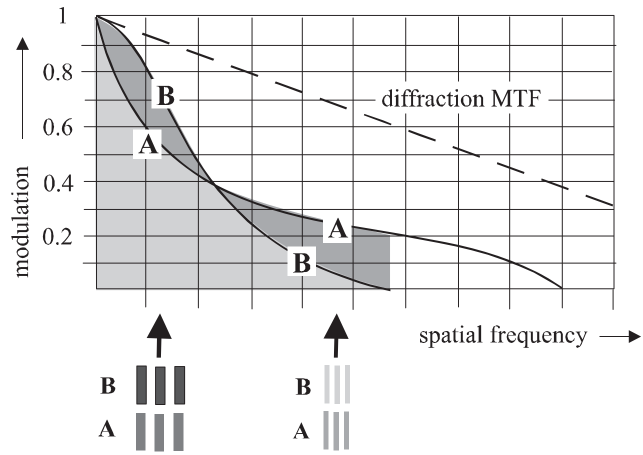

Figure 8.8 Contrast and resolving power. Lens B has better contrast at lower frequencies. Lens A has better contrast at higher frequencies and better resolution.

portrait when wrinkles should be hidden. The lens used for such a purpose is termed a *soft-focus lens*.

8.4 Real Case Demonstration

We will now demonstrate how the remaining aberrations influence the performance of a real lens design.

The double-Gauss camera objective discussed in Ch. 4 will be analyzed. Here is a picture of the lens:

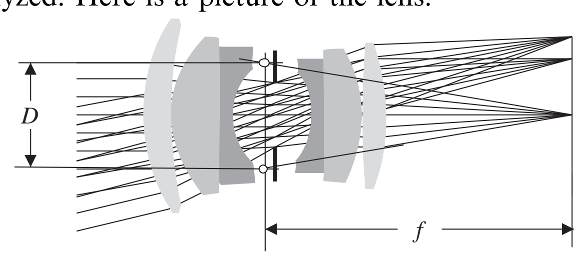

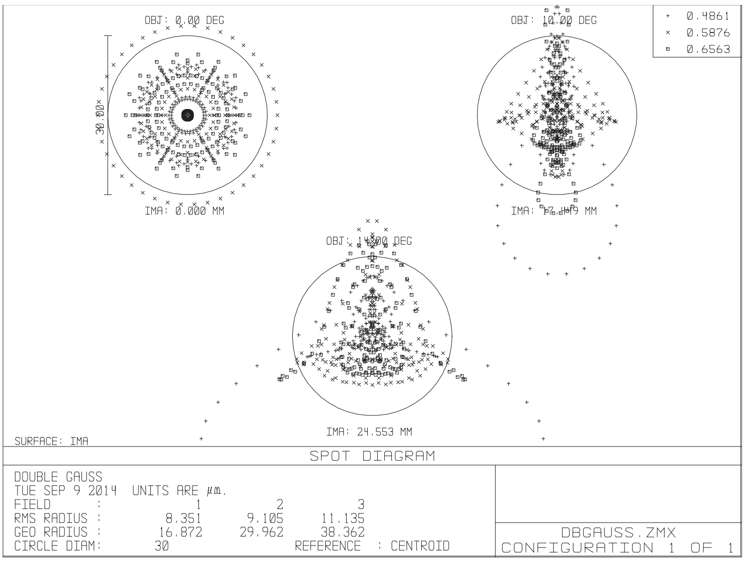

Figure 8.9 Blur spot shapes for the three fields.

Its focal length $f = 100$ mm, and its relative aperture is $f/3$, meaning that the diameter $D = 33.33$ mm. The spectral range was chosen to spread from 0.4861 to 0.6563 μm. Figure 8.9 illustrates the blur spot shapes. These are the F and C Fraunhofer absorption lines. This practice was noted in Ch. 1.

8.4.1 Aberrations

Calculations reveal that the design is not diffraction-limited. A reasonable amount of aberrations remains, which we will learn is acceptable for the application.

This balancing and reducing of the aberration is the job of the lens designer, whereby it is the challenge to meet the requirement without going overboard, which would only increase the cost of the lens. One can understand why lens design is sometimes described as being an art.

8.4.2 Blur spots

Whereas according to Eq. (8.1), the diffraction-limited blur spot size in the longest wave is $B_{Airy} = 2.44\lambda(f/\#) = 2.44\times 0.6563 \times 3 \cong 4.8$ µm, the actual sizes are depicted in Fig. 8.10.

One can clearly see the asymmetry of the pattern caused by the off-axis aberrations: coma, astigmatism, and lateral color. It is also noteworthy that the core of the energy is concentrated in a small area, which has been arbitrarily chosen as a circle 30 µm in diameter for reference. Whereas the Airy disk has been identified as being approximately 6× smaller, the performance of this lens can still be measured by comparing it to a diffraction-limited lens. This is shown in Fig. 8.10, where the top line is the diffraction-limited MTF

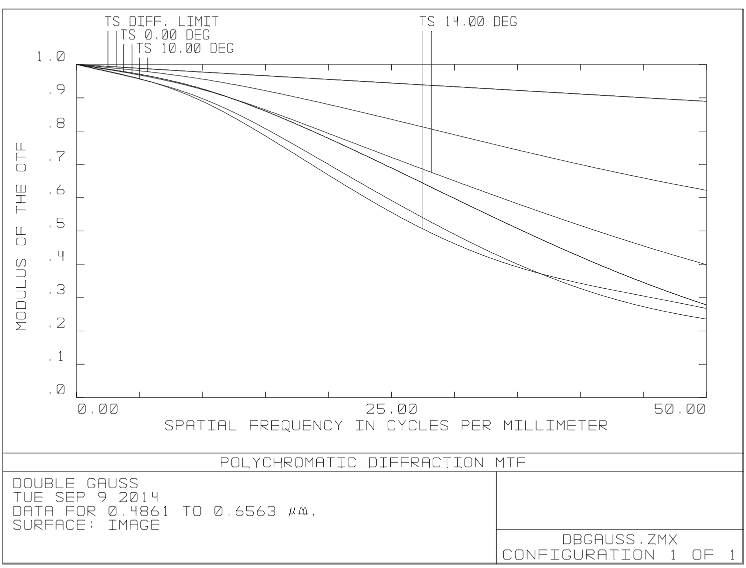

Figure 8.10 Modulation transfer function for a double-Gauss objective.

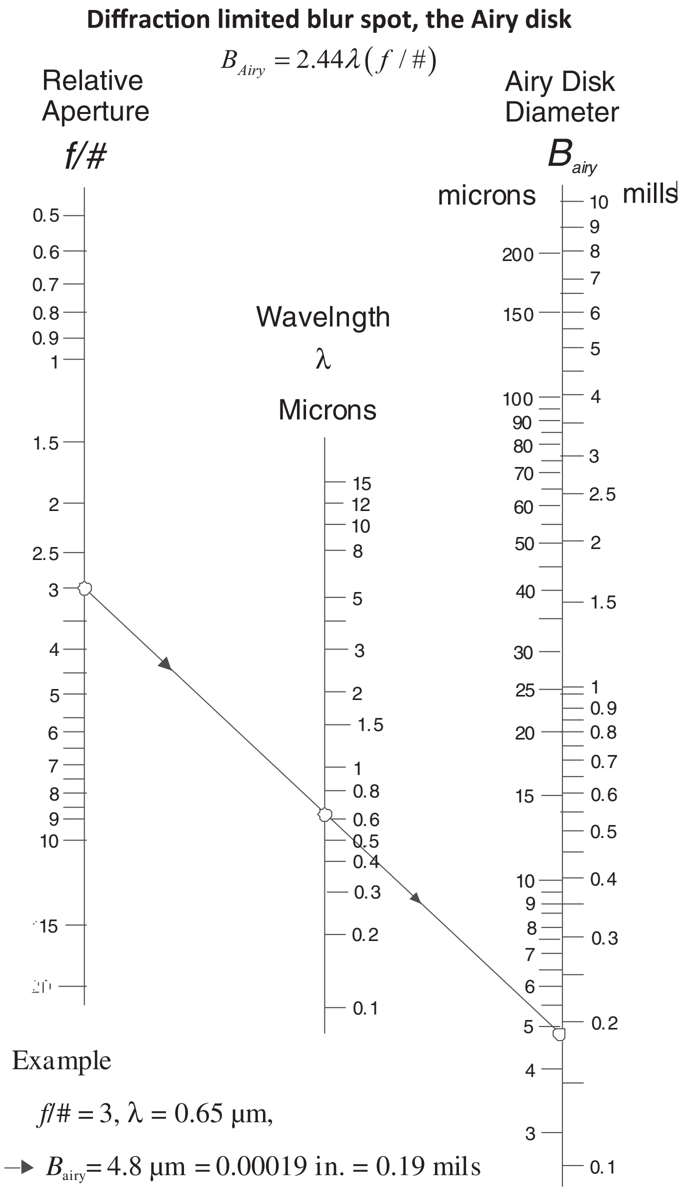

Figure 8.11 Determining the Airy disk diameter from the relative aperture.

curve. The lower lines indicate the symmetry for on-axis imaging and the separations of the tangential and sagittal curves due to astigmatism.

The image quality obtained with a 35-mm camera is generally acceptable if the MTF is approximately 30% for a special frequency of 50 line pairs per mm. This is the case for our lens, as can be seen in the figure.

For convenience, we include a nomogram for the expression of the diffraction-limited blur spot, the Airy disk (see Fig. 8.11). The marked example refers to the previously discussed double-Gauss lens. Of course, one can also use the graph to find the required $f/\#$ for a diffraction-limited system in a given spectral region.

Chapter 9
Optical Coatings

9.1 Introduction

Optical coatings sometimes consist of one layer, but in most cases consist of multiple thin layers of material deposited on an optical element to change the manner in which it reflects, transmits, or absorbs light.

Without optical coatings, applications would be severely hindered. Mirrors must have high reflectance, lenses require high transmittance, and filters and beam dividers require controlled transmission and reflection over specific spectral bands. Some applications require high absorption.

The fundamental law for the relation of these three characteristics is

$$\tau + \rho + \alpha = 1. \tag{9.1}$$

In other words, transmittance τ + reflectance ρ + absorptance $\alpha = 1$.

9.2 Refractive Elements

Augustin Jean Fresnel, a French physicist who lived from 1788 until 1827, is probably best known for his compact lighthouse lens. He derived the fundamental equation for reflection

ρ_s, from a single glass surface, of radiation at normal incidence, which remains a good approximation for tilt angles up to 45°

$$\rho_s = \left(\frac{n-1}{n+1}\right)^2, \tag{9.2}$$

where n is the index of refraction of the medium under observation.

Neglecting absorption, the transmitted fraction τ_s is

$$\tau_s = 1 - \rho_s = \frac{4n}{(n+1)^2}. \tag{9.3}$$

Figure 9.1 indicates that there are internal reflections when light passes through a plane parallel glass plate.

Again, ignoring absorption, but including these internal reflections in the calculation, the total transmitted fraction is

$$\tau = \frac{2n}{(n^2+1)}. \tag{9.4}$$

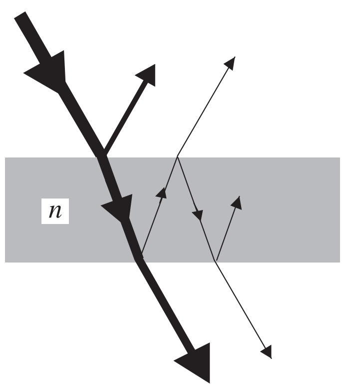

Figure 9.1 Transmission and reflection at a plane parallel plate.

This reveals that the high-index materials used in the infrared spectrum reflect much of the impinging radiation. A single lens made from glass with an index $n = 1.5$ yields

$$\tau = \frac{2n}{(n^2 + 1)} = \frac{2 \times 1.5}{(1.5^2 + 1)} = 92.31\%.$$

There is an expression which neglects the internal reflection

$$\tau \cong \left[\frac{4n}{(n+1)^2}\right]^2. \tag{9.5}$$

For $n = 1.5$, this yields

$$\tau = \left[\frac{4n}{(n+1)^2}\right]^2 = \left[\frac{4 \times 1.5}{(1.5+1)^2}\right]^2 \cong 92.16\%.$$

This indicates that only 0.15% of the light is lost due to internal reflections.

Figure 9.2 compares the transmission through elements comprised of BK7 and germanium, where the index of refraction is 4.

Whereas transmission through glass, which has a low index of refraction (i.e., 1.5), is relatively high compared with infrared (IR) materials, the transmission losses can be quite large.

Another example of how the transmission of light is tremendously reduced by surface reflection is the case of high-resolution objectives for lithographic applications, where a large number of elements is required for aberration correction. In an example shown in Fig. 9.3, where 30 elements comprise the objective, the transmission decreases to

$$\tau_{30} = \left[\frac{4n}{(n+1)^2}\right]^{2\times 30} = \left[\frac{4 \times 1.5}{(1.5+1)^2}\right]^{60} \cong 8.6\%.$$

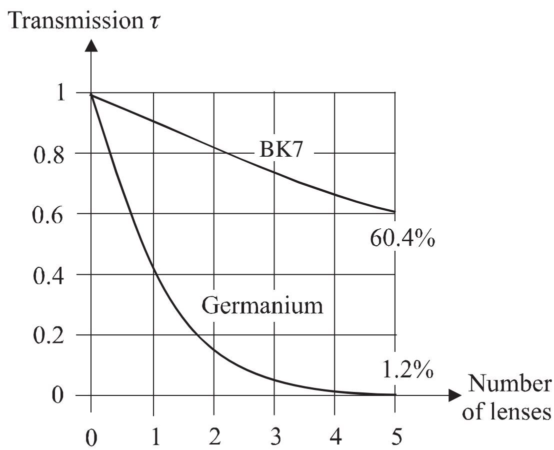

Figure 9.2 Remaining transmitted radiation after passing through a number of lenses.

9.3 Antireflective Coatings

Alexander Smakula, who was born in Ukraine in 1900, invented the antireflective coating scheme in 1935 while employed by Zeiss in Jena, Germany. He immigrated in 1951 to the United States, where he was offered a teaching position at the Massachusetts Institute of Technology. He died in 1983.

The basic principle of this approach is that the index of refraction of the coating film n_f must be equal to the square root of the substrate's index n_s

$$n_f = \sqrt{n_s}. \tag{9.6}$$

Furthermore, the film thickness t_f must meet the requirement

$$n_f t_f = \frac{1}{4}\lambda. \tag{9.7}$$

Equation (9.7) indicates that a maximum transmission can only be achieved for a single wavelength. However, the

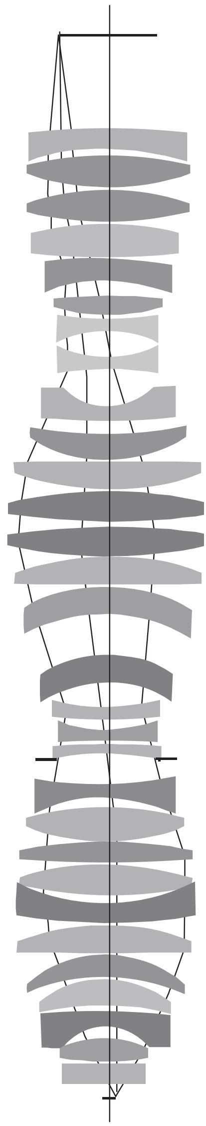

Figure 9.3 Thirty-element objective.

efficiency does not decrease abruptly. The efficiency decreases gradually for shorter and longer wavelengths. For better performance over a broad spectral band, more-sophisticated multilayer coatings are required, whereby the level of reflectance over the visible range can be kept as low as 0.5%.

9.4 Reflective Coatings

Up until the 1930s, the chemical process of depositing a reflective layer on a mirror substrate was simply termed *silvering*. Today, the most common metal films deposited by evaporation are

- aluminium
- silver
- gold
- copper
- rhodium.

Their reflectance varies as a function of wavelength. Therefore, the choice depends on the application. To protect the relatively soft metal layer from environmental influences, so-called *over-coatings* are deposited. The common preferences are magnesium fluoride and silicon monoxide. Dielectric multilayer coatings are applied to meet special protective and/or high-reflecting demands.

9.5 Interference Filters

To control the transmission or reflection (in some cases to also control the absorption), special filters are inserted into the optical train. The type of filters used for this purpose is primarily an interference filter. The name is indicative of the interference effects that occur between the incident and reflected waves at the thin film boundaries (Fig. 9.4). The design and manufacture of such filters is extremely challenging. In some

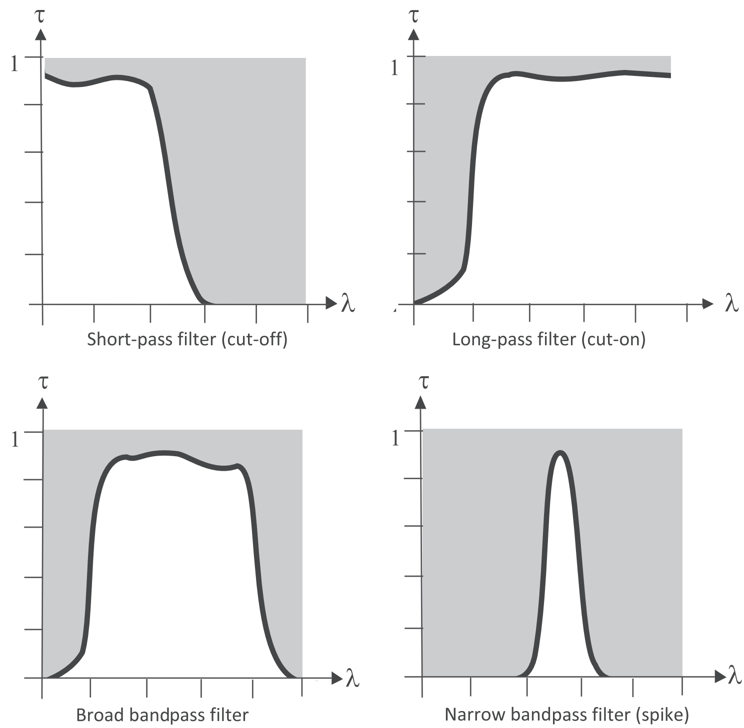

Figure 9.4 Typical interference filters.

cases, the number of individual layers comprising such a filter can reach 100 or even more. Depending on their design, they are named in accordance with the application. Typically they are termed one of the following:

- short-pass filter (cut-off)
- long-pass filter (cut-on)
- broad bandpass filter
- narrow bandpass filter (spike)
- beam splitter.

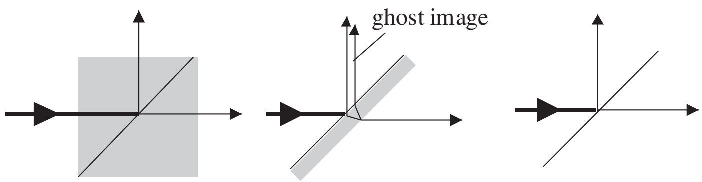

Figure 9.5 Beam splitters, prism, tilted plate, and pellicle.

9.5.1 Beam splitters

As the name implies, a beam splitter is an optical component that splits an incoming beam into two parts, whereby the density and the spectral contents of both the transmitted and reflected light can be controlled. Figure 9.5 shows three basic substrate designs. Each has its characteristic properties.

In the first arrangement, the actual filter is protected. The coating is deposited on the prism diagonal. The combination of the two 45° prisms forms a rather thick parallel plate and introduces sizeable spherical aberration, which can be corrected using the imaging lenses in the optical train. Notice that the path length in both directions is identical.

The second beam splitter arrangement is a relatively thin plane parallel plate with the coating deposited on the front side. As indicated, there may be a faint second image, termed a *ghost image*, which is created by the faint reflection from the second surface. An anti-reflection coating will considerably reduce this effect. In addition to spherical aberration, there is also astigmatism. Furthermore, one must compensate for the lateral displacement according to Eqs. (2.17) and (2.18).

The substrate for the third type of arrangement is a very thin polymer membrane. It is known in the industry as a *pellicle*. Due to its negligible thickness of only a few micrometers, it introduces neither aberrations nor an offset. Of course, it is

Figure 9.6 Pellicle filters and beam splitters mounted in metal rings.

fragile and must be handled with special care. Today, pellicles are also used as beam splitters in the infrared spectrum.

Figure 9.6 shows commercially available pellicles.

9.5.2 Angular sensitivity of filters

There is a shift in wavelength when a filter is tilted. This is expressed as

$$\lambda_\alpha = \frac{\lambda_0}{n_e}\sqrt{n_e^2 - \sin^2\alpha} \tag{9.8}$$

Term n_e is the "effective" index of refraction, which is related to the indices of the film layers and the substrate. Table 9.1 shows the shifts for an effective index $n_e = 1.5$ and a wavelength $\lambda_0 = 0.5$ μm at a temperature of 20°C.

9.5.3 Effect of placing a filter in a converging or diverging light bundle

Recall that if a filter is placed in a diverging or converging bundle of light, there will be a certain amount of spectral

Table 9.1 Shift to shorter wavelength with increasing tilt angle.

Angle α (deg)	0	10	20	30	40	50	60
Wavelength λ_α (μm)	0.5	0.497	0.487	0.471	0.451	0.429	0.408
Shift $\Delta\lambda$ (μm)	0	0.003	0.013	0.029	0.048	0.070	0.092

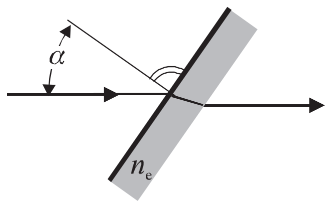

Figure 9.7 Illustration of terms used in Eq. (9.8).

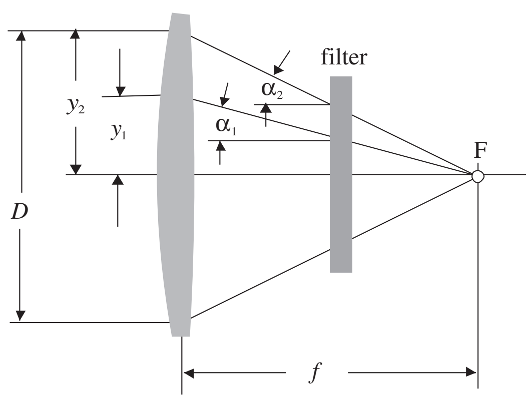

Figure 9.8 Filter inserted in a converging beam.

detuning due to the changing ray angles within the bundle, which is apparent from Eq. (9.8) and illustrated in Fig. 9.7.

Figure 9.8 shows an arrangement in which a filter is positioned in the converging beam of a 100-mm focal length lens with an F-number of 1. The filter has an index $n_e = 1.5$. The wavelength shifts from $\lambda_0 = 0.5$ μm are indicated in

Table 9.2 Wavelength shift due to the change in traveling direction of rays exiting a convex lens.

Ray #	Height position y	tan α	sin α	Wavelength λ (μm)
0	At the axis	0	0	0.5
1	25 mm	0.25	0.243	0.4934
2	50 mm	0.50	0.447	0.4778

Table 9.2, with reference to the ray on the optical axis which passes through the filter in a perpendicular direction.

One of the other two rays passes through the edge of the lens and another passes half way in-between.

It is also important to remember that in addition to this detuning effect, a plane parallel plate also introduces spherical aberration, as noted in Chapter 2.

9.5.4 Thermal sensitivity

Increasing temperature causes the indices of the film layers and their thicknesses to increase. Increasing temperature also results in an increase in wavelength. This is the opposite effect as that observed with the angular position response.

The mathematical relation is

$$\lambda_t = \lambda_0 + \gamma \Delta t, \tag{9.9}$$

where γ is the temperature coefficient, which can vary from approximately 5×10^{-5} to 12×10^{-5} (μm/°C).

Example

A narrow bandpass filter was designed and manufactured for a center wavelength of $\lambda_0 = 0.5$ μm. As usual, 20°C (68°F) was the reference temperature. After the filter was produced at that temperature, it was discovered that the intended application was for an environment with a temperature of 45°C. In that situation, the center wavelength shifts according to Eq. (9.9) as

$$\lambda_t = \lambda_0 + \gamma\Delta t = 0.5 + [(12 \times 10^{-5}) \times 25] = 0.5 + 0.003$$
$$= 0.503\ \mu\text{m},$$

where the temperature coefficient $\gamma = 12 \times 10^{-5}$.

The question to be answered is whether it is possible to correct for that spectral shift by tilting the filter.

Approach to a Possible Solution

We know that by tilting the filter, the wavelength will shift to a lower value. We determined that the effective index $n_e = 1.5$. With this knowledge, we can compare and find whether there is a solution.

We insert the known values into Eq. (9.8) and solve for the tilt angle α

$$0.500 = \frac{0.503}{1.5}\sqrt{1.5^2 - \sin^2\alpha},$$
$$\left[\frac{0.500 \times 1.5}{0.503}\right]^2 = 1.5^2 - \sin^2\alpha$$
$$\sin\alpha = \sqrt{1.5^2 - 1.491054^2} = 0.163582.$$

The tilt angle $\alpha = 9.414845° = 9°\,24'\,53''$.

9.6 Absorption

One must be aware that energy that is neither transmitted nor reflected is absorbed by the optical element. This is of course the case with metal mirrors, where there is no transmittance and the reflectance is never 100%.

Therefore, in that case the radiation that is not reflected is absorbed and causes an increase in the temperature of the mirror substrate. Another very pronounced example is germanium, the lens material used in the longwave infrared (LWIR) spectral region. The absorption greatly increases with the rise in temperature. As an example, for a 10-mm-thick, uncoated Ge lens at 25°C (77°F), the transmission at 10.6 μm (CO_2 laser) is 45.72%, the reflection 52.18%, and the absorption is 2.10%.

At 100°C (212°F), the absorption increases to approximately 60%, and at 200°, the lens will become "blind." The absorbed energy will be reradiated according to thermal laws.

9.7 Interference

The design of many filters and reflective coatings function on the basis of interference, whereby light waves are altered as they collide. This is comparable with the behavior seen when two circular water waves meet, which can be demonstrated by throwing two stones relatively close to each other into calm water. One can observe reinforcement and cancellation. There is a doubling of the amplitude at one extreme and total cancellation on the other, shown graphically in Fig. 9.9.

Application Example

A typical application for a narrow bandpass filter (spike filter) is a non-dispersive gas analyzer, where the very narrow transmission slice is spectrally matched with the absorption band of the gas, the concentration of which must be measured. Figure 9.10 shows an arrangement in which clean air serves as a reference. With the aid of a modulator (rotating chopper), the transmission of the energy from an infrared source is alternately guided through the clean air reference and the sample chambers, and passed through the narrow bandpass filter onto the detector. The signal difference recorded between the two

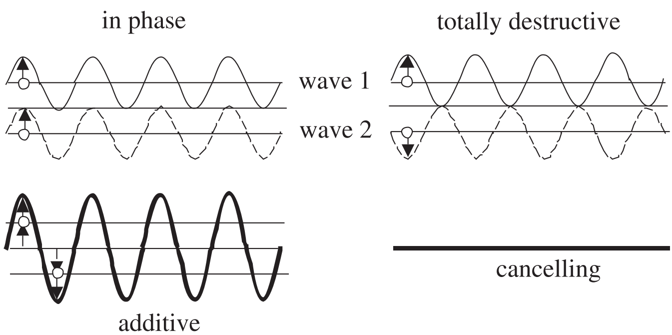

Figure 9.9 Reinforcement and total destruction of two waves.

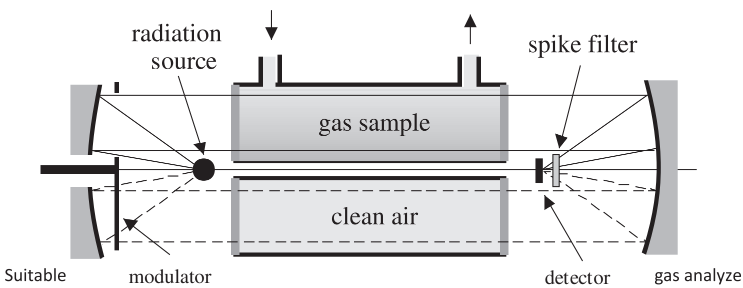

Figure 9.10 Suitable gas analyzer arrangement using a narrow bandpass filter.

measurements is the indicator of the gas concentration. The higher the concentration, the lower the signal received from the sample channel.

Such an arrangement is used to measure the exhaust gases from automobiles, whereby the design is extended to include filters for carbon monoxide (CO) at 4.7 μm, and for the unburned hydrocarbons (HCs) at 3.4 μm. In some cases there is even a third filter incorporated to measure the carbon dioxide (CO_2) at 4.3 μm.

Chapter 10
Manufacturing Processes

10.1 Introduction with Historical Remarks

For centuries the process of generating and finishing optical surfaces remained unchanged. The only suitable surface shape was a flattened sphere with an infinite radius.

Whereas it was well-understood that an aspheric surface would eliminate spherical aberration, it was simply too difficult to produce such a surface routinely.

There have been many changes since then, especially during the second half of the past century. There are now several methods available to produce not only rotationally symmetrical aspheres, but also (as previously mentioned) freeform optical elements.

For economic reasons, the spherical surface is still the most common surface. Therefore, more detailed attention will be given in our discussion to this category. This is also in line with the purpose of this text.

10.2 Conventional Generation of Spherical Surfaces

Figure 10.1 shows the typical setup for generating a spherical lens surface. The rough lens blank is mounted in a suitable fixture on top of a slowly rotating spindle. A diamond cup

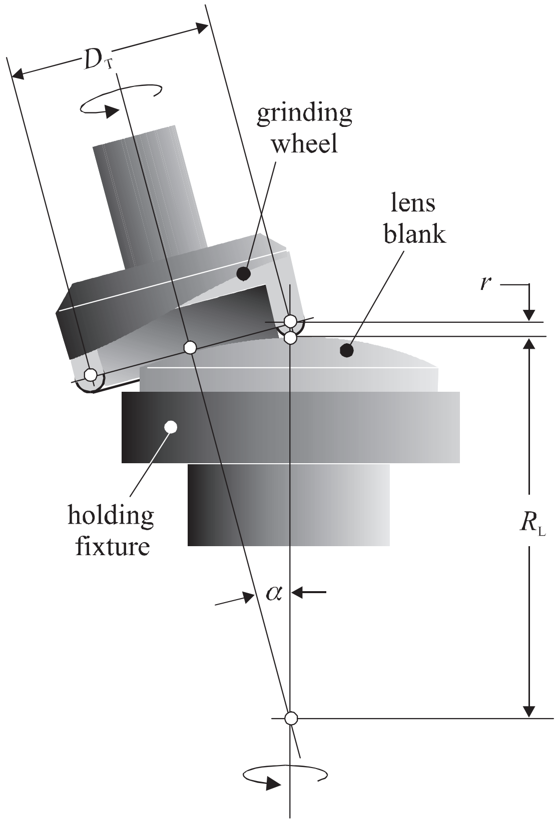

Figure 10.1 Conventional lens generation of spherical surfaces.

grinding wheel, rotating with high speed about a tilted axis, generates the desired spherical surface. Usually, the grinding cup has a rounded profile at its cutting end. The mathematical relation is expressed by

$$\sin \alpha = \frac{D_T}{2(R_L + r)}. \tag{10.1}$$

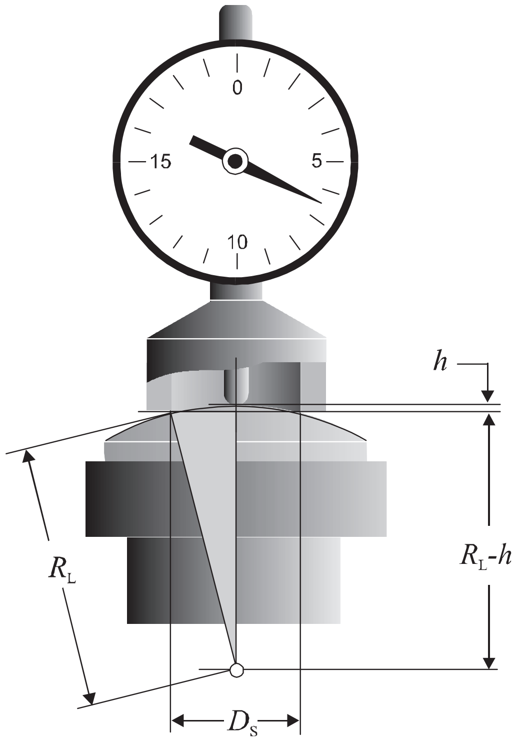

Figure 10.2 Spherometer and its use for measuring the lens surface radius.

The terms are illustrated in Fig. 10.1. Term D_T is the grinding tool diameter, R_L is the surface radius of the lens to be generated, r is the grinding wheel edge radius, and α is the tilt angle of the grinding tool spindle.

To measure the radius, a spherometer, as shown in Fig. 10.2, is used. The principle of a spherometer is easily understood according the Pythagorean relation

$$R_L^2 = (R_L - h)^2 + (D_T/2)^2. \qquad (10.2)$$

Applying again the Pythagorean theorem to the setup shown in Fig. 10.2 results in a relation that is conveniently used to determine the lens radius R_L from the measurement of the sag height h. The sag, or sagittal height h, is also termed in this case the vertex depth.

The contact diameter of the spherometer ring is D_S

$$R_L = \frac{h}{2} + \frac{D_S^2}{8h}. \tag{10.3}$$

Example

In this example, we first determine the tilt angle α of the grinding spindle. Then we measure the generated lens surface with the spherometer.

The grinding tool diameter $D_T = 50$ mm, the small tool edge radius $r = 2.5$ mm, and the lens radius R_L that we want to generate is 150 mm.

Sequence

With the given and chosen parameters, the sine of the tilt angle

$$\sin\alpha = \frac{D_T}{2(R_L + r)} = \frac{50}{2(150 + 2.5)} = 0.1639344.$$

$\alpha = 9.4353387\ \text{deg} = 9°\,26'\,7''$.

When the sag height h was measured, it read 2.2 mm. The spherometer diameter was also 50 mm. With that, the generated lens radius R_L was

$$\frac{h}{2} + \frac{D_S^2}{8h} = \frac{2.2}{2} + \frac{50^2}{8 \times 2.2} = 143.1455\ \text{mm},$$

instead of the desired 150 mm. This means that the tool spindle was tilted too much. We check the result against Eq. (10.1)

$$\sin \alpha' = \frac{D_T}{2(R'_L + r)} = \frac{50}{2(143.1455 + 0.25)} = 0.174343.$$

This indicates an angle $\alpha' = 10.0404296$ deg or $10° \, 2'26''$.

The necessary correction is therefore to reduce the tool spindle angle by $\alpha' - \alpha = 10.0404296 - 9.4353387 = 0.6050905$ deg, which is $36'$ and $18''$.

10.3 Test Plate

After polishing the surface, it can be checked for curvature with a precision test plate. Such a check is based on the principle of interferometry. When the curvatures of two surfaces are nearly identical, an interference pattern can be observed. As indicated in Fig. 10.3, when illuminated from above with a monochromatic light source and viewed in a perpendicular direction, the interference pattern can be seen. If the lens surface is spherical, the pattern consists of concentric rings named after *Isaac Newton*.

The relation between the radius difference ΔR and the observed number of Newton's rings n, also termed *fringes*, is expressed as

$$\Delta R_L = 4\lambda \left(\frac{R_T}{D_L} \right)^2 n. \tag{10.4}$$

Example, continued

When the lens radius was checked with a test plate after polishing, five Newton's rings were counted over the

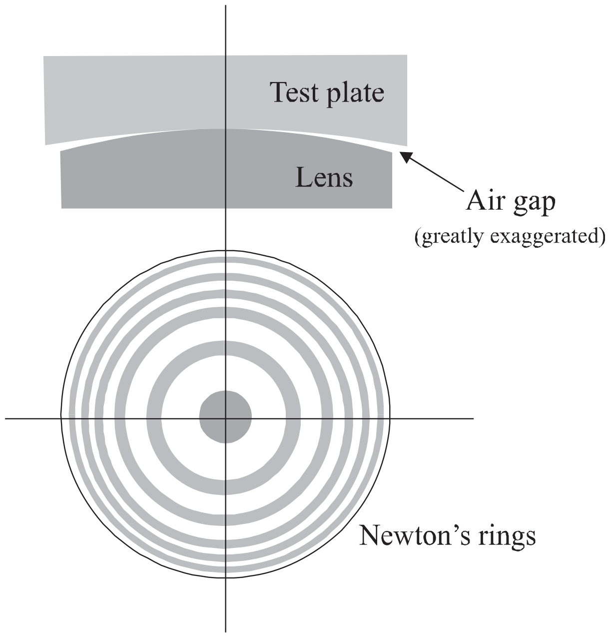

Figure 10.3 Checking a polished lens with a test plate.

60-mm lens diameter. The test plate contacted the lens in the center. Therefore, one knows that the lens radius is smaller than that of the test plate. The light source was a helium–neon laser, the most frequently used source for such applications. Its wavelength $\lambda = 0.6328\ \mu\text{m}$.

Equation (10.4) reveals

$$\Delta R_L = 4\lambda \left(\frac{R_T}{D_L}\right)^2 n = 4 \times 0.6328 \left(\frac{150}{60}\right)^2 \times 5 = 79\ \mu\text{m}.$$

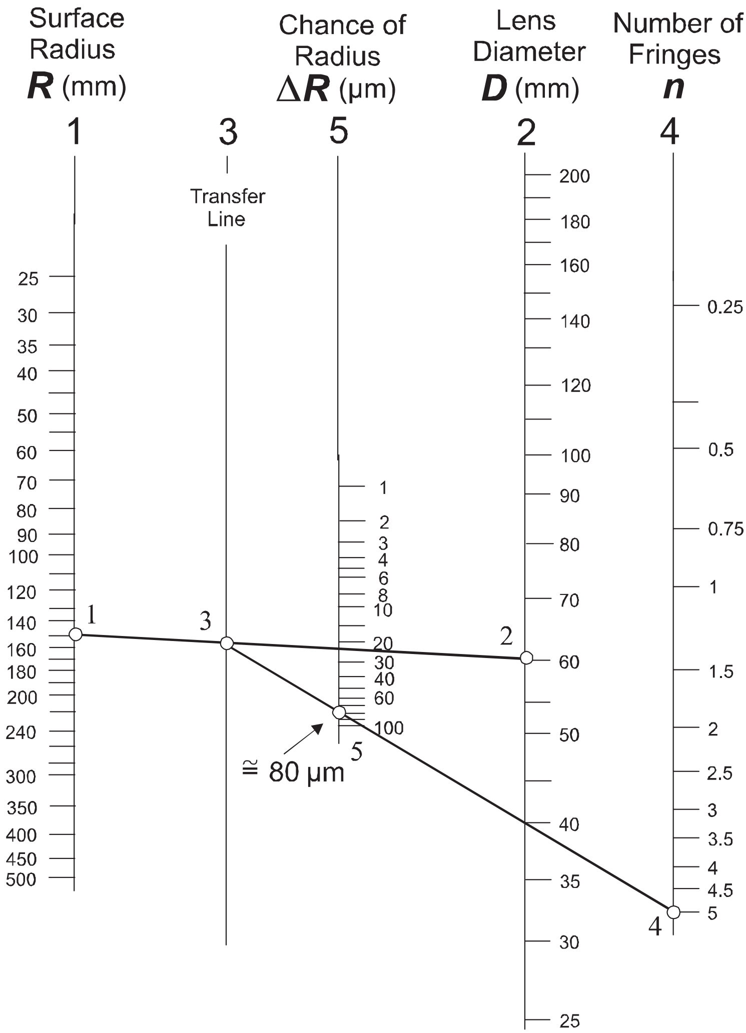

Figure 10.4 Lens radius change as a function of the fringes (Newton's rings).

10.4 Useful Nomogram

The selected case represents the aforementioned example. The first straight line between the surface radius R (150, point 1) and lens diameter D (60, point 2) establishes point 3 on the transfer line. The second straight line between point 3 and the number of the fringe scale n (5, point 4) intersects the ΔR-scale at point 5, which is the answer to the question ($\Delta R \cong 80$ µm).

Question

How does such a variation influence the performance of a lens?

To answer this question, we analyze a diffraction-limited lens with a diameter $D_L = 60$ mm and a second surface radius of $R_2 = -150$ mm. These are the dimensions from our aforementioned lens. Then we alter the design by taking the five Newton rings into consideration, which indicates that the second radius was found to be $R_2 = R_2 + \Delta R_2 = -150 + 0.079 = -149.921$ mm.

To analyze the effect of this deviation, we designed a diffraction-limited lens with a rear radius of -150 mm.

We will compare the performance of the lens in which the second radius has been shortened by 80 µm (0.08 mm).

Then we will examine the effect of refocusing this somewhat degraded lens.

The performance of the diffraction-limited lens is shown in Fig. 10.5.

The performance with the second radius shortened by 80 µm is shown in Fig. 10.6.

The performance after refocusing is shown in Fig. 10.7.

Remark

These observations provide insight into the importance of manufacturing tolerances.

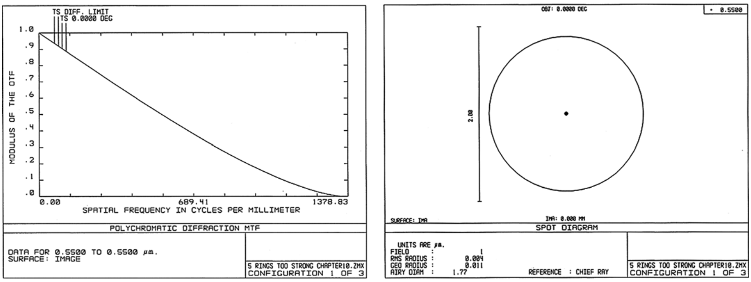

Figure 10.5 Diffraction-limited lens. Circle on the right-hand side indicates the size of the Airy disk. Its diameter is 1.8 μm.

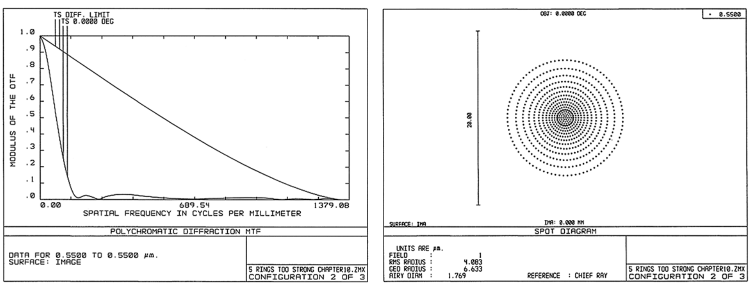

Figure 10.6 Impact on MTF due to five Newton rings of surface deviation. Blur spot diameter has grown to 13.3 μm, more than 7× the size of the Airy disk. Notice the difference in scale by a factor of 10.

General Comments

1. If the fringe pattern is not a set of concentric rings, the surface is not a sphere. Oval shapes indicate a *toroid*, which is a surface with two different radii orthogonal to each other. Waviness in the pattern refers to so-called *irregularities*, which are local deviations from a sphere.
2. In modern shops, one uses interferometers, which are measurement instruments that work on the same

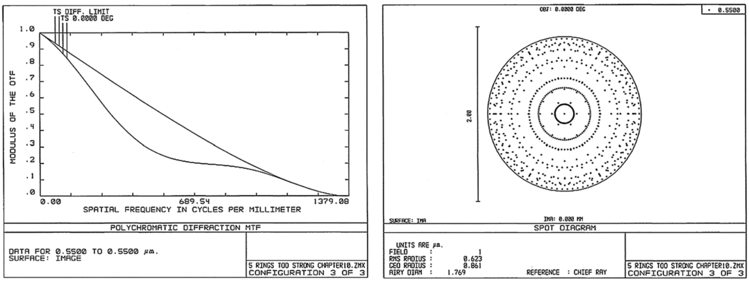

Figure 10.7 After refocusing (14 μm towards the lens) the performance improved considerably. Blur spot reduced to the size of the Airy disk.

principle as test plates, except there is no physical contact between the two surfaces.

3. Interferometers can also be equipped with computer-generated holograms, which enable measurement of aspheres and also freeform surface shapes.

10.5 Aspheric Surfaces

By definition, any surface that is not a sphere is an asphere, whether it is a conic section, rotationally symmetric, symmetric in some directions, or a completely freeform surface. Methods and machines have been developed over the years to generate these shapes successfully. Polishing is difficult when rotational symmetry no longer exists. As one can imagine, testing such freeform surfaces is especially challenging.

Much has been achieved in this polishing research field by applying the magnetorheological finishing (MRF) process. Magnetorheological finishing technology was invented and developed by an international group of collaborators at the Center for Optics Manufacturing in the mid-1990s. Other polishing processes have been applied to achieve the required surface finish. One is the ZEEKO method, which is based on jetting abrasive polishing slurry on a very small region of the surface. The position of the jet nozzle is controlled by a seven-axis computerized numerical control (CNC) machine.

These remarks indicate the difficulty associated with polishing freeform surfaces. Nevertheless, being able to create optical surfaces that send light rays in practically any desired direction is a very potent achievement. Whereas fabricating such elements may be an expensive undertaking, one must remember that the process is in general not intended for mass production, but primarily for producing molds, which are used for high-volume production of optical elements consisting of plastic and other moldable materials. Of course, there are also special cases where cost is secondary compared to the final results. One example is space exploration.

10.6 Surfaces Generated with Single-Point Diamond Turning

One method that provides extraordinary freedom in generating those difficult surfaces is the technology of single-point diamond turning (SPDT). Figure 10.8 shows an overview of the setup.

Single-point diamond turning optical surfaces is the process of mechanically machining such surfaces with the use of a single-point cutting tool, generally on a high-precision machine lathe. Flat and spherical surfaces as well as cylinders have been fabricated by this process for almost a century. To achieve the form accuracy and surface finish required for optical components, a high-precision control mechanism and high-quality bearings are needed. In the early 1970s, these improvements were achieved and diamond

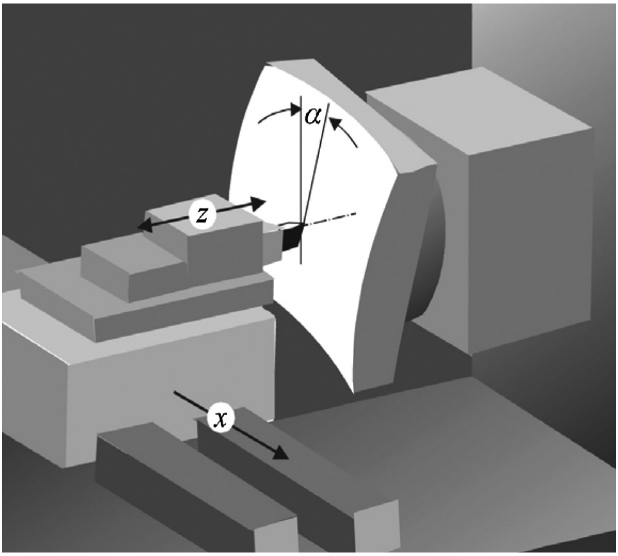

Figure 10.8 Oscillating slow tool servo. Cutting tool movement in the Z direction is a function of the rotation angle α and the lateral position X, the coordinates of which describe the freeform surface.

turning became a suitable process for generating a wide variety of rotationally symmetric surfaces, such as conic sections and other aspheres.

With continued improvements, especially relating to the tool guiding control system, it is now possible to even generate freeform shapes, as indicated previously and illustrated in Fig. 10.8.

Furthermore, it used to be required to "post-polish" diamond-turned surfaces for many applications to obtain the required smoothness. Today, a surface finish can be achieved that meets, in many cases, the demand with respect to the visible spectrum.

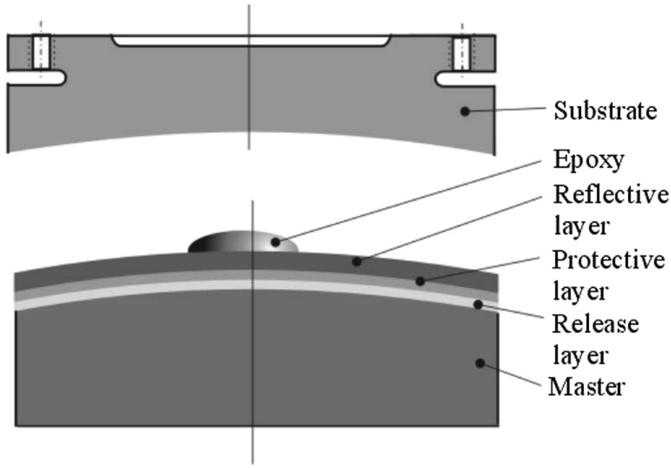

Figure 10.9 Replication process.

10.7 Replicated Optical Elements

Optical replication as we know it today began in 1949 when *John White* and *Walter Fraser*, both of Perkin Elmer, received their patent for a method of fabricating optical elements.

10.7.1 Replication process

Figure 10.9 shows the details of the replication process as it applies to fabricating a reflector. A *master*, frequently fabricated from Pyrex, is first coated with a release layer, which is a component that serves to tack the layers to be transferred to the substrate. This release layer remains, in general, a company-proprietary mixture. Figure 10.10 shows the finished product after the transfer of the reflective and protective layers onto the substrate.

After cleaning the master, it is ready for the next replication. With proper attention and careful handling, many

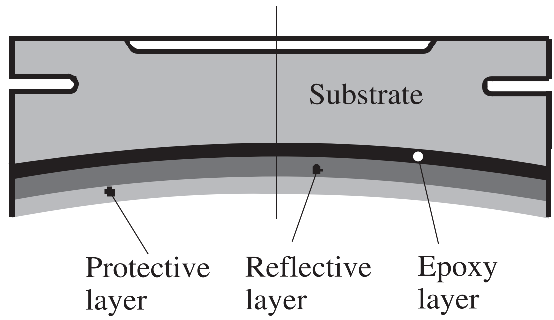

Figure 10.10 Replicated product.

replicas can be produced before the master must be refurbished.

One must ensure that the replicated surface is as smooth as that of the master. Therefore, even applications in the ultraviolet spectrum are possible if the master is prepared to meet such a demand.

In general, many if not most replicated mirrors are flat and serve as scan mirrors. In some cases they are exposed to high accelerations, where they are ideal because they are integrated and part of the mechanical structure.

10.7.2 Lenses

Whereas the replication process was explained in terms of a reflector, it has been used successfully over many decades for aspherizing lenses to eliminate spherical aberration. For this purpose, a thin epoxy shell is attached to a glass lens, which in this case is the substrate. To accelerate the curing process of the epoxy shell, UV-curing adhesives are applied. Figure 10.11 shows a very unique example, an aspherized sphere as it was produced back in 1987.

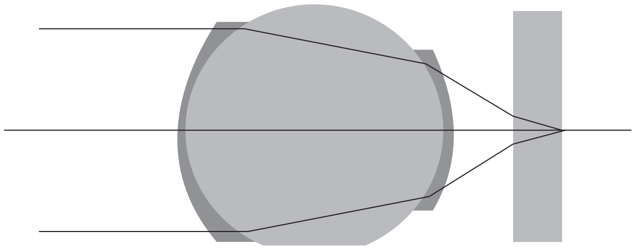

Figure 10.11 Glass sphere with aspheric replicated epoxy shells to serve as a microscope objective.

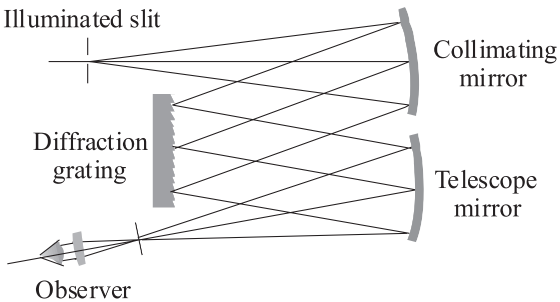

Figure 10.12 Reflective grating spectrometer.

10.7.3 Diffraction gratings

To separate white light into its color components, as described in Chapter 2, diffraction gratings can also be used. There are two basic types: transmissive and reflective gratings. The basic structure of such gratings is very narrowly spaced slits or grooves, which disperse the light into its components. Figure 10.12 shows the arrangement of a reflective grating spectrometer.

There are approximately 600 grooves/mm in such a grating, which means one groove is only 1.67 μm wide.

Producing such gratings mechanically by cutting the grooves one-by-one on a so-called ruling engine is expensive. One can imagine that the ability to replicate such reflective gratings changed an entire industry. This happened in the early 1950s.

To get a good idea of the scale and performance of a reflective grating, one must simply hold a compact disc (CD) under the proper angle to observe the beautiful pure spectrum of the light. These grooves are of the aforementioned dimension, 1.67 μm. This means that there are more than 20,000 grooves on a standard compact disk.

In closing the subject of diffractive elements, one must include that this technique is commonly applied in the infrared region, where the grooves are circularly arranged on lens surfaces to primarily correct chromatic aberration.

The basic principle for chromatic aberration correction with this scheme lies in the fact that a circular diffractive profile focuses the longer wavelengths closer to the lens than the shorter wavelengths. This is the opposite principle of a refractive lens. Properly combing these two features leads to color correction, schematically indicated in Fig. 10.13.

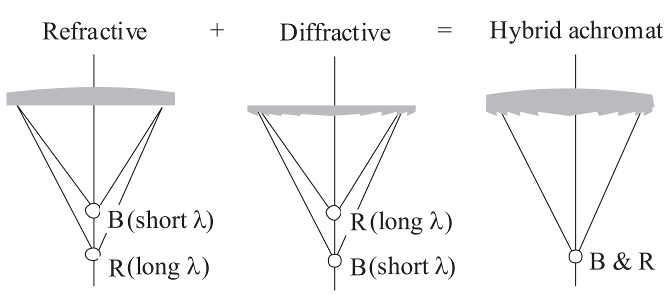

Figure 10.13 Principle of combining refractive and diffractive powers for color correction.

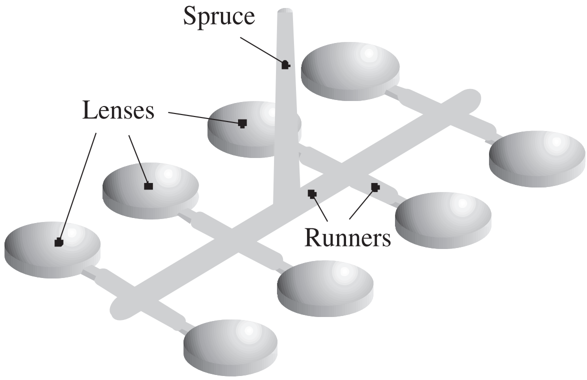

Figure 10.14 Preferred molding arrangement of plastic lenses.

10.8 Molded Plastic Optical Elements

The injection molding process is the primary method for producing plastic lenses. A typical arrangement of multiple-element molding is indicated in Fig. 10.14.

After separation of the lenses from the runners, the remaining "Christmas tree," as the material feeder system is often termed, should not be used again to mold other lenses, because of the change in the refractive index during material recycling.

There are many advances that are linked to molded plastic lenses, including their cost, weight, and the possibility that mounting features and other extensions can be integrated. Surfaces of shape-forming mold inserts can be reworked or replaced. If desired, one mold may be outfitted with different inserts to produce a complete set of components for one assembly.

There are also disadvantages to plastic lenses. Very few materials are suitable for optical applications. The refractive index of available materials covers a range from approximately 1.47 to 1.61. The relative dispersion, the Abbe number, varies from approximately 30 to 57. There are several shortcomings with respect to temperature variations. The index of refraction change is approximately -12×10^{-5}/°C, and the thermal coefficient of linear expansion is 65×10^{-6}/°C. This compares, respectively, to 7.1×10^{-6} and 0.8×10^{-6} for the glass BK7. Besides the big difference in these numbers, one must also be aware of the sign reversal with a temperature increase for the index change relating to the plastic.

An important application of injection-molded optics is the automotive market, where the glass headlight components have been replaced for some time now with plastic components, taking advantage of the additional available freedom in form-shaping.

Chapter 11
Optical Bench

11.1 General Remarks

An optical bench is a basic setup to measure certain parameters of lenses and lens systems, such as the focal lengths, lens radii, and even aberrations.

We limit ourselves here to demonstrate only a few basic examples.

11.2 Basic Bench

Figure 11.1 shows a basic setup with a collimator, the function of which is to generate parallel bundles of light, simulating the condition of a target located at infinity. There are two parallel rails, which provide the means to move lens holders and other components, including a measuring microscope along the optical axis established by the axis of the collimator. There are additional attachments, such as a nodal slide and others, supporting special requirements to perform the requested measurements. There is also a precision scale attached to the rails to measure the movements of the sliding elements and the measuring devices along the optical axis. The length of the bench, which is usually several meters long, is shown at a

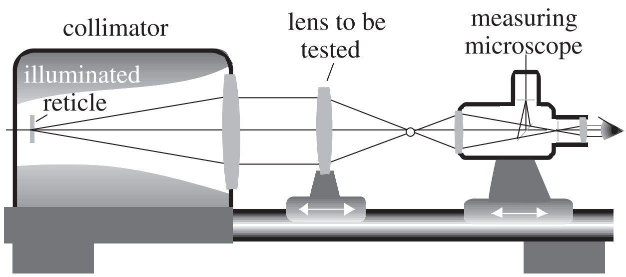

Figure 11.1 Layout of a basic optical bench.

much reduced length to fit the width of the page and still maintain clarity of detail.

The setup shown in Fig. 11.1 illustrates the determination of the focal length of a lens. The procedure is as follows.

With the knowledge of the collimator's focal length f_{coll}, the object size at the collimator's reticle h_{object}, and the image size h_{image}, measured with the aid of the microscope, there is a simple relation. The focal length f_{lens} of the lens under test is

$$f_{lens} = \frac{h_{image}}{h_{object}} f_{coll}. \tag{11.1}$$

Example

With a collimator focal length of 500 mm and object height in the collimator's reticle of 20 mm, the image height was measured as 2 mm. The focal length of the test lens is then

$$f_{lens} = \frac{h_{image}}{h_{object}} f_{coll} = \frac{2}{20} \times 500 = 50 \text{ mm}.$$

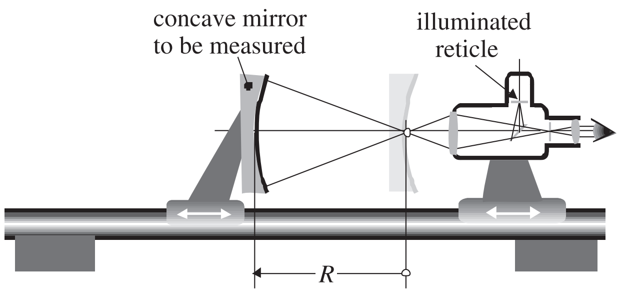

Figure 11.2 Setup for measuring the radius of a concave mirror.

11.3 Evaluating a Concave Mirror

In this example, we determine the radius of a spherical concave mirror (Fig. 11.2). First, we focus on the center of the mirror and mark the position of the mirror holder. Subsequently, the mirror holder slide is moved away from the microscope until the returned image, which is the microscope-projected reticle, or illuminated pinhole, is in focus. By this procedure, the mirror has been moved a distance equal to its radius R. The travel is indicated by the markings on the linear scale of the bench.

The same basic approach is used to determine the back focal distance of a lens or lens assembly.

11.4 Bessel's Method to Determine the Focal Length

The German astronomer and mathematician *Friedrich Wilhelm Bessel* (1784 to 1846) suggested an interesting approach to measure the focal length of a lens. However, it has certain shortcomings with respect to accuracy. Because it provides an opportunity for a good derivation exercise, we present his method here with a numerical example. Figure 11.3 shows the required setup.

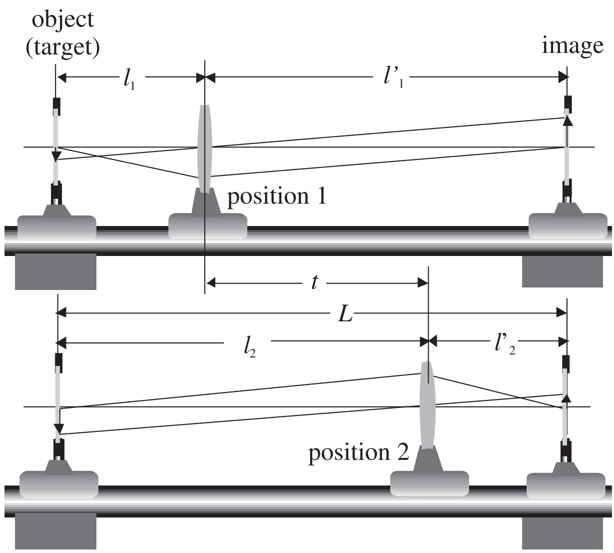

Figure 11.3 Setup for Bessel's method to determine the focal length of a lens.

Procedure

1. Place the target (object) and the image screen at the bench, separated by a distance L, which must be larger than $4\times$ the focal length of the lens to be tested.
2. As shown in the upper part of Fig. 11.3, move the lens into position 1, which is where the image seen at the screen is the sharpest. Mark the position of the lens as read out on the bench scale.
3. Now move the lens slide to the right until the image at the screen appears sharp again. This is position 2 as shown in the lower part of the sketch. The lens is now exactly the same distance from the image screen as it was in position 1 from the target (object). The distance from position 1 to position 2 is the measurement of the separation t.

With the knowledge of L and t, the focal length f_{test} can be calculated with the equation

$$f_{test} = \frac{L^2 - t^2}{4L}. \tag{11.2}$$

Exercise

Derive the previously stated equation.

Approach and Solution

To satisfy Eq. (2.10), which was $1/l' = (1/l) + (1/f)$, we must determine the distances l and l'.

With reference to the upper part of Fig 11.3, it can be seen that $l_1 = (1/2)(L - t)$. Furthermore,

$$l_1' = t + \frac{1}{2}(L - t) = t + \frac{L}{2} - \frac{t}{2} = \frac{1}{2}(L + t).$$

We rearrange Eq. (2.10) to read $1/f = (1/l_1') - (1/l_1)$ and substitute to yield

$$\frac{1}{f} = \frac{2}{(L + t)} + \frac{2}{(L - t)} = \frac{2(L - t) + 2(L + t)}{(L + t)(L - t)}$$
$$= \frac{2L - 2t + 2L - 2t}{(L - t)^2} = \frac{4L}{(L - t)^2}.$$

The reciprocal is then

$$f = \frac{(L^2 - t^2)}{4L} \quad \text{(q.e.d)}.$$

Example

In analyzing a lens, we opted to set $L = 500$ mm, and measured $t = 100$ mm.

The focal length of the lens is therefore

$$f = \frac{(L^2 - t^2)}{4L} = \frac{(500^2 - 100^2)}{4 \times 500} = \frac{240{,}000}{2000} = 120 \text{ mm}.$$

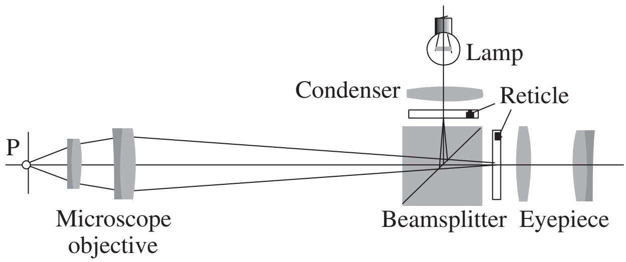

Figure 11.4 Autoreflecting microscope.

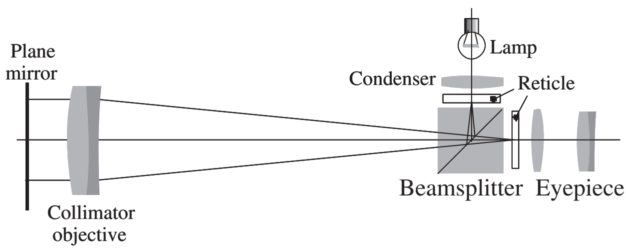

Figure 11.5 Autocollimator.

11.5 Autoreflecting Microscope and the Autocollimator

Figure 11.4 shows a more detailed cross section of the microscope used for measurements made on an optical bench.

The reticles are either simply cross hair lines, scales, or have other suitable patterns. At the illuminating side, a pinhole aperture may be the best choice for the task. At point P the light is reflected and redirected to the eyepiece. This is the method used in the case discussed in Sec. 11.3. Note that the reflecting surface must not necessarily be a plane.

The objective, which forms an image at its focal plane, turns this instrument into an autocollimator. The light is reflected from a plane mirror surface, as indicated in Fig. 11.5.

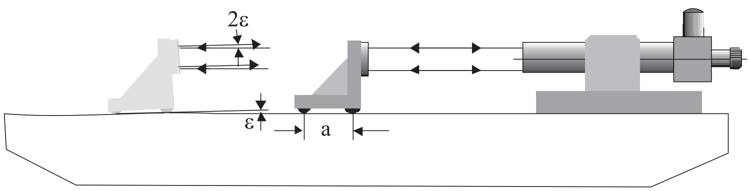

Figure 11.6 Checking the straightness of a surface with an autocollimator.

Figure 11.7 Total profile.

A typical application for an autocollimator is to check the straightness of a surface. This is demonstrated in an exaggerated manner in Fig. 11.6.

Procedure

A flat mirror is moved along the surface to be measured and readings of the angular shifts 2ε are taken in intervals of *a*, the distance between the support points of the mirror. Figure 11.7 shows a greatly exaggerated combined effect over the total length.

Chapter 12
Mounting Optical Components

12.1 Declaration

Paul Yoder stated it precisely in the preface of the first edition of his book, *Opto-Mechanical Systems Design* (M. Dekker, 1986), with the sentence,

"In the design of any optical instrument, optical and mechanical considerations are not separate entities, they are merely two phases of a single problem."

This is immediately recognizable by looking at one of his illustrations (Fig. 12.1), which shows the assembly of an eyepiece.

We will limit ourselves here to some fundamental mounting techniques of optical components and note the integration possibility with metal mirror systems.

12.2 Basic Lens Mounting Methods

There are some basic methods for securing lenses in their mounts. Three of them are shown in Fig. 12.2.

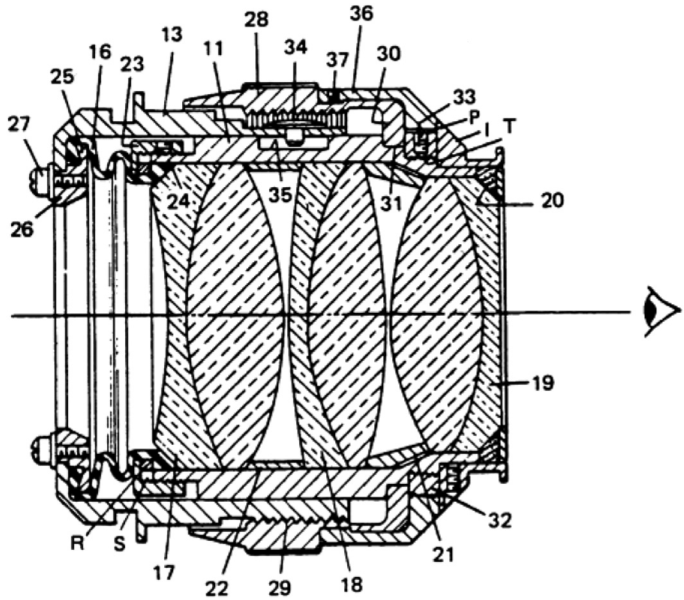

Figure 12.1 Yoder's opto-mechanical layout of an eyepiece.

Probably the most frequently used mounting method is shown in case 1, where a threaded lock ring secures the lens in its mount. In the second sketch, a spring ring is employed to hold the lens in place. The third layout suggests that the lens is

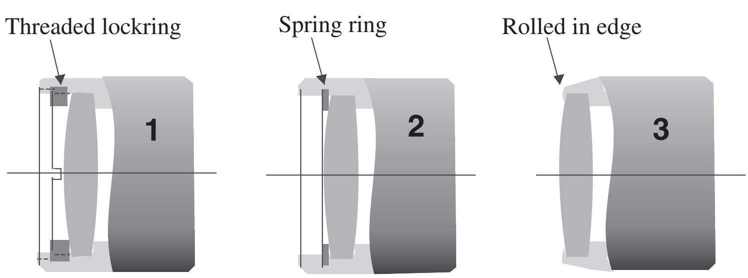

Figure 12.2 Common lens mounting techniques.

held by a brim, which is roll-formed on a lathe. This type of lens securing was commonly used when housings consisted of brass. Recall that aluminum and plastic appeared much later, and adhesives were introduced as an additional method to mount lenses and other optical elements.

12.3 Plastic Lenses and Mounts

With respect to plastics as mounting or housing material, there is first the advantage of shaping the elements for effective integration, as indicated in Fig. 12.3. This sketch shows the layout of the Kodak *Starmatic* camera optics as it was produced in the millions at the middle of the last century. The second lens is imbedded in the structure of the front element. The darker shade of the negative second lens element indicates that it is comprised of a different material than the first element. It has a higher refractive index and a lower Abbe number to correct chromatic aberration. Typical plastic materials for such an achromatic assembly are acrylic for

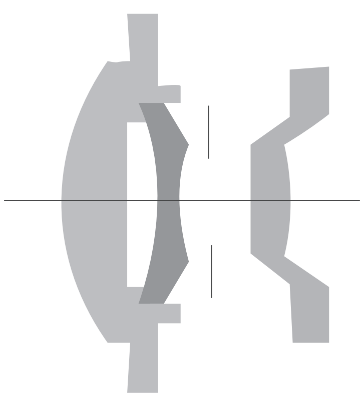

Figure 12.3 Three-element plastic *Starmatic* camera objective.

the positive lens with an index $n_d = 1.491$. The Abbe number for this material is $\nu = 57.2$. The negative element, the second lens consists of styrene with an index $n_d = 1.59$ and Abbe number $\nu = 30.8$. The location of the aperture stop is also shown in the figure.

A second example shows the use of a split assembly housing, which allows one to position the elements properly. In this case, the lenses can of course be comprised of glass or other suitable materials. They are held in place by flexible lips. The identical second shell is then placed on top and the two parts are cemented together, as indicated in Fig. 12.4.

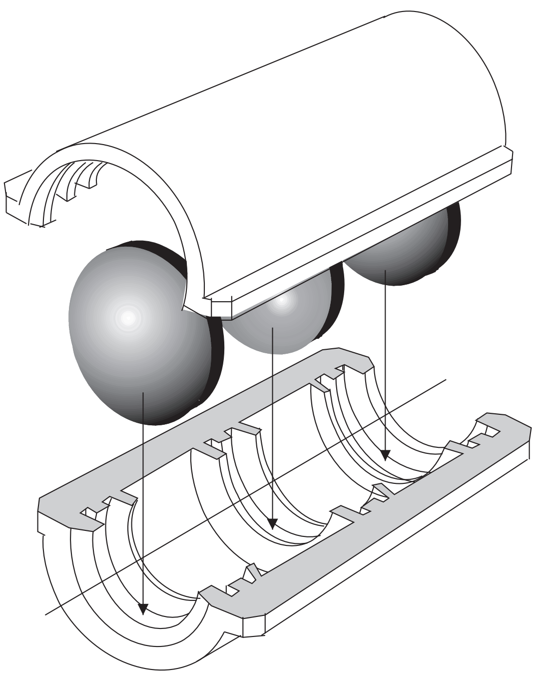

Figure 12.4 Clam shell mounting of lens elements.

12.4 Mirrors

Round mirrors are usually mounted in a similar manner as lenses. Other mirrors are either mounted spring-loaded or pressed against some soft pads. When flat mirrors are small in size, they are frequently glued onto a metal mount. Both suggestions are shown in Fig. 12.5.

12.5 Prisms

Besides clamping (one example is shown in Fig. 12.6), arrangements are used whereby the prism is bonded to a stud and then secured in a suitable mounting structure with screws or other fasteners (indicated in Fig 12.7).

12.6 Metal Mirrors

Replicated mirrors, and especially diamond-turned mirrors, provide freedom of design with respect to configuration, limited only by one's imagination. Whereas a surface smoothness, suitable even for the ultraviolet spectral region, can be achieved by the replication process, there are some difficulties in attaining alignment requirements in the transfer process of the epoxy and the coating stack.

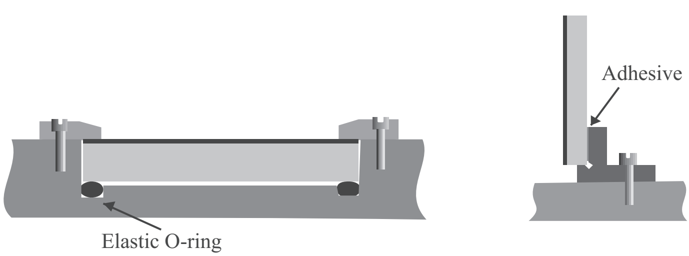

Figure 12.5 Two suggestions for mounting mirrors.

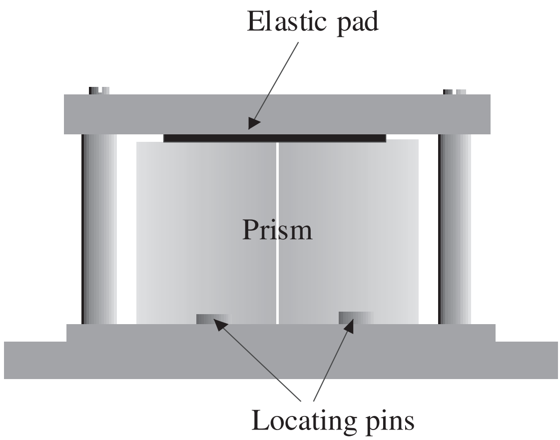

Figure 12.6 Clamped prism positioned by locating pins.

This problem is not a factor with respect to single-point diamond turning; however, the surface finish is of lower quality. Nevertheless, without post-polishing, the demand for the visible spectrum can be met, which has been mentioned in Ch. 9.

Figure 12.8 shows a design of this type, a monolithic collimator which was been manufactured some years ago for the infrared spectrum.

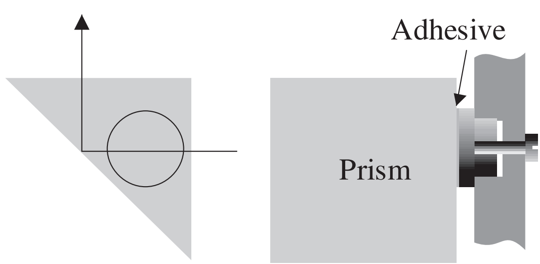

Figure 12.7 Prism bonded to a metal stud.

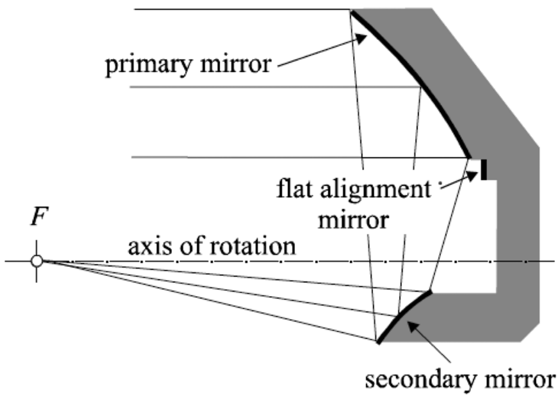

Figure 12.8 Monolithic collimator, fabricated from aluminum.

The importance of the flat alignment mirror must be noted. As the name implies, its purpose is to help align the system. This is achieved by *squaring on*. An autocollimator is positioned and angularly adjusted until the returned image from the flat alignment mirror section of the monolith coincides with the projected reticle mark (cross hair). The optical axis of the autocollimator is now parallel to the axis of the reflective collimator. Moving either system only laterally until the full autocollimator aperture falls within the primary mirror's area will facilitate location of the reflector's focal point, whereby a screen is moved along the optical axis, indicated in Fig. 12.8 as the axis of rotation.

This clever configuration allowed one to not only produce two of the systems in one setup in the lathe, but also provided the required balancing effect for the machining process. This ingenious scheme was the creation of my good friend and college, *Dieter Korsch*, who has left us all too early.

The system was produced by Corning, which provided the photo.

12.7 Thermal Effects

Materials expand at different rates with increasing temperature. In addition, the refractive index of the optical substrates changes.

The combined effect of a lens consisting of BK7 with a 100-mm focal length, mounted in an aluminum housing, is a focus shift of +0.1 mm when the assembly is exposed to a temperature increase of 40°C (72°F). The shift of a germanium lens under the same conditions is 6× as large.

By selecting a suitable material for the housing, increasing the number of lens elements with different characteristics, correction within limits can be achieved. This is known as *passive athermalization*.

Active athermalization is a method by which the position of the optical elements within an assembly is changed. These shifts are actuated by a drive mechanism which responds to the temperature changes. Such arrangements are primarily used for infrared systems, as can be imagined by the comparison noted in the aforementioned example.

An exception is if the system consists of only one material, as is the case in the diamond-turned collimator design shown

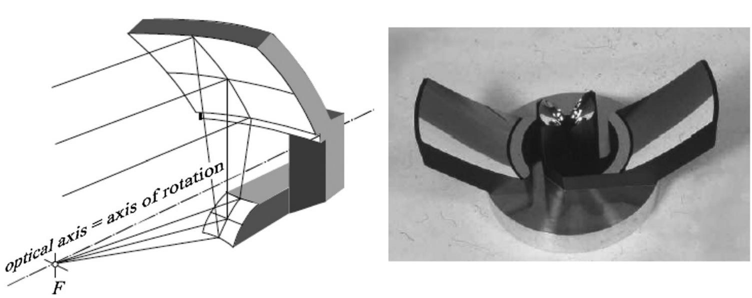

Figure 12.9 Three-dimensional view and dual setup for balanced setup during machining.

in Fig. 12.9. The aluminum structure simply expands uniformly, and consequently there is only a scaling effect.

With an expansion coefficient of $\alpha_{alu} = 24 \times 10^{-6}$ (mm/mm)/°C, the entire assembly "grows" by a factor of 1.000024/°C.

If a system is exposed to temperature differentials, which occurs when, for example one side is unprotected against sunshine and the other is in the shade, much damage occurs. Actual "bending" of the optical axis ensues and one can imagine the problems that arise.

If necessary and possible, the best solution is of course to install the entire system in a temperature-controlled housing.

Chapter 13
Exercises with Elaborations

In this Section we shall present exercises with discussions referring to the subjects covered in all of the chapters.

13.1 Exercise 1.1

Sunlight requires 500 s to reach the Earth, but light requires only 1.25 s to travel from the Moon to the Earth. Interestingly, both subtend an angle from the earth of approximately 32 min arc. ($\approx 1/2$ deg).

Question

How far are the Sun and the Moon from the Earth, and what are their diameters?

Answer

Knowing that the speed of light is approximately 300,000 km/s, the distance to the sun $d_{sun} = v_{light}\,t = 300{,}000 \times 500 = 1.5 \times 10^8$ km. The distance to the moon $d_{moon} = v_{light}\,t = 300{,}000 \times 1.25 = 375{,}000$ km. This is a

Figure 13.1 Solar eclipse.

ratio of 400:1, easy to remember. To convert arc minutes into radians, recall that 180 deg are π radians (the circumference of a circle being 2π), and 1 deg has 60 arc min. Therefore, 32 arc min are $[\pi/(180 \times 60)] \times 32 = 0.00931$ rad. We multiply this value by the distance to the sun and obtain for the sun diameter $0.00931 \times (1.5 \times 10^8) \cong 1.4 \times 10^6$ km.

The fact that the moon extends at essentially the same angle can be observed during a solar eclipse, where only a peripheral glow (corona) from the sun can be seen (demonstrated in Fig. 13.1).

With this information, the diameter of the moon can be found with the ratio 400.

The aforementioned value is

$$D_{moon} = \frac{D_{sun}}{400} = \frac{1.4 \times 10^6}{400} = 3{,}500 \text{ km}.$$

With all this information, we should recall that when we watch a sunset, the sun has already past the horizon more than 8 min previously.

13.2 Exercise 1.2

In any other medium, light travels at a slower speed than it does in vacuum. The ratio of the velocity in vacuum to the velocity in the medium is termed the index of refraction. This is stated by Eq. (1.1):

$$n = \frac{v_{vacuum}}{v_{medium}}.$$

Questions

Two questions are as follows:

1. What are the velocities at which light travels through different materials at the chosen reference wavelengths?
2. How does this impact Snell's law?

Response

With respect to part 1, Table 13.1 lists different materials used in the VIS, MWIR, and LWIR spectral regions. For

Table 13.1 Velocity of light in different optical materials.

Medium (substrate)	Reference wavelength (μm)	Index of refraction n_{medium}	Velocity in medium (km/s)
Crown glass	0.5	1.5	200,000
Flint glass	0.5	1.8	166.667
Zinc selenide	4	2.4	125,000
Silicon	4	3.4	88,235
Germanium	10	4.0	75,000

simplicity, the numbers are rounded off. The speed of light in vacuum is assumed to be $v_{vacuum} = 300{,}000$ km/s. This leads to the expression

$$v_{medium} = \frac{300{,}000}{n_{medium}}.$$

With respect to part 2, to answer this question we only refer to the two extreme values in the table: the crown glass and germanium.

Equation (1.2) states Snell's law as $n' \sin i' = n \sin i$. Rearranged, it indicates the direction at which a ray travels after impinging a substrate at an angle i

$$\sin i' = \frac{n}{n'} \sin i.$$

Since we are considering that the substrate is in air, for which we substitute $n = 1$, the equation changes to $\sin i' = (1/n') \sin i$, where n' is n_{medium}, the index of the substrate. If we assume for our example the incoming angle $i = 45$ deg, we obtain

$$\sin i' = \left(\frac{1}{n_{medium}}\right)(\sin 45 \text{ deg}) = \frac{0.7071}{n_{medium}}.$$

This yields, for crown glass of $n = 1.5$,

$$\sin i' = \frac{0.7071}{1.5} = 0.4710.$$

Therefore, $i'_{crown} = 28.13$ deg.

For germanium,

$$\sin i' = \frac{0.7071}{4} = 0.17678.$$

Hence, $i'_{germanium} = 10.18$ deg.

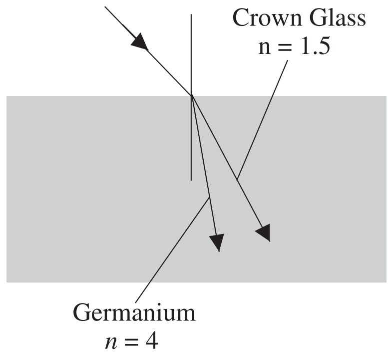

Figure 13.2 Bending of light as a function of the index of refraction.

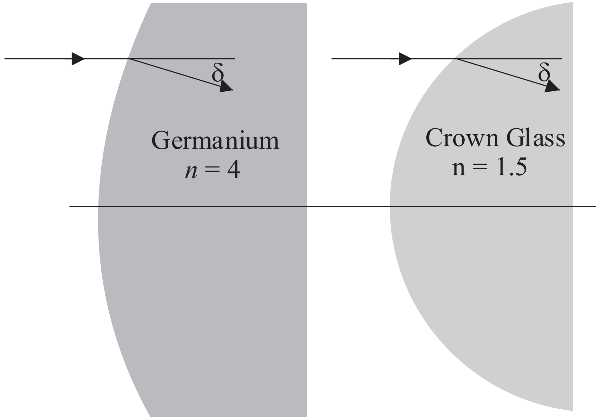

Figure 13.3 Surface radius, a function of substrate index for the same ray deviation angle.

This strong impact is depicted in Fig. 13.2.

This indicates that the radius of a lens (Fig. 13.3) can be much longer with a high-index medium compared to a lower-index medium to achieve the same directional change after refraction.

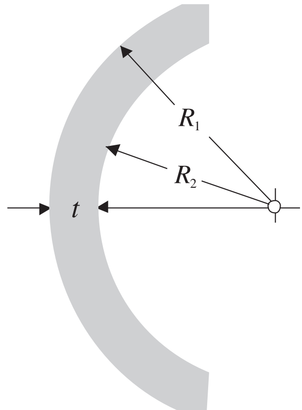

Figure 13.4 Optical dome.

13.3 Exercise 2.1

An optical dome, as used, e.g., for missiles, is typically formed by an element with two concentric spherical surfaces (Fig. 13.4). In other words, the two radii have a common center, which means that the second radius is shorter than the first radius by the thickness of the element.

Question

Does such an element have any optical power? Analyze a dome with a front radius of 50 mm and a thickness of 10 mm. The index of the glass is 1.5.

Answer

Equation (2.1) states,

$$\phi = \frac{1}{f} = (n-1)\left[\frac{1}{R_1} - \frac{1}{R_2} + \frac{(n-1)t}{nR_1R_2}\right].$$

We insert $R_1 = 50$, $t = 10$, and $n = 1.5$, and recall that $R_2 = R_1 - t = 50 - 10 = 40$. This yields

$$\begin{aligned}\phi = \frac{1}{f} &= (n-1)\left[\frac{1}{R_1} - \frac{1}{R_2} + \frac{(n-1)t}{nR_1R_2}\right]\\ &= (1.5-1)\left[\frac{1}{50} - \frac{1}{40} + \frac{(1.5-1)\times 10}{1.5\times 50\times 40}\right]\\ &= 0.5(0.02 - 0.025 + 0.0016667)\\ &= -0.0016667.\end{aligned}$$

The focal length is

$$f = \frac{1}{\phi} = \frac{1}{-0.0016667} = -600 \text{ mm}.$$

It is a dispersing lens.

13.4 Exercise 2.2

Snell's law indicates that there is a limit set by the fact that the maximal value of the sine of an angle is 1, which refers to an angle of 90 deg.

The law states that $n' \sin i' = n \sin i = \sin i'$.

When a ray travels from a dense material into air, the index $n' = 1$.

Inserting the limit of the angle, $i' = 90$ deg, and the equation reduces to $\sin i = 1/n$. At that limit, the angle $i = \arcsin(1/n)$.

We can now determine the limiting angle i for different optical materials (Table 13.2). When the angle i is larger than this limit, the ray will not exit the substrate; it will be reflected. This effect is termed *total internal reflection*.

The arrangement is shown in the sketch of Fig. 13.5.

The right-hand sketch of Fig. 13.5 indicates the limit. The dotted lines identify an internally reflected ray.

Table 13.2 Examples of total internal reflection.

Material	Glass	Zinc selenide	Silicon	Germanium
Index n	1.5	2.4	3.2	4.0
Limiting angle i (deg)	41.8	24.6	18.2	14.5

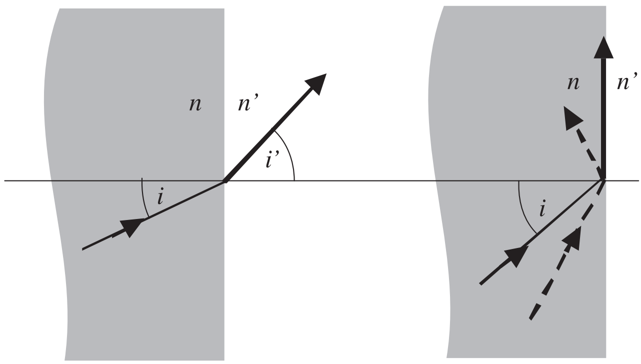

Figure 13.5 Exiting ray and limiting angle i.

13.5 Exercise 3.1

It is often helpful to analyze specific cases because they frequently lead to relationships that are easy to remember. For that reason, let us evaluate two such exceptional cases relating to the shape of a thin lens.

Questions

Two questions are as follows:

1. What is the focal length of a thin (zero thickness) equi-convex lens? This is a positive lens, the radii of which are equal but opposite in direction.

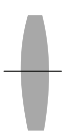

2. What is the focal length of a thin plano-convex lens? This positive lens has one curved and one flat surface.

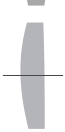

Answer to Question 1

We begin with Eq. (3.1)

$$\phi = \frac{1}{f} = (n-1)\left[\frac{1}{R_1} - \frac{1}{R_2}\right],$$

and set $R_2 = -R_1$ to describe the shape of an equi-convex lens.

This leads to

$$\phi = \frac{1}{f} = (n-1)\left[\frac{1}{R_1} - \frac{1}{-R_1}\right] = \frac{2(n-1)}{R_1}.$$

The focal length is therefore $f = R_1/[2(n-1)]$. One can see that with $n = 1.5$, $f = R_1$.

Remember that *when* $n = 1.5$, *the focal length of an* ***equi***-*convex thin lens is equal to the front radius.*

Answer to Question 2

Selecting the second surface to be flat ($R_2 = \infty$) simplifies Eq. (3.1) to read as

$$\phi = \frac{1}{f} = \frac{(n-1)}{R_1}.$$

Hence $f = R_1/(n-1)$. For $n = 1.5$, $f = 2R_1$.

Remember that *when* $n = 1.5$, *the focal length of a* ***plano***-*convex thin lens is equal to twice the front radius.*

These observations are also valid for thin equi-**concave** and plano-**concave** lenses. However, in these cases the focal lengths are negative.

13.6 Exercise 4.1

Question

How large is the minimum blur spot caused by spherical aberration of an optimally shaped thin positive lens when the object is located at infinity?

Compare the following materials for a lens with a 100-mm focal length and a relative aperture of $f/2$ (Table 13.3).

Answer

In the text, the minimum blur spot was calculated with the use of Eq. (4.3) for glass with an index of $n = 1.5$. We use the same equation and insert the appropriate indices.

The equation is

$$B_{sphere} = \frac{n(4n-1)f}{128(n-1)^2(n+2)(f/\#)^3}.$$

Inserting 100 for f and $2^3 = 8$ for $(f/\#)^3$ changes the equation to

$$B_{sphere} = \frac{n(4n-1)\cdot 100}{128(n-1)^2(n+2)\times 8} = \frac{n(4n-1)}{10.24(n-1)^2(n+2)}.$$

The results are shown in Table 13.4.

Table 13.3 Different lens materials and their indices.

Material	Glass	Zinc selenide	Silicon	Germanium
Index n	1.5	2.4	3.2	4.0

Table 13.4 Blur spot sizes as a function of the lens material.

Material	Glass	Zinc selenide	Silicon	Germanium
Index n	1.5	2.4	3.2	4.0
B_{sphere} (mm)	0.837	0.234	0.147	0.107

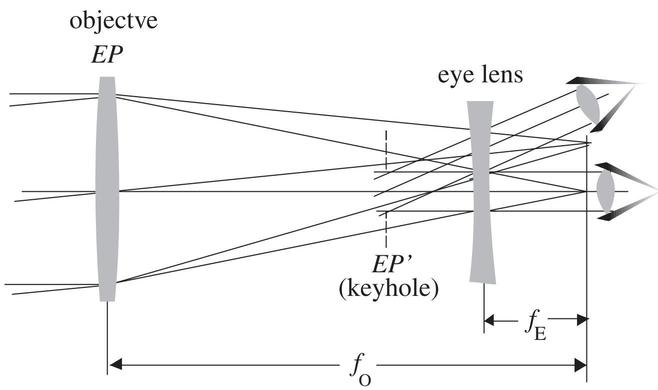

Figure 13.6 Galilean telescope.

As mentioned previously, a spherical mirror with the same focal length and relative aperture compares very favorably with

$$B_{mirror} = \frac{f}{128(f/\#)^3} = \frac{100}{128 \times 2^3} = 0.098 \text{ mm}.$$

13.7 Exercise 5.1

In this exercise, we analyze the situation that exists with respect to the location of the exit pupil in a Galilean telescope.

The basic layout is as shown in Fig. 13.6.

The location of the objective lens is also the position of the entrance pupil. Imaging via the eye lens into the image space results in a virtual exit pupil, located to the left of the eye lens, as indicated in the figure. Typically, the eye should be placed at the exit pupil of a viewing device. In this arrangement, this is not possible, as can be seen from the layout. To cover an extended field of view, the observer must position his or her eye as indicated (somewhat exaggerated) in

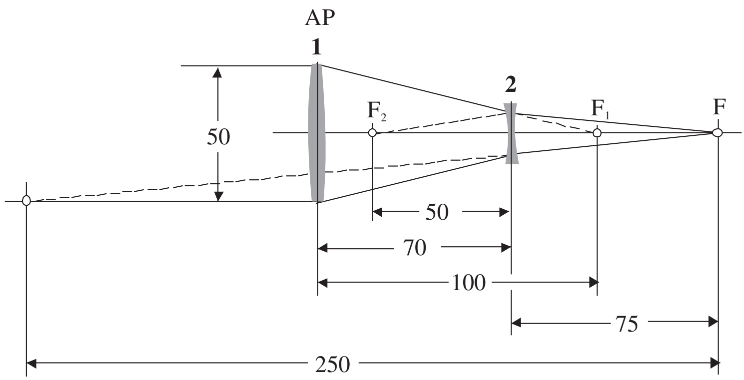

Figure 13.7 Layout of the discussed telephoto objective.

the figure. One can easily understand why this observing method is termed *keyhole viewing*.

13.8 Exercise 6.1

Calculate the focal length and the back focal length of a telephoto objective with the following components: The focal length of the positive front element is 100 mm. Behind (70 mm) the front element is the negative second element with a focal length of -50 mm. The diameter of the front lens, which is also the aperture stop, is 50 mm.

Sketch the objective.

Approach and Solution

Let us first identify the given data to match the symbols of the equations given in Ch. 6, i.e., $f_1 = 100, f_2 = -50$, and the separation of the two lenses $d = 70$ mm.

Using Eq. (6.6), we find the focal length of the system

$$f = \frac{f_1 f_2}{f_1 + f_2 - d} = \frac{100 \times (-50)}{100 - 50 - 70} = 250 \text{ mm}.$$

The back focal length, according to Eq. (6.7), is

$$bfl = \frac{f(f_1 - d)}{f_1} = \frac{250(100 - 70)}{100} = 75 \text{ mm}.$$

Remarks on the Sketch

One finds the focal length of the system by extending the exiting ray backwards until it crosses the entering marginal ray.

The focal points of the components have been identified in the sketch for additional clarity.

The relative aperture of the system $f/\# = f/D = 250/50 = 5$.

13.9 Exercise 7.1

The predominant shape of an imaging reflector is the parabola, a conic section. We analyze this profile in some detail as an example of an aspheric surface and compare it with the shape of a sphere.

Without derivations, we present the equations for the sagittal heights for a parabola and a circle, the contour of a sphere. The sagittal height is a measure of the height of an arc.

Equations

The expressions for the two shapes are as follows:

1. circle (sphere)

$$x_{sphere} = R - \sqrt{R^2 - y^2}.$$

2. parabola

$$x_{para} = \frac{y^2}{2R}.$$

Example

Let us look at a concave mirror with radius $R = 200$ mm and a relative aperture of $f/1$.

With this input, the relative aperture is

$$(f/\#) = 1 = \frac{f}{D} = \frac{f}{2y_{max}} = \frac{100}{2y_{max}} = \frac{50}{y_{max}},$$

and $y_{max} = 50$ mm.

Now we can determine the difference between the distances at the edges of spherical and parabolic mirrors.

$$x_{sphere,max} = R - \sqrt{R^2 - y_{max}^2} = 200 - \sqrt{200^2 - 50^2}$$
$$= 6.351 \text{ mm}$$

$$x_{parabola,max} = \frac{y_{max}^2}{2R} = \frac{50^2}{2 \times 200} = 6.25 \text{ mm}$$

The difference is a sizeable 6.351–6.25 = 0.101 mm.

Figure 13.8 is a schematic sketch and illustrates the principle. It is not to scale. It is exaggerated to amplify the effect.

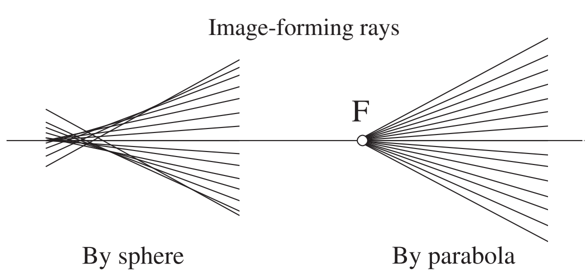

Figure 13.8 Difference between the sagittal heights between a parabola and a circle.

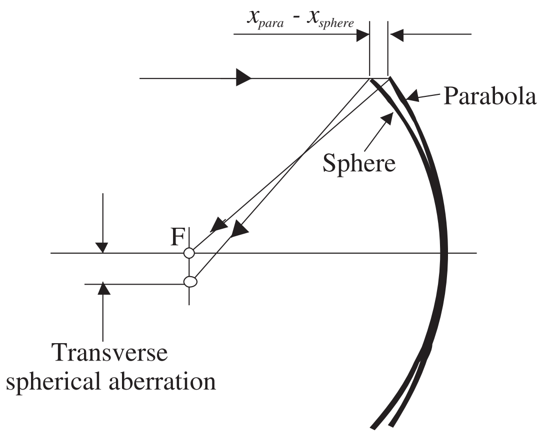

Figure 13.9 Rays formed by a spherical mirror compared to a parabolic mirror.

Figure 13.9 is an illustration of the image forming rays from a spherical mirror and a parabolic mirror. It is to scale. It is from a computer ray trace and demonstrates the optical effect, the hallmark of spherical aberration, contributed by the spherical mirror. The parabolic mirror is diffraction-limited. All rays meet at the focal point.

13.10 Exercise 8.1

Question

What is the best suitable relative aperture $f/\#$ for an imaging system that is to be used in the longwave infrared (LWIR) spectral region, when the diffraction-limited blur spot size diameter should be as large as the side of the square detector element, which is 25 μm? The reference wavelength $\lambda = 10$ μm.

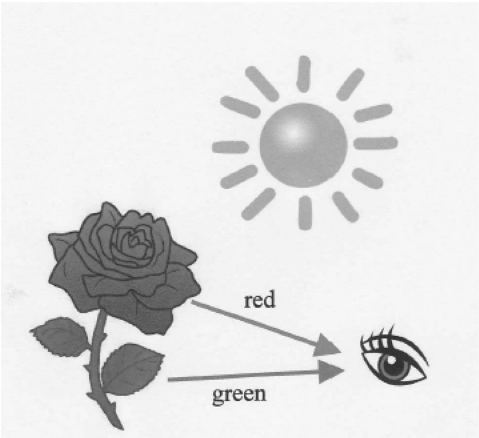

Figure 13.10 Rose illuminated by the sun, reflecting selected colors.

Answer

The diffraction-limited blur spot size, the Airy disk is, as stated in Eq. (8.1), $B_{Airy} = 2.44\lambda(f/\#)$. The request is that $B_{Airy} = 25$ μm with $\lambda = 10$ μm.

Therefore,

$$f/\# = \frac{B_{Airy}}{2.44\lambda} = \frac{25}{2.44 \times 10} \cong 1.$$

> The answer could also have been found with the help of the previously presented nomogram.

13.11 Exercise 9.1

This exercise is intended to explain why we see objects in color. We limit ourselves to the case when the illuminator is the sun (see Fig. 13.10).

Equation (9.1) states that $\tau + \rho + \alpha = 1$, which means that the sum of the transmission, reflection, and absorption must add up to 1. This applies to each individual wavelength of the spectrum. Therefore, some of the wavelengths may be reflected, whereas others are transmitted or absorbed. Therein lies the answer to why we see images in color. Let us look at a flower.

The rose blossom absorbs the orange, yellow, green, blue, and violet wavelengths emitted by the sun, and only reflects the red wavelengths. The leaves and the twig absorb all wavelengths except green, which is reflected.

The absorbed radiation changes into thermal energy and the flower becomes a radiation source.

Depending on the angle at which the sun's rays hit the flower, there may be some scattered transmission.

Scattered transmission can be compared with the scattered reflection of a rough surface. One can observe the radiation, but not an image.

For various reasons, colors are sometimes presented in print by different shades of grey as in this book. In this case, the picture reflects all wavelengths. The total intensity determines the degree of grey, which can vary from white to black.

13.12 Exercise 10.1

If the spherical surface to be measured is concave, the outside diameter of the spherometer is in contact, as shown in Fig. 13.11. This is in contrast to the case shown in Fig. 10.2, where the inner ring diameter touches the lens surface.

In the example discussed in Ch. 10, the sagittal height h of the convex surface is 2.2 mm, measured with a spherometer, the inside diameter of which is 50 mm. The resultant lens radius is 143.1455 mm.

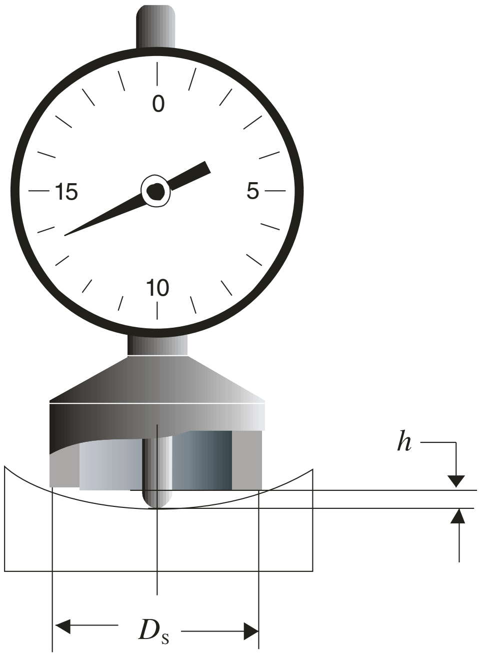

Figure 13.11 Measuring a concave surface.

Question 1

What is the radius of a concave surface with the same reading, with an outside spherometer diameter of 60 mm?

Answer

Applying Eq. (10.3) indicates that

$$R_L = \frac{h}{2} + \frac{D_S^2}{8h} = \frac{2.2}{2} + \frac{60^2}{8 \times 2.2} = 205.6455 \text{ mm}.$$

Question 2

What is the reading for the sagittal height h when the radius of the concave surface is equal, but opposite in sign, to that measured for the convex surface? In this case, $R_L = 143.1455$ mm.

Answer

Because the ring diameter of the spherometer used for this measurement is different ($D_S = 60$ mm), we find that

$$h = R_L - \sqrt{R_L^2 - \frac{D_S^2}{4}} = 143.1455 - \sqrt{143.1455^2 - \frac{60^2}{4}}$$
$$= 3.18 \text{ mm}.$$

> It is possible to measure the sagittal height of any rotationally symmetric conic section at the spherometer ring diameter. One must be extremely careful when aligning the spherometer axis with the axis of rotation of the conic section.

13.13 Exercise 11.1

Among the many uses of an optical bench, we present here the measurement of back focal length (BFL) of a camera objective.

The arrangement is shown in Fig. 13.12. The procedure is as follows: One focuses an auto-reflective measuring microscope at the rear focal point of the objective. This is achieved when the reflected light by the plane mirror appears sharply concentrated at that point. The position of the lens holder slide is indicated on the measuring scale. Next, the lens holder slide is moved towards the microscope until the last surface of the objective is in "focus." The distance the lens holder slide

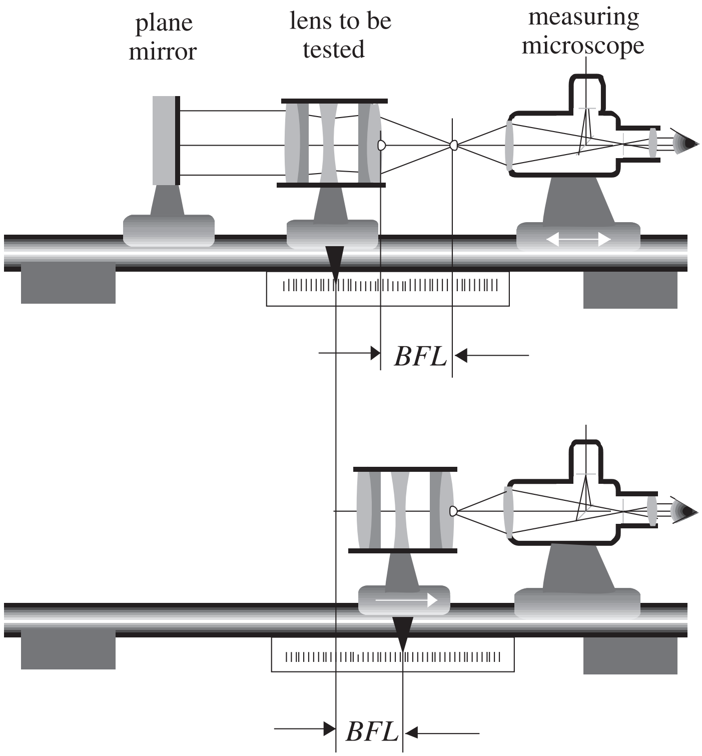

Figure 13.12 Measuring the back focal length of an objective on an optical bench.

was moved is indicated by the measuring scale. This distance is the sought-after back focal length of the objective. In this process, one must of course avoid refocusing the microscope separately.

As noted in the opening remarks of Ch. 12, mounting of optical elements is a very special challenge, and requires extraordinary considerations and special attention, which is beyond the scope of this text.

Index

A
Abbe number, 30
absorption, 123
achromat, 80, 82
Airy disc, 97
angular measure, 55
angular sensitivity, 119
antireflective coating, 114
aperture stop, 63
aspheric singlet, 93
aspheric surface, 134
astigmatism, 56
autocollimator, 148
autoreflecting microscope, 148
axial chromatic aberration, 53
axial marginal ray, 41
axial ray, 41

B
back focal length (bfl), 10, 12, 15, 18
ball lens, 24
beamsplitter, 118
blockage, 71

C
Cassegrain telescope, 82
chief ray, 41
circle of least confusion. *See* minimum blur spot
clipping. *See* blockage
coma, 56
concave mirror, 35
conic section, 91
convex mirror, 37
crown glass, 82
curvature differences, 44

D
decentered lens, 33
diffraction grating, 139
diopter, 11
dispersion, 29
distortion, 57
doublet, 80

E
étendue. *See* throughput

F
Fermat's principle, 3
field curvature,
49, 56
field stop, 63
flint glass, 82
F-number, 42
focal fength of two
separated elements, 86
focal length, 10
freeform surface, 93
front focal length (ffl), 15

G
Galileo Galilei, 74
Gaussian form, 16
gradient index (GRIN) lens,
94

H
Hubble telescope, 83
human eye, 22, 23

I
image location, 43
index of refraction, 3
interference filter, 116

J
Johannes Kepler, 75

L
lateral chromatic aberration.
See lateral color
lateral color, 58
lens bending, 44
lenses, 9
light, 1
longitudinal chromatic
aberration contribution,
55

M
magnification, 15, 41
magnifier, 21
magnifying power (MP), 21
microscope, 76
microscope objective, 84
minimum blur spot, 49
minimum deviation, 31
modulation transfer
function (MTF), 100
molded plastic optical
element, 141
monolithic collimator, 157

N
negative lens, 17
Newton's rings, 129
nodal point, 13
Nyquist frequency, 104

O
off-axis aberration, 49

on-axis aberration, 49
optical bench, 143
optical coating, 111
optical elements, 9
optical path length (OPL), 95

P
paraxial region, 41
pellicle, 118
Petzval curvature. *See* field curvature
plane parallel plate, 25
plastic lens, 153
positive lens, 10
primary aberrations, 47
principal planes, 14
principal ray, 41
prism, 28
  one-diopter, 33
prism spectrometer, 31
projector system, 78
pupils, 63

Q
quarter-wave criterion, 99

R
Rayleigh criterion, 99
reciprocal relative dispersion. *See* Abbe number
reflective coating, 116
relative aperture, 42
relay system, 77
replicated optical elements, 137
reverse telephoto objective, 79

S
sagittal height, 173
Schwarzschild microscope objective, 86
secondary spectrum, 80
separated imaging mirror, 82
sign convention, 14
single-point diamond turning (SPDT), 135
Snell's law, 4, 5
  for a mirror, 34
solar eclipse, 162
spherical aberration, 49

T
telephoto objective, 78
telescope, 73
telescope objective, 82
test plate, 129
thermal effects, 158
thermal sensitivity, 121
thin lens, 39

thin lens third-order aberration theory, 47
thin prism, 32
throughput, 68
tilted plate, 27
total internal reflection (TIR), 167
transverse axial contribution, 55
two-element systems, 73

V
velocity of light, 3
vignetting, 71

W
wavefront spread, 98
windows, 63
working *F*-number, 42
working relative aperture, 42

About the Author

Max J. Riedl was born in Kempten, Germany, where he was educated at the Mathematisch Mechanisches Institut. He graduated from the Akademie für Angewandte Technik, now named the University of Applied Sciences in Munich, where he studied precision mechanics and optics. He has worked in the fields of mathematical and optical instruments for many years, and has been awarded numerous patents for mechanical and electro-optical devices. He held technical as well as business leadership positions during the 45 years he lived in the United States. He has published and presented many papers on fundamental lens design as well as on replicating optical elements and diamond turning diffractive optical components for applications in the infrared spectrum.

For many years he has been presenting short courses on the subjects of *Optical Design Fundamentals for Infrared Systems* and *Precision Machining of Optics* at international conferences of SPIE.

He is the author of the well-received texts *Optical Design Fundamentals for Infrared Systems* and *Optical Design, Applying the Fundamentals*. He is currently retired and lives in Bavaria, Germany.